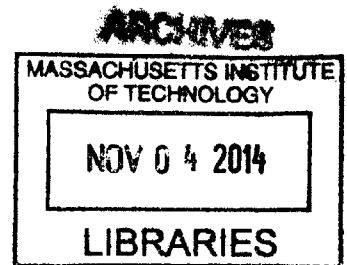


Linking dopaminergic physiology to working memory related  
neural circuitry

By

Andrew D. Bolton  
BS Biomedical Engineering  
Boston University, 2004



SUBMITTED TO THE DEPARTMENT OF BRAIN AND COGNITIVE SCIENCES IN  
PARTIAL FULFILLMENT OF THE REQUIREMENTS FOR THE DEGREE OF

DOCTOR OF PHILOSOPHY IN NEUROSCIENCE

AT THE  
MASSACHUSETTS INSTITUTE OF TECHNOLOGY

SEPTEMBER 2014

© 2014 Massachusetts Institute of Technology  
All rights reserved

Signature redacted

Signature of Author: \_\_\_\_\_  
Andrew D. Bolton  
Department of Brain and Cognitive Sciences  
June 27, 2014

Certified By: \_\_\_\_\_  
Martha Constantine-Paton  
Professor of Biology  
Thesis Supervisor

Accepted By: \_\_\_\_\_  
Matthew A. Wilson  
Sherman Fairchild Professor of Neuroscience  
Director of Graduate Education for Brain and Cognitive Sciences

# Linking dopaminergic physiology to working memory related neural circuitry

By

Andrew D. Bolton

Submitted to the Department of Brain and Cognitive Sciences on June 27, 2014 in  
Partial Fulfillment of the Requirements for the Degree of  
Doctor of Philosophy in Neuroscience

## ***ABSTRACT:***

Working memory is the ability to hold information “online” over a delay in order to perform a task. This kind of memory is thought to be encoded in the brain by persistent neural activity that outlasts the presentation of a stimulus. Interestingly, patients with schizophrenia, a heritable neurological disorder, perform poorly in working memory tasks that require the retention of a target in space, indicating that persistent neural activity related to spatial locations may be impaired in the disease. At the biophysical level, NMDA receptors and dopamine receptors have been continually implicated in supporting persistent activity during spatial working memory. Perhaps relatedly, drugs that target the dopamine system are regularly used in the treatment of schizophrenia, and drugs that target NMDARs induce schizophrenia-like symptoms in healthy individuals. In this thesis, I seek to further examine the possible connection between NMDA receptors, the dopamine system, and schizophrenia-related working memory deficits. We find that homocysteine, a dopamine breakdown product that is upregulated in the blood of schizophrenia patients, strongly impacts NMDAR currents by reducing channel desensitization and altering peak amplitude. Additionally, we find that the dopamine system itself, which is traditionally studied in areas like striatum and prefrontal cortex, is organized in a behaviorally relevant pattern in the superior colliculus (SC), a brain region that shows persistent activity during spatial working memory tasks. The electrophysiological effects of dopamine on the SC suggest that dopamine dysregulation could have previously unexplored effects on spatial attention, sensorimotor integration, and working memory.

Thesis Supervisor: Martha Constantine-Paton, Ph. D.

Title: Professor of Biology, Investigator of the McGovern Institute

## **Andrew D. Bolton**

15 Fairmont Ave Unit #1  
Cambridge, MA 02139  
[abolton@mit.edu](mailto:abolton@mit.edu)

### **Education and Training:**

**Massachusetts Institute of Technology**, Cambridge, MA (2007-pres)

PhD Candidate, Brain and Cognitive Sciences

PI: Martha Constantine-Paton

**Harvard Medical School**, Boston, MA (2004-2007)

Research Assistant, BWH/HMS Department of Genetics

PI: David Beier, Jennifer Moran

**Boston University**, Boston, MA (2000-2004)

BS Biomedical Engineering

Minor in English

Senior Thesis: "DNA Analysis of Genes Linked to Schizophrenia"

PI: Cassandra Smith

### **Fellowships and Awards:**

**NDSEG** - National Defense Science and Engineering Graduate Fellowship

**NSF GRFP** - National Science Foundation Graduate Research Fellowship

**Angus MacDonald Award** - Excellence in Undergraduate Teaching at MIT

### **Bibliography:**

Moran JL, Bolton AD, Tran PV, Brown A, Dwyer ND, Manning DK, Bjork BC, Li C, Montgomery K, Siepka SM, Vitaterna MH, Takahashi JS, Wiltshire T, Kwiatkowski DJ, Kucherlapati R, Beier DR. "Utilization of a whole genome SNP panel for efficient genetic mapping in the mouse." *Genome Research*, 2006 Mar;16[3]:436-40.

Smits P, Bolton AD, Funari V, Lei L, Hong M, Merriman D, Nelson S, Krakow D, Cohn DH, Kirchhausen T, Warman ML, Beier DR. "Lethal Skeletal Dysplasia in Mice and Humans Lacking the Golgin GMAP-210", *New England Journal of Medicine*, 2010 Jan; 262[3] 206-216

Foster KA, McLaughlin N, Edbauer D, Phillips M, Bolton A, Constantine-Paton M, and Sheng M. "Distinct Roles of NR2A and NR2B Cytoplasmic Tails in Long-Term Potentiation", *Journal of Neuroscience*. 2010 30: 2676-2685

Smith CL, Bolton AD, Nguyen G. "Genomic and Epigenomic Instability, Fragile Sites, Schizophrenia and Autism". *Current Genomics*. 2010 September; 11(6): 447–469.

Bolton AD, Phillips MA, Constantine-Paton M. "Homocysteine reduces NMDAR desensitization and differentially modulates peak amplitude of NMDAR currents depending on GluN2 subunit composition", *J Neurophysiol*. 2013 Oct;110(7):1567-82

Phillips MA, Bolton AD, Chen Z, Brown E, Constantine-Paton M "NR2A and NR2B subunit chimeras for the study of NMDA receptors in developmental plasticity", in preparation.

Bolton AD, Murata Y, Kirchner R, Dang T, Constantine-Paton M. "The organization of the dopamine system in the superior colliculus: segregation of D1 and D2 receptors to behaviorally relevant zones", in preparation.

### **Research Experience:**

#### **McGovern Institute for Brain Research at MIT**

PI: Martha Constantine-Paton

Project Descriptions:

1. Analyzing the effects of dopamine and its breakdown product homocysteine on the electrophysiological properties of superior colliculus neurons
2. Modeling and testing the role of NMDA receptors in persistent neural activity during working memory tasks.
3. Designing and testing devices to track mouse eye movements during a short term memory task

#### **Harvard Medical School / BWH Dept. of Genetics**

PI: David Beier, Jennifer Moran

Project Descriptions:

1. Design, implementation, and analysis of SNP panels for forward genetic screening in the mouse.
2. Genetic, phenotypic, and molecular characterization of an ENU mouse mutant with omphalocele, bone defects, and laminar disorganization in the brain.

#### **Boston University Center for Advanced Biotechnology**

PI: Cassandra Smith

Project Descriptions:

1. Examining the relationship between fragile DNA, nutrition, and schizophrenia
2. Sampling the DNA of twins discordant for schizophrenia and comparing the differences between their genomes at unstable repeat sites

## **Teaching Experience:**

Teaching Assistant, "Brain Structure and Its Origins", Prof. Gerald Schneider

Teaching Assistant, "Systems Neuroscience Lab", Prof. Chris Moore, Prof. Jim Dicarlo

## **Relevant Coursework:**

### **Neuroscience**

Systems Neuroscience  
Cellular and Molecular Neuroscience  
Computational Neuroscience  
Genetic Neurobiology  
Human Brain Mapping  
Neural Basis of Learning and Memory

### **Electrical Engineering**

Engineering Computation  
Intro to Electronics  
Signals and Systems  
Control Systems  
Electric Circuit Theory

### **Math/Physics**

Differential Equations  
Calculus I-III  
Linear Algebra  
Neural Networks  
Probability and Statistics  
Statistics for Brain and Cognitive Sciences  
Physics I-II  
Engineering Mechanics I-II  
Biomechanics

### **Biology**

Systems Physiology  
Molecular Biotechnology  
Intro to Biochemistry  
Intro to Biology

## **Technical Skills:**

***Electrophysiology:*** Patch clamp recording of cultured neurons, acute slices, and human embryonic kidney cells. Miniature, spontaneous, and evoked currents; spike recording, dual patch. Expert in fast-application of agonist techniques using piezo-electric amplifiers and fast solution exchange manifolds.

***Computational Methods / Programming:*** Python. MATLAB. Processing. Novice at functional programming (Haskell, Scheme). Neural network modeling, biophysical modeling, MATLAB for probability and statistics.

***Molecular Biology:*** Primary neuron and HEK293 cell culture, transfection of cloned DNA. Brain anatomy (paraffin + cryo sectioning for histology, immunofluorescence, in situ hybridization). Gel electrophoresis, plasmid prep, microsatellite and SNP/RFLP PCR, DNA cloning, Sequenom mass spectrometry, RNA extraction + cDNA preparation.

***Genome Analysis:*** dCHIP genotype analysis software [see Moran, Bolton et al. publication], Sequencher DNA sequence analyzer, Genome database browsers [including NCBI, Mouse Phenome Database, Mouse Genome Informatics, Mouse BLAT, HMS SNP2RFLP].

**Imaging:** Confocal imaging with Nikon C2 system, calcium imaging of Fura2 and GCAMP, imaging of neurobiotin filled / nickel stained neurons and reconstruction with NeuroLucida.

## **Software:**

### ***Mouse Eye Tracker***

Authors: Rory Kirchner and Andrew D. Bolton

<https://github.com/roryk/Mouse-tracker>

### ***Open Source Electroporator and Cell Counter***

Authors: Andrew D. Bolton

<https://github.com/LarryLegend33>

## **Invited Talks:**

“Seldom Studied Aspects of the Dopamine System”

Picower Institute Plastic Lunch Series

Cambridge, MA May 2013.

“How the brain overcomes biophysical constraints on persistent neural activity”

1<sup>st</sup> Annual NIGMS Symposium

Cambridge MA, July 2012

“Homocysteine impacts the activation and desensitization of NMDARs”

McGovern Institute Retreat

Cambridge MA, May 2012

“Utilization of a whole genome panel for efficient genetic mapping in the mouse”

5th Annual Meeting of the Complex Trait Consortium,

Chapel Hill NC, May 2006

“ENU Mutagenesis and SNP genotyping with Sequenom”

Harvard Partners Center for Genetics and Genomics

Cambridge MA, February 2005

“DNA analysis of genes linked to schizophrenia”

Boston University Biomedical Engineering Day

Boston MA, April 2004

## **Poster Presentations:**

Bolton AD, Murata Y, Dang T, Constantine-Paton M. "Exploring the Dopamine Projection to the Superior Colliculus"

Society For Neuroscience Meeting  
San Diego CA, November 2013

Bolton AD, Phillips M, Constantine-Paton M. "Homocysteine reduces NMDAR desensitization and differentially modulates peak amplitude of NMDAR currents depending on GluN2 subunit composition"

Society For Neuroscience Meeting  
New Orleans LA, October 2012

Phillips M, Bolton AD, Chen Z, Brown E, Constantine-Paton M

"NR2A and NR2B subunit chimeras for the study of NMDA receptors in developmental plasticity"

Society For Neuroscience Meeting  
Washington DC, November 2008

Bolton AD, Manning DK, Moran JL, Dwyer ND, Beier DR

"An ENU-induced mouse mutant with severe embryonic defects in endochondral and intramembranous bone formation"

Gordon Research Conference  
Ventura CA, March 2007

Smith CL, Abdolmaleky H, Bolton AD

"Schizophrenia: A Consequence of Perturbations in Nucleic Acid Metabolism"

CNS Diseases Congress  
Boston, MA June 2007

Moran JL, Bolton AD, Tran PV, Brown A, Dwyer ND, Manning DK, Bjork BC, Li C, Montgomery K, Siepka SM, Vitaterna MH, Takahashi JS, Wiltshire T, Kwiatkowski DJ, Kucherlapati R, Beier DR

"Utilization of a whole genome SNP panel for efficient genetic mapping in the mouse."

5th Annual Meeting of the Complex Trait Consortium  
Chapel Hill NC, May 2006

Moran JL, Bolton AD, Brown A, Dwyer ND, Nelson DK, Tran PV, Yun Y, Chesebro A, Bjork B, Li C, Kwiatkowski DJ, Kucherlapati R, Wiltshire T, Beier DR.

"Efficient genetic mapping in the mouse using a whole genome SNP panel."

19th International Mammalian Genome Conference  
Strasbourg France, November 2005.

**ACKNOWLEDGEMENTS:** I would first like to thank my amazing wife Kirsten for her unwavering support and for loving a science nerd. I'd like to thank my daughter Cora for smiling at me when I walk in the door at night and my boxer Kima for licking my face. My parents Susan and Donald Bolton have always provided unbelievable guidance and I can't thank them enough.

Thanks to Jerry Schneider for constant advice on my anatomy data; some of my best times in grad school were sitting in Jerry's office with him and his wife Amy, listening to stories about keeping alligators in the building and watching hamsters orient to sunflower seeds.

Thanks to Sebastian Seung for being a fantastic committee member and Neural Nets teacher. How lucky I was to have a committee member that actually read my proposal, gave me a point-by-point response, and recommended a paper (Ingle et al. 1975) that started me down my current path of frog investigation.

Thanks to Martha Constantine-Paton, a wonderful friend and advisor. One thing that was always a constant in grad school was Martha's complete openness to any idea or project. How many other advisors have a constantly open door, willing to talk to you about anything at any time? How many would drive you home on snowy days, or after late nights trying to bash out a paper? Martha is a real scientist; she taught me to think broadly and consider all angles, and her brave battle with cancer will always be a model of perseverance for me.

Thanks to my outside member Venki Murthy for joining my thesis committee and for offering helpful experimental advice. I knew he was a good choice when he liked my Thelonious Monk desktop picture.

Finally, thank you to all the incredible friends I made in grad school. Marine Phillips is my scientific idol, showing me that careful and personal scientific work is better than flash and pomp any day of the week. Rory Kirchner is the most trustworthy human being I've ever encountered and taught me 75% of what I learned in grad school. Yarden Katz is a brilliant man who does the second best Bob Horvitz impression I know of. Greg Hale and Stuart Layton enhanced my grad school experience 10-fold. Kartik Ramamoorthi and Andrew Young are excellent scientists and friends. I could always tell how Nikhil Bhatla felt about an idea by his indifference (good) or grimaces (bad). Mike Sidorov was always willing to talk slices or sports. Yasunobu Murata: a gracious and honorable scientist with a voracious taste for the NBA. Akira Yoshii always provided a stern, practical, and realistic point of view. Tatsuo Okubo will someday discover something profound. Tru Dang was an outstanding UROP. Thanks to Sam Cooke for reading almost everything I wrote in grad school and for teaching me about George Best and David Ginola.



**TABLE OF CONTENTS:**

**Chapter 1 - Broad Introduction to the Relevance of the Dopamine System in Schizophrenia-Related Working Memory Deficits..... 16**

1.1 - Linking Schizophrenia, Dopamine, NMDARs and Working Memory ..... 17

    1.1.1 – Schizophrenia and Dopamine ..... 17

    1.1.2 – Schizophrenia and NMDARs ..... 18

    1.1.3 – Schizophrenia and Working Memory ..... 21

    1.1.4 – The Superior Colliculus - A Working Memory Storage Device ..... 25

1.2 – The Biophysics of Persistent Activity ..... 28

    1.2.1 – Excitatory Feedback Mechanisms for Persistent Activity..... 29

    1.2.2 – Biological Evidence Supporting the NMDAR Feedback Model ..... 32

    1.2.3 – The PFC, Dopamine, and Persistent Activity ..... 33

1.3 – Summarized Hypothesis ..... 42

**Chapter 2 - Homocysteine Reduces NMDAR Desensitization and Differentially Modulates Peak Amplitude of NMDAR Currents, Depending on GluN2 Subunit Composition ..... 44**

2.1 – Introduction..... 45

2.2 – Materials and Methods ..... 47

    2.2.1 - Primary Neuron Culture..... 47

    2.2.2 - NMDA Receptor Expression in HEK293T Cells ..... 47

    2.2.3 - Electrophysiology Drugs Used / Prepared..... 48

    2.2.4 - Neuron and HEK Cell Electrophysiology..... 49

    2.2.5- Acute Hippocampal Slice Preparation..... 50

    2.2.6 - Slice Electrophysiology and Glutamate Uncaging ..... 51

    2.2.7 - Current Analysis and Statistics..... 52

2.3 – Results..... 53

    2.3.1 - HCY Reduces NMDAR Desensitization and Peak Amplitude in Cultured Neurons ..... 53

    2.3.2 - HCY Effects are Dose Dependent and are Occluded by Saturating Glycine ..... 55

    2.3.3 - HCY Reduces Desensitization of all NMDAR Subtypes, with Effects on Peak Amplitude that are GluN2 Subunit Dependent ..... 57

2.3.4 - HCY Effects in DIV30 Cultured Neurons.....	61
2.3.5- A Free Sulphur Group is Critical for HCY's Effects on NMDARs .....	62
2.3.6- Is HCY Acting at the NMDAR Glycine Site? .....	67
2.3.7 - Are NMDARs in the Brain Susceptible to HCY? .....	68
2.4 – Discussion.....	71
2.4.1 - Site of HCY's action .....	72
2.4.2- HCY and NMDAR Gating .....	73
2.4.3 - HCY Effects are Age Dependent.....	74
2.4.4 - Relevance to Disease.....	75
<b>Chapter 3 - D1 and D2 Dopamine Receptors Segregate to Behaviorally Relevant Zones in the SC: An Anatomical and Electrophysiological Characterization .....</b>	<b>78</b>
3.1 – Introduction.....	79
3.2 – Materials and Methods .....	81
3.2.1 – Animals .....	81
3.2.2 – RNA Sequencing.....	82
3.2.3 – Animal Surgery .....	82
3.2.4 – Anatomy and Histology.....	83
3.2.5 – Cell Counting.....	84
3.2.6 – Slice Electrophysiology .....	84
3.3 – Results.....	85
3.3.1 – RNA Seq .....	85
3.3.2 - D1+ and D2+ Cells are Spatially Segregated in the SC.....	86
3.3.3 – Characterizing the Location, Overlap, and Inhibitory / Excitatory Identity of D1 and D2 Neuron Populations.....	87
3.3.4 – Dopamine Source to the SC is DAT Negative .....	96
3.3.5 - Retrobead Injections to the SC Reveal A13 as a Dopaminergic Input.....	99
3.3.6 - Dopamine Alters Electrophysiology of D1 and D2 Neurons.....	103
3.4 - Discussion .....	106

<b>Chapter 4 – Conclusions and Future Directions .....</b>	<b>110</b>
<b>4.1 – Introduction.....</b>	<b>111</b>
<b>4.1.1 – Issues and Future Directions Concerning the Homocysteine Project ..</b>	<b>113</b>
<b>4.1.2 – Issues and Future Directions Concerning the Dopamine SC Project ....</b>	<b>117</b>
<b>REFERENCE LIST .....</b>	<b>123</b>

**FIGURE LIST:**

<b>Figure 1.1 - Molecular Biology of Dopamine Signaling .....</b>	<b>18</b>
<b>Figure 1.2 - Homocysteine is upregulated in schizophrenia. ....</b>	<b>19</b>
<b>Figure 1.3 - Persistent activity occurs in many different species. ....</b>	<b>23</b>
<b>Figure 1.4 - Schematic of the Memory Guided Saccade Task .....</b>	<b>24</b>
<b>Figure 1.5 - SC Anatomy .....</b>	<b>25</b>
<b>Figure 1.6 - SC and PFC neurons show delay activity. ....</b>	<b>28</b>
<b>Figure 1.7 - NMDAR feedback model.....</b>	<b>30</b>
<b>Figure 1.8 - Recurrent excitation in the intermediate SC.....</b>	<b>31</b>
<b>Figure 1.9 - U-shaped curve of D1 function.....</b>	<b>36</b>
<b>Figure 1.10 - DA enhancement of persistent activity.....</b>	<b>36</b>
<b>Figure 1.11 - D2 impacts saccade neurons of the PFC .....</b>	<b>37</b>
<b>Figure 1.12 - Method of dopamine clearance differs across the brain. ....</b>	<b>41</b>
<b>Figure 2.1 - HCY induces a small depolarization in neurons and reduces desensitization of NMDAR currents.....</b>	<b>54</b>
<b>Figure 2.2 - HCY effects on NMDAR current amplitude and desensitization are dose dependent.....</b>	<b>56</b>

<b>Figure 2.3 - Increasing bathing glycine concentrations occlude HCY's desensitization effects. ....</b>	<b>58</b>
<b>Figure 2.4 - HCY effect on NMDAR currents depends on GluN2 subunit composition. ....</b>	<b>60</b>
<b>Figure 2.5 - HCY reduces desensitization of GluN2A and GluN2B, but not GluN2D NMDAR currents, at 1 <math>\mu</math>M glycine without affecting NMDAR decay kinetics. ....</b>	<b>61</b>
<b>Figure 2.6 - HCY does not reduce peak amplitude in old neuronal cultures ....</b>	<b>62</b>
<b>Figure 2.7 - Opening the thiol ring of HCY-thiolactone creates L-HCY, which reproduces D,L HCY effects. ....</b>	<b>64</b>
<b>Figure 2.8 - Cysteine enhances NMDAR charge transfer through neurons and GluN2A and GluN2B expressing HEK cells. ....</b>	<b>66</b>
<b>Figure 2.9 - Low dose NMDA application does not recapitulate HCY induced reduction of desensitization. ....</b>	<b>66</b>
<b>Figure 2.10 - HCY does not rescue effects of partially blocking the glycine site with DCKA. ....</b>	<b>68</b>
<b>Figure 2.11 - Caged glutamate induces HCY-reducible desensitization in hippocampal cultures. ....</b>	<b>69</b>
<b>Figure 2.12 - HCY induces a small initial depolarization and reduces glycine-dependent NMDAR desensitization in neurons from acute CA1 slices during uncaging of 1 mM MNI-caged glutamate. ....</b>	<b>71</b>
<b>Figure 3.1 - RNA sequencing of dopamine receptor related genes in the SC... </b>	<b>86</b>
<b>Figure 3.2 - D1-Cre and D2-Cre positive cell populations segregate to different SC layers. ....</b>	<b>87</b>

<b>Table 3.1 – Total neuron counts for D1,D2 overlap and D1 VGAT, D2 VGAT experiments. ....</b>	<b>88</b>
<b>Figure 3.3 – D1 tdTomato neurons are enriched in the SGS while D2 EGFP neurons avoid the SGS and are concentrated in the SO and SGI. ....</b>	<b>92</b>
<b>Figure 3.4 – D1 tdTom x VGAT Venus mice show strong overlap between D1 and Venus in the SGS. ....</b>	<b>93</b>
<b>Figure 3.5 – D2 tdTom x VGAT Venus mice show that D2 is expressed primarily in non-GABAergic ....</b>	<b>94</b>
<b>Figure 3.6 - D1 SGS cells are primarily GABAergic while D2 SO neurons are mainly excitatory.....</b>	<b>95</b>
<b>Figure 3.7 – D1 SGS cells are primarily GABAergic while D2 SO neurons are mainly excitatory.....</b>	<b>96</b>
<b>Figure 3.8 – TH axons in the SC are DAT negative. ....</b>	<b>97</b>
<b>Figure 3.9 - Retrobeads do not label SNr dopamine neurons and SNr dopamine neurons do not express VGAT. ....</b>	<b>100</b>
<b>Figure 3.10 – Retrobead injection into the SC labels the locus coeruleus and A13.....</b>	<b>102</b>
<b>Figure 3.11 - DAT tdTom +, TH- neurons in the dorsal hindbrain project to the SC.....</b>	<b>103</b>
<b>Figure 3.12 - D1 expressing neurons respond to dopamine with reduced spiking and decreased AMPA currents. ....</b>	<b>104</b>
<b>Figure 3.13 - D2 neurons respond to dopamine with resting voltage hyperpolarization. D2+ cells were recorded in the intermediate SC in current clamp. ....</b>	<b>105</b>

**Figure 4.1 - NMDAR feedback model “on HCY” ..... 116**

**Figure 4.2 - D1-Cre injected with AAV-Flex-EGFP ..... 121**

**CHAPTER 1:**

***Broad Introduction to the Relevance of the Dopamine System in Schizophrenia-Related Working Memory Deficits***

**\*\* Portions of this introduction have been previously submitted as part of ADB's thesis proposal. Other portions are modified from an R03 NIH application written by ADB.**



## **1.1 - Linking Schizophrenia, Dopamine, NMDARs and Working Memory:**

Schizophrenia is an inheritable neurological disorder marked by hallucinations, delusions, disorganized thoughts, and social withdrawal. Antipsychotic medications, which cause a wide array of detrimental side effects, alleviate symptoms but do not cure the disease and in some cases are ineffective. There is currently no structural biomarker for schizophrenia resembling Alzheimer's or Parkinson's-related neurodegeneration: brains of schizophrenia patients appear anatomically normal (Schnieder and Dwork 2011). With no simple explanation from anatomy, investigators have focused on neurochemical dysregulation, genetic predisposition, and behavioral endophenotypes. These lines of research ask the following questions: Which drugs are relatively effective and what are their targets? Which genes appear linked to schizophrenia? What are some simple behaviors that may reveal functional deficits in the disease? Each of these questions will be addressed.

***1.1.1 - Schizophrenia and Dopamine:*** Dopamine has been the neurotransmitter most closely associated with schizophrenia. Clozapine and Seroquel, both comparatively effective antipsychotic medications, bind multiple dopamine receptor subtypes with a proposed antipsychotic role at the D2 dopamine receptor. Zyprexa and Risperdal, the other two most commonly used schizophrenia treatments, also bind both the D1 and D2 dopamine receptor (Tauscher et al. 2004, Kapur and Remington 2001). Understanding how these drugs work on their target receptors, and how these receptors affect the circuits they are expressed in, may reveal the basis of schizophrenia symptoms and pave the way for more effective treatments.

***1.1.1a - Dopamine Receptor Signaling:*** Since antipsychotic drugs bind dopamine receptors, it is important to understand how these receptors work. D1- and D2-type dopamine receptors are G-protein coupled receptors that act primarily by altering levels of cyclic AMP (cAMP) in neurons (Figure 1.1a). D1 receptors couple to the alpha G-protein  $G_s$ , which stimulates adenylate cyclase and increases cAMP in the postsynaptic neuron. D2, which activates the alpha G-protein  $G_i$ , does the reverse, inhibiting adenylate cyclase and decreasing cAMP. Dopamine receptors can also signal through beta/gamma G-proteins to influence neuronal conductances

(Whorton and Mackinnon 2013). The exact mechanisms concerning how these changes in cAMP and G-protein signaling modulate the electrophysiology of neurons will be addressed in section 1.2.3b. For now, though, it is important to note that the effectiveness of drugs that bind dopamine receptors has convinced many schizophrenia researchers that a defective dopamine system is a main cause of the disease (i.e. the “Dopamine Hypothesis of Schizophrenia”, for review see Howes and Kapur 2009).

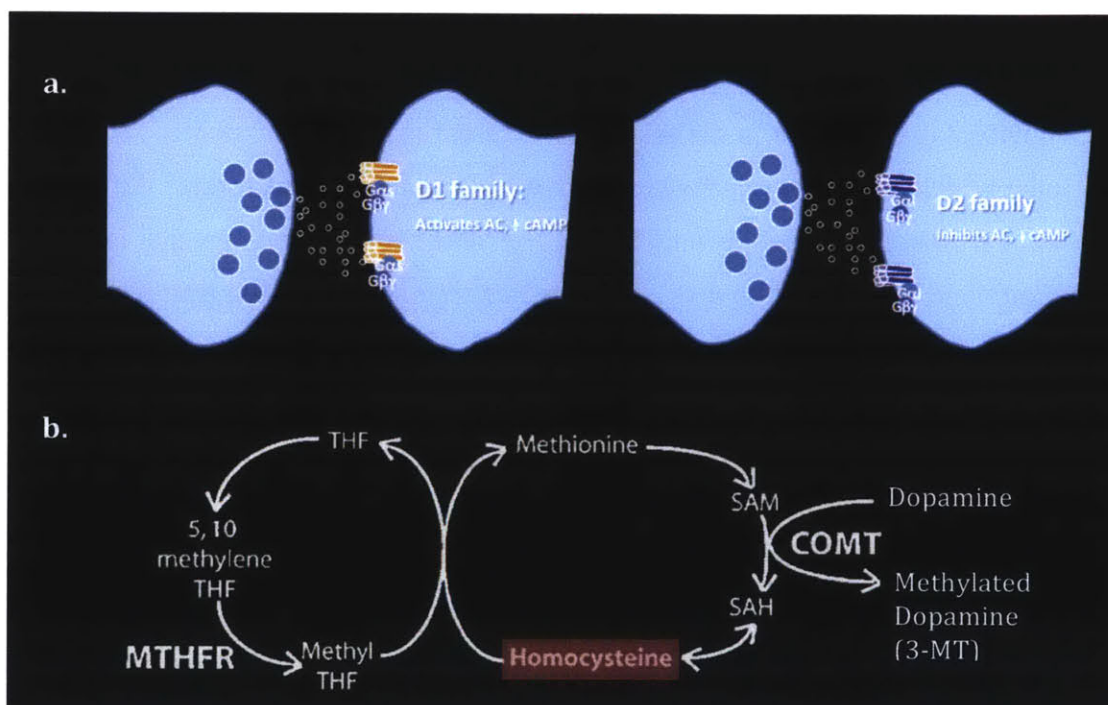


**FIGURE 1.1 – Molecular biology of dopamine signaling. a)** D1 and D2 receptors have opposite effects on cAMP levels. D1 receptors activates G<sub>s</sub>, which stimulates adenylate cyclase and increases cAMP. D2 receptors activate G<sub>i</sub>, which reduces adenylate cyclase activity and decreases cAMP. Both subtypes also couple to beta-gamma G-proteins. **b)** After dopamine has activated its receptors, dopamine is broken down in a pathway involving COMT. COMT methylates dopamine using a methyl group from S-Adenosylmethionine (SAM). When this methylation occurs, a molecule of homocysteine is created, which is eventually re-methylated to methionine in a pathway involving MTHFR [modified from Tunbridge et al. 2008].

**1.1.2 - Schizophrenia and NMDARs:** A second line of pharmacology-based schizophrenia research focuses on N-methyl-D-aspartate receptors (NMDARs). NMDARs are glutamate-activated excitatory cation channels that are essential for normal brain function. The role of these receptors in coincidence detection is critical

for neural plasticity (Bi and Poo 1998), activity-dependent development (Constantine-Paton et al. 1990, Phillips et al. 2011) and persistent neural activity related to short-term memory (Wang 2001, Seung et al. 2000 – to be addressed in section 1.1.3b). NMDARs are also strongly linked to neurological disease. For example, the “NMDAR hypothesis of schizophrenia” has arisen because NMDAR antagonists like ketamine induce schizophrenia-like symptoms in healthy individuals (Newcomer and Krystal 2001). It is unclear, however, how dysregulation of endogenous neurotransmitters could give rise to a ketamine-like environment in the schizophrenic brain. One hint comes from a meta-analysis showing that homocysteine (HCY), an amino acid that binds NMDARs and modulates NMDAR-mediated long-term potentiation, is abnormally high in the blood of schizophrenia patients (Lipton et al. 1997, Christie et al. 2009, Muntjewerff et al. 2006). The analysis concluded that humans with a 5  $\mu\text{mol/L}$  higher than average concentration of HCY in their blood are 70% more likely to have schizophrenia (Muntjewerff et al. 2006; Figure 1.2).

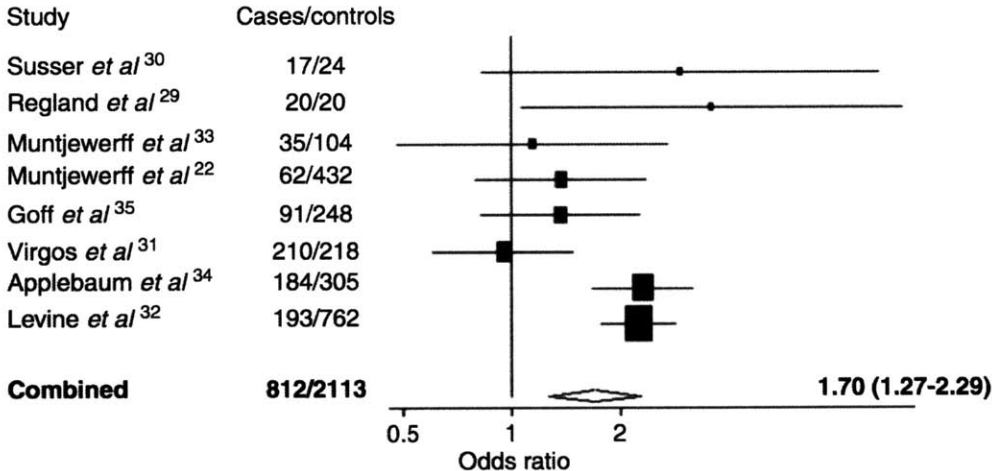


**FIGURE 1.2 - Homocysteine is upregulated in schizophrenia.** Eight case-control studies were analyzed by Muntjewerff et al. (2006) and the question “how likely is an individual to have schizophrenia if they have a 5  $\mu\text{mol/L}$  higher than average HCY level?” was asked. Odds ratios are plotted for each study with 95% confidence intervals (i.e. 1 = subject is equally likely to have schizophrenia or be healthy, 2 = subject is twice as likely to have schizophrenia). All studies but one show a greater likelihood of schizophrenia diagnosis given an increased plasma HCY level. Combined statistics show that individuals are 70% more likely to have schizophrenia given a 5  $\mu\text{mol/L}$  higher than average HCY level.

Importantly, HCY is present in the brain and has been found to be elevated in the cerebrospinal fluid of schizophrenia patients (Regland et al. 2004). HCY arises in the brain after a primary dopamine clearance enzyme, catechol-o-methyltransferase (COMT), inactivates synaptically released dopamine (Tunbridge et al. 2008). A molecule of HCY is generated *every time* COMT removes a methyl group from methionine and places it on a dopamine molecule (Figure 1.1b); this process is a vital step of dopamine metabolism in many brain areas (Tunbridge et al. 2006). After COMT mediated dopamine inactivation, cells release HCY to the extracellular space, where it is free to interact with membrane-bound molecules (Huang et al. 2005). Considering the fact that HCY binds NMDARs, it can be surmised that the glutamate and dopamine systems, and thereby the two main hypotheses of schizophrenia (Dopamine and NMDAR), may be directly linked through COMT. However, this relationship has never been addressed experimentally and is only rarely suggested in the literature.

At the genetic level, hypermorphic and hypomorphic COMT variants have been linked to schizophrenia in numerous studies (Abdolmaleky et al. 2006, Nicodemus et al. 2007, Tunbridge et al. 2006). This association could either stem from COMT's ability to control HCY levels in humans (Tunbridge et al. 2008,) or from COMT's capacity to influence extracellular dopamine levels (Gogos et al. 1998, Tunbridge et al. 2004). However, the importance of HCY is further stressed by research showing that hypomorphic polymorphisms in MTHFR (methyl-tetrahydrofolate reductase), the enzyme that enables the metabolism of HCY after COMT methylations (Figure 1.1b), have also been linked to schizophrenia (Tunbridge et al. 2008, Muntjewerff et al. 2006). These MTHFR polymorphisms, in association with hyperactive COMT, correlate with increased HCY levels in the blood of human subjects (Tunbridge et al. 2008) and could be a driving factor behind the HCY elevations seen in patients (Figure 1.2, Muntjewerff et al. 2006). We suspect that dopamine *and* HCY dysregulation are likely involved in schizophrenia pathology and that proper levels of dopamine and HCY are important for normal brain function. This hypothesis is the reason that, in this thesis, I sought to further

illustrate both HCY and dopamine's effects on receptors and circuits relevant to schizophrenia.

Intriguingly, the same polymorphisms in the COMT and MTHFR genes that heighten HCY levels and predispose individuals to schizophrenia interact to reduce performance on working memory tasks and tests of executive function (Roffman et al. 2008a, Roffman et al. 2008b). This is crucial when considering that working memory appears to be impaired in schizophrenia patients, as will be addressed in section 1.1.3.

**1.1.3 - Schizophrenia and Working Memory:** Because inheritable diseases like schizophrenia are behaviorally complex and confounding to study, researchers have tried to divide these diseases into their component behavioral parts. For example, schizophrenia patients explicitly express psychotic symptoms, but it is thought that these symptoms may be rooted in sensory gating and working memory deficits (Gottesman and Gould 2003). These “endophenotypes” are simpler deficits that co-segregate with the disease and also appear to a milder degree in healthy first-degree relatives. Poor sensory gating and working memory performance, if studied in isolation, could yield insight into more complex schizophrenia symptoms like hallucinations, flattened affect, and avolition (Gottesman and Gould 2003, Durstewitz and Seamans 2008). In this thesis, I focus on the working memory endophenotype because working memory has been strongly linked to both NMDARs and dopamine, the two major molecular players in schizophrenia. But before discussing the NMDAR and dopamine relationship to working memory, it is first important to define our endophenotype of choice.

**1.1.3a - Introduction to working memory:** Working memory is the ability to briefly retain information that is no longer explicitly present in the environment “online” in order to perform a task or make a decision. For example, Romo and Brody (Romo et al. 1999) famously designed and implemented the following working memory task: First, a monkey is presented a vibration on his finger. After a short delay, the monkey is presented with a second vibration at a different frequency. He must then indicate if the first or second frequency was higher to gain

a reward (Figure 1.3a, top). Successful comparison requires the monkey to remember the first frequency until the second is presented; the short-term memory of the first vibration frequency is the “working memory” in this case. Monkeys perform this task very accurately (90% +), indicating that there is a high fidelity short-term storage mechanism in the brain (Romo et al. 1999).

With regards to a neural correlate of working memory, Romo and Brody observed “persistent neural activity” in the prefrontal cortex as monkeys remembered the first vibration (Figure 1.3a, bottom). Remarkably, this persistent activity monotonically encoded the frequency to be remembered. For example, if the monkey remembered a 40 Hz frequency, a set of “memory neurons” in the prefrontal cortex would fire at 40 Hz throughout the entire memory period. If the monkey remembered a 20 Hz frequency, the neurons would fire at 20 Hz. This amazing result, along with the bulk of other work that shows stimulus-specific persistent activity during working memory (for review, see Goldman-Rakic et al. 1996, Arnsten et al. 2012, Compte 2006), suggests that working memory could be studied by examining the basis of persistent neural activity in the brain.

#### 1.1.3b - Persistent Activity and Working Memory Across the Animal Kingdom:

Although the most pioneering work in the field has been performed in the monkey by the group of Patricia Goldman-Rakic (Goldman-Rakic 1996), persistent activity is not restricted to primates. On the contrary, persistent activity appears to be a fundamental form of neural dynamics observed across many species during working memory. For example, in rats performing a delayed turning task, the direction of a future turn is stored via persistent activity in the superior colliculus (Felsen et al. 2012, Figure 1.3b). Frogs also use persistent activity in the optic tectum (the non-mammalian homolog of the superior colliculus; Ingle et al. 1975, Figure 1.3c) to remember locations of prey. Lastly, the “memory” of eye location can be read out from persistent neural activity in the fish medulla (Seung et al. 2000, Aksay et al. 2007).

A short-term storage buffer like working memory is vital to the every day life of humans as well. On a minute-to-minute basis, we are storing information for short periods of time (location of our coffee relative to our hand so we don't knock it

over, the topic of the conversation we're having, the ever-changing location of our samples in lab so we don't dump brains on the floor) only to throw it away when it is no longer useful.

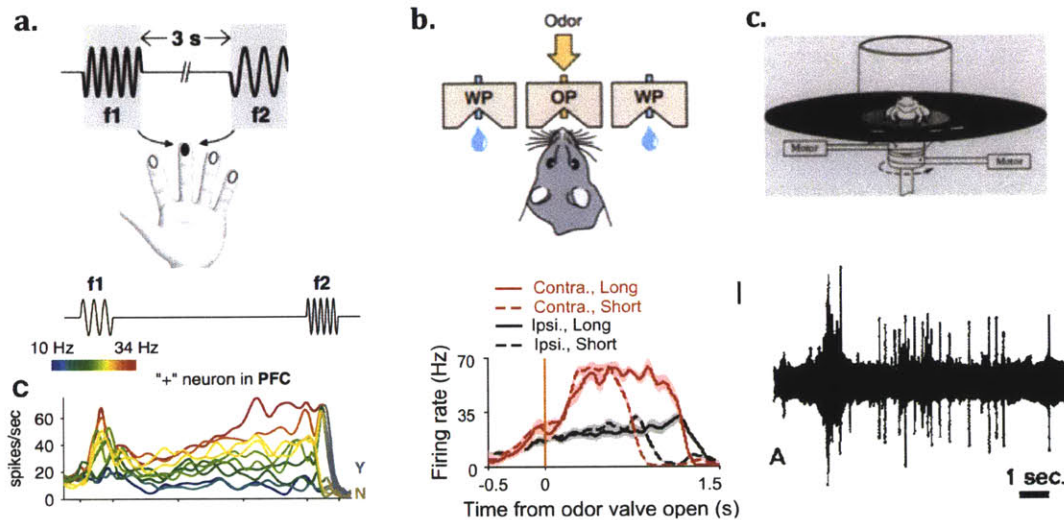


**FIGURE 1.3: Persistent activity occurs in many different species.** a) During a monkey somatosensory working memory task, the subject must remember the frequency of a vibration on his finger (f1) and compare it to a second vibration (f2) occurring 5 seconds later. During the 5 second delay, neurons in the PFC monotonically encode the remembered frequency (i.e. cells fire at 20 Hz if remembering a 20 Hz f1 frequency). Adapted from Machens et al. 2005. b) Rats that have associated a particular odor with a left or right turn are delivered the odor at a port (OP). After a 1-1.5 second delay, the animal is allowed to choose to turn left or right depending on the remembered odor. The animal remembers which direction it will turn using persistent activity in the contralateral superior colliculus. c) If a prey item vibrates in space, a frog will remember the location of the vibrating prey until the prey vibrates a second time, causing the animal to strike. The frog remembers the location of the first prey item using persistent activity in its optic tectum. (Ingle et al.1975).

*1.1.3c - Schizophrenia Memory Deficits are Spatial:* Like the aforesaid rat and frog examples (Figure 1.3b and 1.3c), the working memory tasks schizophrenia patients tend to fail are **spatial** in nature. In one of many examples, Park and Holtzman (1992) showed that during a memory-guided saccade task, schizophrenia patients performed significantly worse than both healthy controls and a cohort of non-schizophrenic bipolar patients with psychosis. This task requires the subject to remember a cued spatial location over a delay of 5 or 30 seconds then saccade to the remembered location (Figure 1.4). Over a 30 second delay, schizophrenia patients dropped to only 60% accuracy and tended to perseverate on previously correct

answers. The same investigators, along with Patricia Goldman-Rakic, later repeated this result and showed that the deficit carries over to first-degree relatives (Park, Holtzman and Goldman-Rakic, 1995).

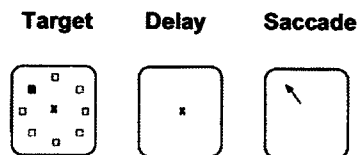


**FIGURE 1.4: Schematic of the Memory Guided Saccade Task.** A monkey or human is shown an array of possible targets surrounding a fixation point (X). One of the targets then flickers. The subject must remember the location of this target over a short delay until the fixation point turns off. A correct saccade to the remembered location warrants a reward.

Spatial working memory deficits in schizophrenia patients and their relatives carry over when the readout is an arm movement or button press instead of a saccade. This indicates a deficit in a memory system versus a defect in a specific motor system. Moreover, the deficits have been shown in patients and relatives from both Caucasian and Pacific Island populations, indicating a common endophenotype amongst various human populations (Glahn et al. 2003; Myles-Worsley and Park 2002; Park and Holtzman 1992).

Critically, in many studies, *only spatial working memory is impaired* while verbal working memory stores appear to be normal (Park and Holtzman, 1992, Cannon et al. 2000) or not reflected in relatives' performance (Pirkola et al. 2005). The most convincing studies on this front have come from the lab of Tyrone Cannon. His findings have all been extracted from twin pairs that are either discordant for schizophrenia or completely unaffected. These studies show that a healthy unmedicated monozygotic twin (i.e. a twin with the **exact** same genetic background as his/her schizophrenic brother or sister) mirrors the schizophrenia-related spatial working memory deficit in their ill sibling while failing to show a deficit in verbal working memory (Cannon et al. 2000, Pirkola et al. 2005). Like schizophrenia itself, it appears that schizophrenia-related spatial working memory deficits are genetic in nature, representing a true endophenotype of the disease. *The brain region or*



regions involved in this deficit must therefore be primarily involved in encoding spatial information.

#### 1.1.4 - The Superior Colliculus – A Spatial Working Memory Storage

**Device:** The superior colliculus (SC) is an inherently spatial structure located on the roof of the midbrain (Figure 1.5a). The upper “superficial” layer (SGS) of the SC receives retinal ganglion cell axon projections that terminate topographically along the SC surface (Figure 1.5b). This means that specific locations in space are represented in specific areas of the SC in a *visuotopic map*. The visual axons forming the map enter the SC through the stratum opticum (SO), which also contains neurons with visual receptive fields and is considered “superficial” SC (Figure 1.5b).

Superficial cells project directly downward to the intermediate SC layers (SGI, SAI, Figure 1.5b), endowing intermediate layer neurons with visual receptive fields. Unlike the superficial layer, excitatory intermediate layer cells are reciprocally connected to each other by recurrent collateral axons (Pettit et al. 1999, Saito and Isa 2003). Recurrent collateral axon connections are the exact architecture predicted by computational models to mediate persistent activity – these models will be addressed in Part 2 of this chapter.

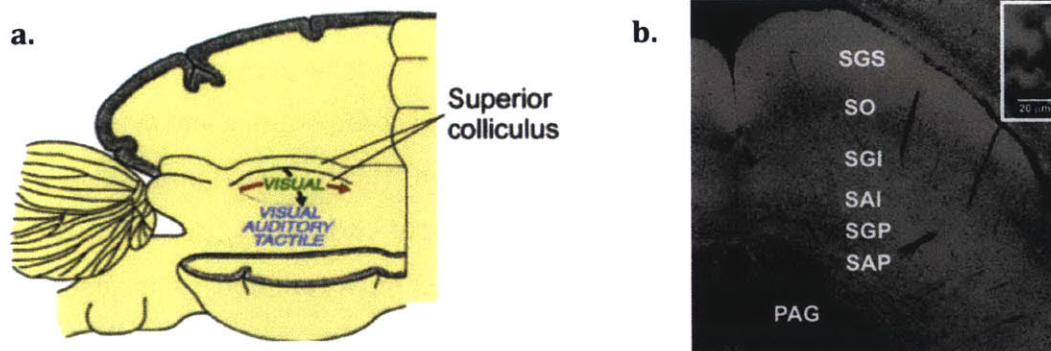


**FIGURE 1.5 - SC Anatomy.** a) The SC is a structure located in the dorsal midbrain beneath the cortex. b) Like the cortex, the SC is multi-layered structure. This figure shows a coronal section of the rodent SC. Visual input terminates on neurons in the superficial SC (SGS, SO), which then project downward to topographically organized premotor neurons in the SGI and SAI. The SGI, SAI, SGP, and SAP all receive multimodal input, especially somatosensory, with the deepest layers (SGP, SAP) receiving the bulk of SC auditory input. [Modified from Sooksawate et al. 2012].

In addition to receiving **sensory** input from the superficial SC layers, intermediate layer cells also have topographically organized **motor** fields. That is, a *motor map* exists within the SC. Stimulating the SGI in monkeys induces saccades whose amplitude and direction correspond to location within the SC structure (Robinson 1972, Schiller and Stryker 1972). Correspondingly, stimulating the SGI/SAI of rats (Dean et al. 1986) or hamsters (Northmore et al. 1988) induces orienting movements whose direction corresponds to SC location, and stimulating the intermediate layers of the frog tectum induces snapping motions that correspond to topographic location in the SC (Ewert 1984).

It is therefore clear that the SC receives topographic visual input in the superficial layers that can be translated into a spatially precise, intermediate-layer mediated, movement towards a stimulus. Central to this dissertation, moreover, is the fact that SGI cells in the SC display persistent activity during the delay period of the exact delayed saccade task that schizophrenia patients fail (Munoz and Wurtz 1995). During the task, when the visual target is presented for memorization, an intermediate SC cell will spike strongly if the target is in its visual receptive field (Figure 1.6). However, after disappearance of the target at the beginning of the delay period, the cell's activity does not return to baseline (Figure 1.6). The cell maintains persistent firing during the delay as previously described in section 1.1.3. This delay activity is thought to encode the remembered location of the target and/or the intention to saccade to that target. After the delay period ends, the cell "ramps up" to a burst that is causal for the ensuing saccade (Munoz and Wurtz, 1995). Therefore, individual intermediate SC neurons receive visual input, remember that input, and transform the sensory input into a motor output. Amazingly, it appears that the three actions a subject must complete to perform the delayed saccade task (see target, remember target, saccade to target) are all reflected in the activity of single neurons in the intermediate superior colliculus!

Importantly, the PFC also shows delay activity during the delayed saccade task, but the three portions of the task are separately represented by three kinds of spatially tuned neurons: cue, memory, and response cells (Figure 1.6b; Goldman-Rakic 1996). The PFC also shows a semblance of topographical mapping of space

(Hagler Jr. and Serano 2006, Sawaguchi and Iba 2001). However, it is unclear why researchers have almost exclusively focused on the PFC as a working memory site if species as ancient as frogs can perform spatial working memory with only an optic tectum and no neocortex whatsoever (Ingle et al. 1975, Ingle and Hoff 1990). Moreover, lesions of the PFC produce subtle deficits in terms of overall mental capacity. After losing much of his frontal lobe in a construction accident, Phineas Gage went on to become a successful stagecoach driver and even learned a second language (Kean 2014). If the PFC were the sole site of spatial working memory, it would certainly be surprising that Phineas Gage could perform the complex spatial navigation required for driving a taxi around Chile.

The SC, on the other hand, is a vastly underappreciated and understudied structure with new research pointing to its role in spatial attention (Muller et al. 2005, Lovejoy and Krauzlis 2010), decision making (Ratcliff et al. 2003), and even more ethereal roles like consciousness (Merker 2007, Strehler 1991). Removing the SC, unlike the PFC, causes profound deficits. Monkeys with SC lesions become expressionless, stare aimlessly into space, stop grooming, and return to apathy immediately after stimulation from the environment. The only reported SC lesion in a human rendered the patient expressionless, un-reactive to the environment, and resigned to staring into space (Denny Brown 1962). These symptoms **strongly resemble the negative symptoms of schizophrenia**, which include inexpressive faces, blank looks, few gestures and lack of socialization (Komaroff 1999).

To summarize, the SC shows task-bound activity during delayed saccade tests that schizophrenia patients fail. We therefore hypothesize that defects in the fundamentally spatial SC, which contains spatial maps of both visual input and motor output, contributes to the spatial working memory deficits observed in schizophrenia. However, to understand the mechanisms of working memory-related SC persistent activity, it is important to now address the biophysical mechanisms that allow persistent activity to come about.

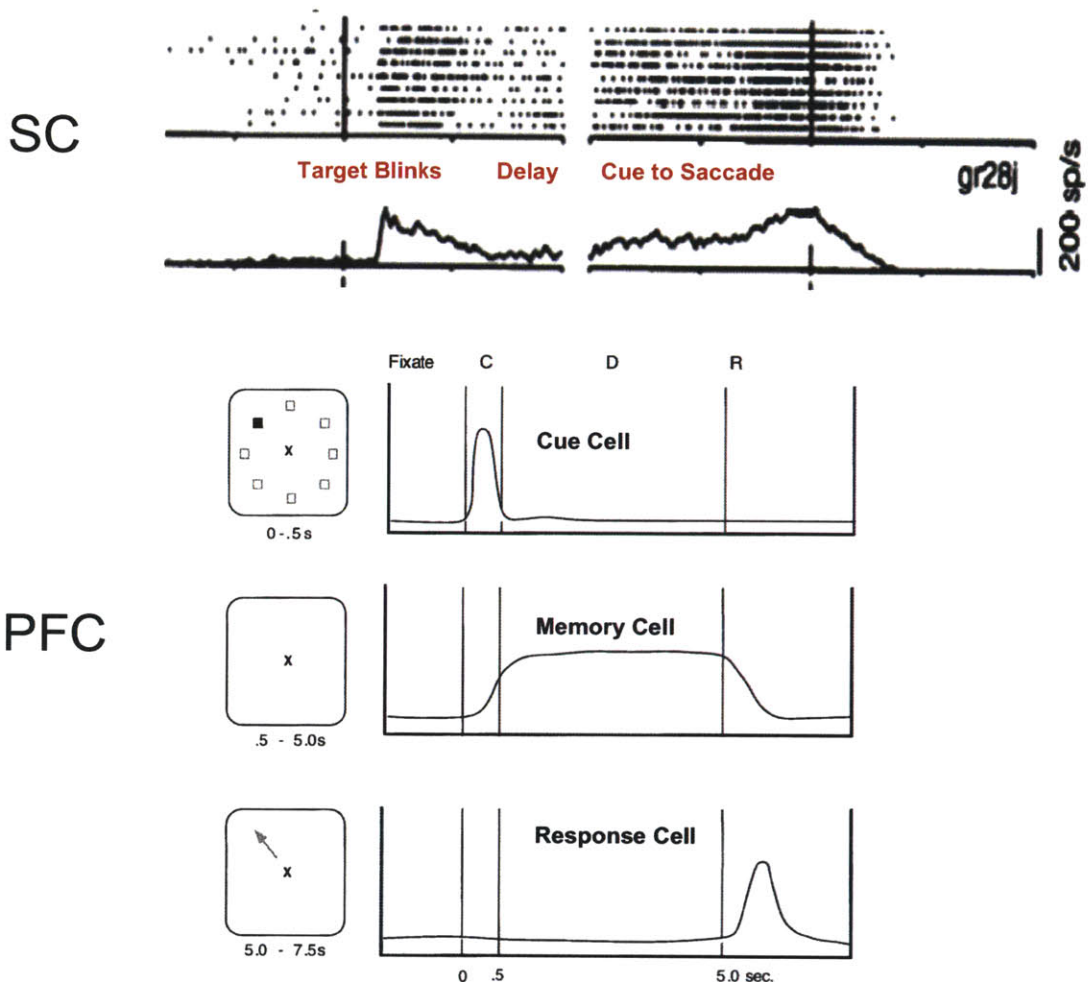


**FIGURE 1.6: SC and PFC neurons show delay activity.** Here, a neuron is recorded in the SGI while a monkey performs the memory guided saccade task. When the target to be remembered first appears, the neuron shows a bursting visual response. This response decays but remains persistent at ~40Hz after the target has disappeared. When the fixation point turns off, allowing the animal to saccade, the activity ramps up to over 200Hz and the eye moves to the remembered target position. (Taken from Munoz and Wurtz, 1995). PFC neurons also activity during the delayed saccade task, but the three facets of the task are spread amongst three different cell types that show activity related to seeing, remembering, and responding to a remembered stimulus (Goldman Rakic 1996).

## 1.2 - The Biophysics of Persistent Activity:

The connection between NMDARs, dopamine, working memory, and schizophrenia has been addressed. How could these topics converge at the level of neurons and synapses? Which properties of neural circuits allow the storage of

persistent activity and how could this go wrong in disease states? These questions will be addressed here in Part 2 of Chapter 1.

**1.2.1 - Excitatory Feedback Mechanisms for Persistent Activity:** It must be stressed that when a PFC memory cell or an SGI neuron in the SC remains firing during the delay period of a memory guided task, there is *no environmental information driving the cell*. How neurons remain persistently active with no input to drive them is still poorly understood at the cellular level and is even less understood at the level of synapses and molecules (i.e., ion channels, synaptic receptors, required signaling pathways). At the cellular level, persistent activity could arise from:

1) Intrinsic mechanisms = sensory-driven changes in the persistently active cell itself that outlast the stimulus

2) Network mechanisms = Ongoing dynamics of the multi-neuronal circuit within which the active cell is synaptically connected.

Biophysically, the intrinsic mechanism could be a “plateau potential” carried by a non-desensitizing voltage-gated cation channel. Sensory driven depolarization would drive the neuron past the activation voltage of this channel, allowing it to open and continually depolarize the cell until deactivated by inhibition. There is precedent for this intrinsic mechanism in the entorhinal cortex, where calcium channels drive cell autonomous persistent activity (Egorov et al. 2002). On the other hand, the hypothesized network mechanism for persistent activity is recurrent excitatory feedback mediated by NMDAR containing synapses (Figure 1.7).

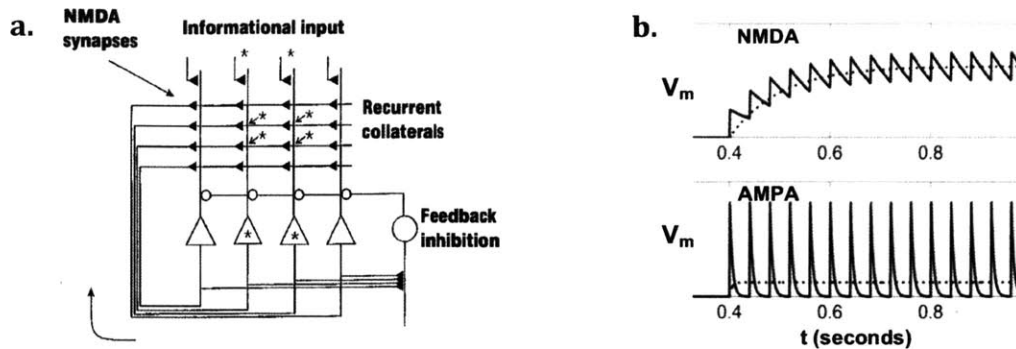


**FIGURE 1.7 - NMDAR feedback model.** **a)** Recurrent excitation allows the storage of a short-term memory in selected cells (\*). Each neuron in the network is connected to every other neuron via recurrent collaterals with NMDA synapses. Informational input arrives only at the starred neurons. These neurons fire action potentials which backpropagate and relieve their dendritic NMDA  $Mg^{2+}$  block. Recurrent synapses thereby become operational exclusively on the starred cells promoting reverberatory activity on those cells only via feedback excitation. Runaway excitation and noise is prevented by feedback inhibition. **b)** Feedback excitation can drive further action potential firing in starred neurons because the NMDA response, unlike the AMPA response, decays slowly (see  $\tau = 100ms$  vs.  $\tau = 5ms$ ). This allows temporal summation of recurrent input EPSPs, bringing the neuron towards action potential threshold. AMPA receptors decay too quickly for temporally delayed inputs to stack (Taken from Lisman et al. 1998 and S. Seung lecture notes).

NMDARs are unique receptors in that they are the “AND gates” of the brain. When a neuron is at rest, its NMDARs are plugged with  $Mg^{2+}$  ions that prevent the receptor from passing current. The  $Mg^{2+}$  ions only exit the NMDAR if the neuron is depolarized. This sets up a scenario whereby the NMDAR can detect coincident presynaptic glutamate release and postsynaptic depolarization. Only then will the NMDAR pass depolarizing sodium and calcium into the postsynaptic neuron.

The excitatory feedback model of persistent activity takes advantage of the coincidence detection properties of NMDARs. In the model, all neurons in the network share excitatory feedback connections containing NMDARs (Lisman et al. 1998). If a subset of neurons in the network is activated by an external stimulus to be remembered (Figure 1.7a, starred cells), the sensory induced depolarization of the cell will relieve the  $Mg^{2+}$ -block from dendritic NMDA receptors. Excitatory feedback synapses on activated neurons thus become operational. In the absence of further sensory input, spiking neurons will persistently activate each other through these feedback synapses in an excitatory loop. NMDA receptors remain blocked with  $Mg^{2+}$  on the dendrites of cells that were not activated by the external stimulus,

causing failure of feedback neurotransmission onto these neurons. Therefore, neurons not activated by the original input will not participate in a persistently active ensemble and will remain silent.

NMDARs serve a second purpose of “remembering” previous inputs; the long decay time of NMDA currents allows temporal summation of postsynaptic potentials (EPSPs) as long as subsequent inputs arrive within ~100-400ms (Seung et al. 2000). Stacking of EPSPs during excitatory feedback allows successive inputs that are staggered in time (as occurs during feedback amplification) to cooperate in driving the neuron towards firing threshold. Non-NMDA AMPA EPSPs have extremely fast decay times -- staggered inputs onto fast decaying synapses would not be able to summate, causing a lesser total depolarization at the soma that would fail to fire reverberating neurons (see Figure 1.7b).

Importantly, the kind of feedback architecture predicted by biophysical models of persistent activity is present in both the PFC (for review, see Arnsten et al. 2012) and the SC (Saito and Isa 2003, Pettit et al. 1999). In the SC, if one excitatory cell is stimulated with caged glutamate (Figure 1.8), recurrent excitatory activity amongst neighboring connected neurons evokes continuous EPSCs that resemble stacked EPSCs in Figure 1.7b. Moreover, this type of reverberatory activity does not occur in the SGI if NMDA receptors are blocked with AP5 (Saito and Isa 2003), which fits perfectly with the NMDAR-mediated excitatory feedback model.

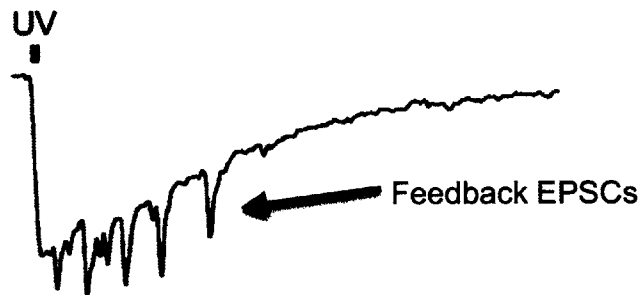


**FIGURE 1.8 – Recurrent excitation in the intermediate SC.** Neurons in the SGI of the SC are connected in recurrent excitatory loops. If a single excitatory cell is stimulated to threshold with caged glutamate (UV), its firing triggers the firing of nearby connected neurons, which feed back onto the originally excited neuron. This feedback induces a run of EPSCs that do not occur if TTX is present (indicating the requirement of neighboring neuron firing). Taken from Pettit et al. 1999.

To summarize and reiterate how Lisman's computational model of persistent activity relates to SC circuitry:

1) Neurons in the superficial SGS receiving topographic input from the eye provide input to the recurrent network through the SGS -> SGI vertical projection (i.e. SGS is "informational input" in Figure 1.7a).

2) After visual input activates the SGS and is translated to the SGI, SGI neurons encoding the presented location in space will fire, relieving the dendritic  $Mg^{2+}$  block. Through recurrent excitatory feedback synapses in the SGI (Pettit et al. 1999, Saito and Isa 2003, Figure 1.8), neurons sharing the same spatial receptive field can recurrently activate themselves through NMDAR-containing feedback synapses. Meanwhile, the  $Mg^{2+}$  block remains intact on SGI neurons whose receptive fields do not correspond to the presented visual input. These neurons will not respond to the continual recurrent excitation because their NMDARs are inoperative, allowing specific encoding of spatial memory by the activated cells.

**1.2.2 - Biological Evidence Supporting the NMDAR feedback model:** The  $Mg^{2+}$  block and long decay time of the NMDAR make this receptor an ideal biological device for mediating stimulus-specific persistent activity. However, if NMDAR based models of persistent activity are indeed correct, then NMDAR binding drugs should modulate persistent activity and working memory performance. This appears to be the case.

Aultman and Moghaddam (2001) found that IP injection of the NMDAR antagonist MK801 prevented rats from performing a working memory-based delayed alternation task; these rats performed at chance levels for all delay periods tested. In monkeys, systemic administration of the broad NMDAR antagonist ketamine diminished performance on the delayed saccade task and reduced task related persistent firing of memory cells in the PFC (Wang et al. 2013). Local application of NMDAR antagonists for both the GluN2A and GluN2B NMDAR subtypes leads to a decrease in persistent firing in PFC memory cells (Wang et al.



2013). Finally, humans also show working memory deficits when under the influence of ketamine (Krystal et al. 2005, Newcomer and Krystal 2001). These results strongly suggest a role for NMDARs in working memory and persistent activity.

**1.2.3 - The PFC, Dopamine, and Persistent Activity:** In Part 1 of this chapter, the SC was proposed as a possible site of schizophrenia related working memory deficits. Considering the recurrent feedback architecture in the intermediate SC and the fact that NMDAR antagonists abolish SC reverberatory activity, it is likely that the persistent activity that stores working memories in the SC is NMDAR feedback mediated.

In section 1.1.2, we illustrated that the dopamine breakdown product HCY is upregulated in schizophrenia patients and that HCY is known to bind NMDARs. We propose that HCY could affect the NMDAR feedback model by influencing NMDAR currents. This could explain why upregulated HCY, working memory deficits, and schizophrenia pathology are linked. However, HCY's effect on NMDAR currents has never been examined in depth, which was an original goal of this dissertation and is addressed in Chapter 2.

Also mentioned in section 1.1.2 is the idea that dopamine itself is the major neurotransmitter involved in schizophrenia pathology. If our proposal that the SC is disrupted in schizophrenia is correct, and this leads to the working memory deficits observed in the disease, then we must understand how the dopamine system influences activity in the SC.

There is currently no evidence concerning how dopamine might affect the SC's ability to store spatial memories. If the NMDAR feedback model is correct, it is critical to place dopamine modulation into the context of the model. One hint about how dopamine may influence circuits that support working memory in the SC comes from the PFC literature.

**1.2.3a - Dopamine Agonists and Antagonists Modulate PFC Persistent Activity:**  
The dopamine system's role in altering working memory performance and persistent activity in the PFC has been intensively, but not necessarily successfully,

studied. The modulation of PFC persistent activity and working memory by dopamine agonists and antagonists is complex and the mechanism by which dopamine works is debatable. Even papers from the same lab are conflicting at times. These complexities are likely due in part to the proposed “U-Shaped Curve” of dopamine function (Goldman-Rakic et al. 2000), but this theory could not capture the entire breadth of contradictory results. It is at least important to address dopamine’s effects on PFC persistent activity in order to better understand how it might affect similar activity in the SC.

The “U-Shaped Curve” theory postulates that optimal function of the PFC requires a set point of dopamine, and that PFC processing will be compromised if this setpoint is either not met *or* exceeded. This hypothesis is supported by the fact that both the addition of dopamine antagonists and agonists can reduce working memory performance; moreover, hypo- *and* hyper-active polymorphisms in COMT, the aforesaid enzyme that breaks down dopamine and controls total dopamine levels in the PFC, can both be detrimental to PFC function (Goldman-Rakic et al. 2000, Sawaguchi and Goldman-Rakic 1991, Zahrt et al. 1997, Tunbridge et al. 2006, Tunbridge et al. 2008). In addition to behavioral readouts, the U-shaped function seen with dopamine related drugs can also be observed at the level of single neurons. For example, Williams et al. (1995) showed that applying the D1 antagonist SCH39166 enhanced delay period persistent activity in the monkey PFC during the delayed saccade task (Figure 1.9a, trace 2). However, if the concentration of the drug was increased, the delay period persistent activity was abolished (Figure 1.9a, trace 3). Moreover, on the same set of neurons where D1 antagonists enhance persistent activity, D2 antagonists depress activity (Figure 1.9b). Therefore, both D1 and D2 antagonists appear to be able to alter activity related to working memory, convincing most researchers that dopamine is at least involved in supporting persistent neural activity.

The question of dopamine involvement in PFC persistent activity was re-addressed by the work of Sawaguchi (2001). In this study, the idea proposed by Williams et al. (1995) that D1 antagonists enhance activity was contradicted. Sawaguchi found that application of the D1 antagonist SCH23390 only rarely

enhanced activity (5/62 neurons at high concentration, 1/11 neurons low concentration); it was nearly always depressive (43/62 high concentration, 10/11 neurons low concentration). When Sawaguchi applied dopamine to persistently active neurons in the PFC during working memory, it enhanced activity only in the preferred direction of the neuron (i.e. the center of the receptive memory field, Figure 1.10). This effect was blocked with the D1 antagonist SCH23390. Moreover, SCH23390 did not impact background activity of the recorded neurons nor activity related to other aspects of the task; the effect of D1 receptors appeared specific to working memory-related delay activity that theoretically supports memory.

Considering Sawaguchi's result that *D1 receptors are specifically required for maintaining delay activity*, it is not surprising that detrimental effects on working memory have been observed when using SCH23390 on both rodents and monkeys (Aultman et al. 2001, Sawaguchi et al. 1994). In fact, Aultman et al. showed in rats that this D1 antagonist had no effect on a delayed alternation spatial working memory task if the delay was short (1 second), but saw increasing effects of the drug if the delay was longer (10 sec) and significantly poorer performance if the delay reached 40 seconds. This was exactly mirrored in monkeys (Sawaguchi et al. 1994), where D1 antagonist infusion to the PFC impacted working memory more severely with longer delays, and did not affect performance if the same task was devoid of a delay.

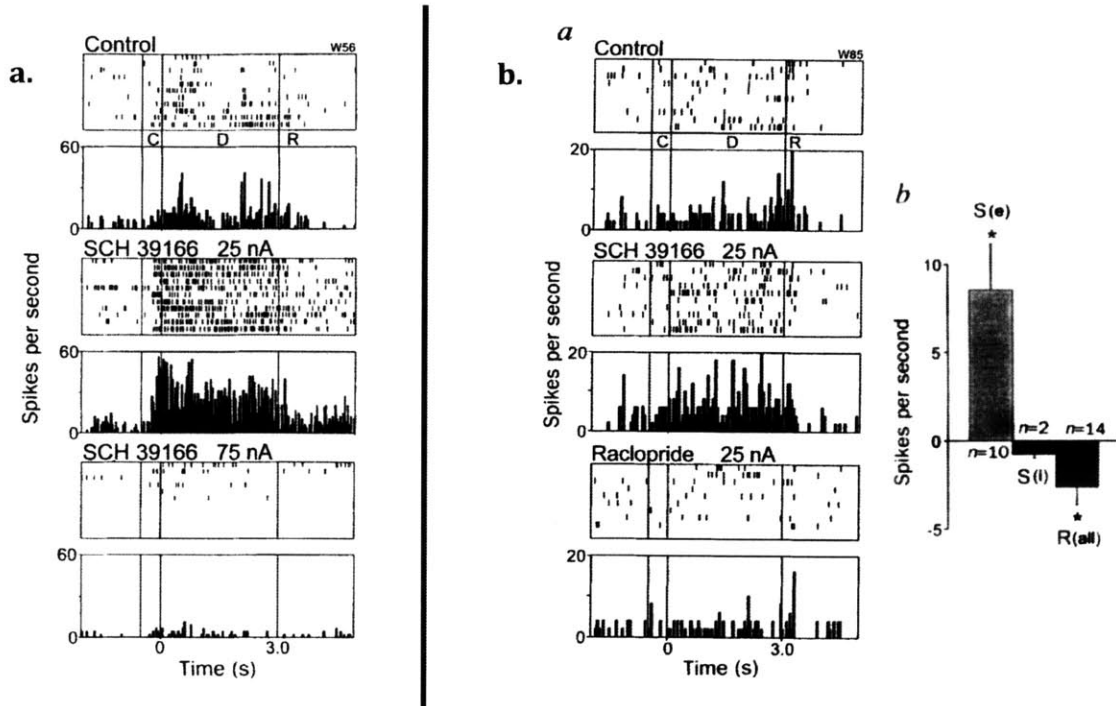


**FIGURE 1.9 - U-shaped curve of D1 function.** a) In control conditions (top trace), persistent activity is observed as the monkey remembers a location in space. This persistent activity is spatially precise: the neuron's receptive field is restricted to one spatial target. If D1 antagonist SCH39166 is added at low concentrations iontophoretically, the delay activity is enhanced (middle trace); however, at higher concentrations, delay activity is significantly depressed (bottom trace). b) If raclopride, a D2 antagonist, is added iontophoretically, delay activity is suppressed similarly to high concentration SCH39166. The bar chart on the right indicates that on average, low D1 antagonist enhances delay spiking by 8 spikes/sec, while D2 antagonist depresses activity by ~3 spikes/second (figures taken from Williams et al. 1995).

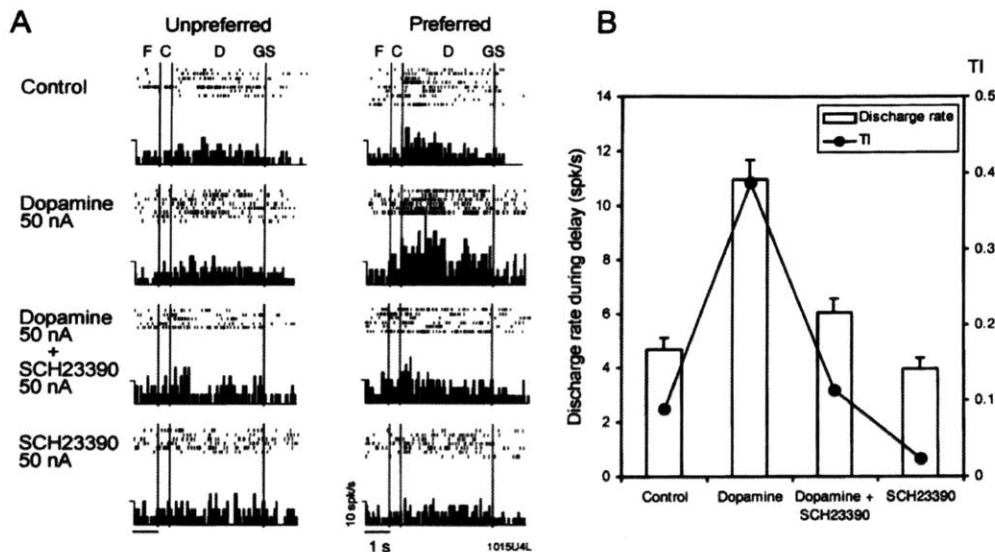


**FIGURE 1.10 – DA enhancement of persistent activity.** Dopamine application to neurons firing persistently during working memory enhances spike rate in the preferred direction of the cell. This effect is blocked using the D1 antagonist SCH23390. SCH23390 reduces activity during the delay if applied without dopamine (figures taken from Sawaguchi 2001).

The effect of D2 receptor antagonists and agonists is even more controversial than D1. In Sawaguchi's study (2001), only 2 of 15 neurons responded significantly to the D2 antagonist sulpiride. Unlike Williams et al. (1995) where the D2 antagonist raclopride significantly decreased persistent activity, these two neurons showed significant enhancement. Others, however, have seen drastic results with D2 antagonists. Wang et al. (2004) infused D2 antagonist raclopride into the PFC during the delayed saccade task and saw no effect on persistent activity; however, the activity of "saccade neurons" was significantly suppressed by raclopride. These are the "response" cells in Figure 1.6. Moreover, Wang saw the *reverse* result of Sawaguchi in terms of D1's role. Like in Williams and Sawaguchi's study, D1 had a role only in persistent activity and did not affect "saccade neurons"; however, the D1 agonist SKF38393 significantly suppressed persistent activity, which is in complete contradiction to Sawaguchi's result especially (Figure 1.11).

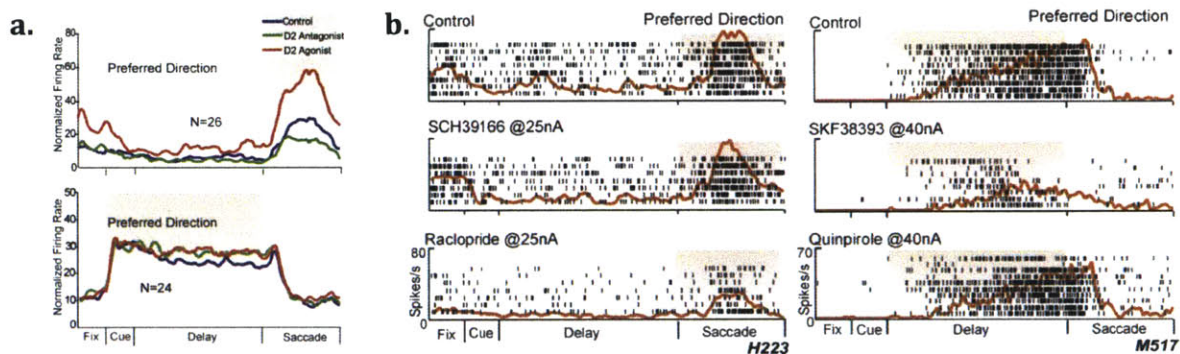


**FIGURE 1.11 – D2 impacts saccade neurons of the PFC.** A subset of neurons in the PFC show activity locked to the third phase of the delayed saccade task (recall Figure 1.4). This is the "response" phase, where after remembering the stimulus using "delay" or "memory" neurons, the monkey initiates a movement towards the remembered target. There are cells in the PFC that activate only when the saccade is initiated. The saccade related activity of these cells is significantly depressed by D2 antagonist raclopride (a, top; b, bottom left) and enhanced by the D2 agonist quinpirole (a, top). Raclopride and quinpirole had no effect on delay activity in memory neurons. D1 antagonist SCH29166 did not replicate raclopride's depression of saccade related activity (b, left middle), but D1 agonist SKF38393 did affect delay activity with a significant depression (b, right middle). Modified from Wang et al. 2004.

With regards to *behavioral* effects of D2 acting agents, Arnsten et al. (1995) showed that D2 agonist quinpirole, if injected systemically into monkeys, impaired working memory at low concentrations but improved memory performance on the same spatial delayed choice task at high concentrations. Luciana et al. (1992) and Mehta et al. (2001) report that systemic injection of D2 agonist bromocriptine enhances working memory in humans and Mehta et al. (1999, 2004) shows that the D2 antagonist sulpiride reduces working memory response latency (1999) and accuracy (2004) in humans during spatial but not non-spatial working memory tasks.

On the other hand, Sawaguchi et al. (1994) saw no behavioral effects of PFC injected D2 antagonist (sulpiride) during the delayed saccade task, and a more recent study by Mehta (2005) did not confirm her previous two results that sulpiride affects spatial working memory exclusively.

#### 1.2.3b - What is the Basis of Largely Contradictory Dopamine Effects in PFC?:

It is clear that dopamine is doing *something* during working memory tasks that require persistent activity. It is also not surprising that dopamine alters activity related to working memory because slice electrophysiology experiments have documented numerous effects of dopamine on neural excitability and neural communication. D1 receptor activation has been shown to reduce glutamate release (Gao et al. 2001, Seamans et al. 2001a), enhance NMDAR currents (Seamans et al. 2001a), increase spike rate in response to injected current (Onn et al. 2006), enhance activity of GABAergic cells (Trantham Davidson et al. 2007, Seamans et al. 2001b), alter resting potential (Pickel et al. 2006, Podda et al. 2010), and enhance HCN currents (Chen and Yang 2007). D2 receptor activation induces bursting in excitatory neurons (Onn et al. 2006), decreases inhibitory current frequency and amplitude (Seamans et al. 2001b), and activates GIRK type potassium channels that hyperpolarize neurons and heterologous cells (Lacey et al. 1987, Williams et al. 1989, Werner et al. 1996).

1.2.3c - What is Wrong with Previous Approaches?: One major problem with the *in vivo* PFC studies is the lack of knowledge about whether the cells being recorded even express dopamine receptors. A recent study of the mouse PFC using a

D1-tdTomato reporter mouse revealed that only a sparse population of PFC neurons expresses D1 receptors (Seong et al. 2012). D1+ and D1- pyramidal cells represent two different populations of neurons; D1+ cells are bursting cells with no HCN currents whose activity is increased in response to D1 agonists. D1- cells spike regularly, possess hyperpolarization-activated currents, and are not modulated by D1 agonists. Therefore, even though it is still questionable how the mouse PFC maps onto the monkey PFC, Seong et al. (2012) reveals how critical it may be to examine neurons that actually express the receptor in order to understand how dopamine impacts circuit function.

The sparseness of dopamine receptor expressing cells in the PFC suggests that the behavioral effects of systemic agonist / antagonist injection (Arnsten et al. 1995, Luciana et al. 1992, Mehta et al. 1999, 2001) may not be entirely due to drug actions on the PFC. In fact, D2 receptor density is 10-20 times lower than D1 receptor density in the PFC (Lidow et al. 1991). D2 is much more highly expressed in the striatum, a region also known to be involved in spatial short term memory (Ingle and Hoff 1990). Our personal observations suggest that D2 is expressed far more strongly in the superior colliculus than the PFC, and D1 is also strongly expressed in the SC. No studies have ever addressed the role of D1 or D2 receptors in the superior colliculus. Studying D1 and D2 in the SC is compelling because it could explain the discrepancy between the well-accepted dopamine dysregulation in schizophrenia and the present lack of a clear association between dopamine and the working memory deficit observed in the disease.

A second major problem with present *in vivo* work is the lack of consideration of the various components of the PFC neural circuit. Current understanding of how the 6-layered structure of the PFC operates with regards to inputs, outputs and function is limited. It is impossible to understand the true role of dopamine without considering its overall actions on a well defined microcircuit. The SC presents a more tractable circuit with direct sensory input, premotor output, and defined roles played by each layer. However, despite both dopamine and the SC's strong link to working memory, no studies have ever examined dopamine's effect on SC electrophysiology.

Lastly, the *in vivo* studies may miss how dopamine dysregulation impacts working memory because dopamine breakdown products are disregarded. Little attention is paid to the notion that after dopamine activates its receptors, it must be cleared from synapses for future transmission to occur. *Dopamine's effects can only be understood if all neuroactive molecules that arise after its release are considered.* Interestingly, the mechanism of dopamine clearance from synapses differs across the brain, meaning that the combined effects of dopamine and its breakdown products vary according to brain region. For example, not every area in the brain uses COMT mediated breakdown as a means of dopamine clearance. In fact, the brain area that contains the most dopamine innervation, the striatum, uses the dopamine transporter (DAT) to reuptake dopamine into the presynaptic terminal (Sesack et al. 1998, Figure 1.12). Meanwhile, in the frontal cortex, DAT is not expressed at synaptic terminals (Sesack et al. 1998, Figure 1.12); instead, COMT mediated breakdown appears to be the major method of dopamine clearance (Tunbridge et al. 2006). This is also the case in the SC, where dopamine concentrations are higher than frontal cortex (Versteeg et al. 1976) and dopamine breakdown products are also present at high levels (Weller et al. 1987). Notably, COMT activity in the SC is higher than in frontal cortex, and COMT methylations in the SC can be induced by visual stimulation (Bigl et al. 1974).

As mentioned, the COMT generated dopamine byproduct HCY is strongly and consistently upregulated in the blood (Muntjewerff et al. 2006) and CSF (Regland et al. 2004) of schizophrenia patients. Detailed results concerning HCY's effect on the nervous system will be addressed in Chapter 2. However, in this broad introduction, it is critical to note that the COMT will create HCY in the SC, and HCY molecules will be free to interact with synaptic molecules like NMDARs (Lipton et al. 1998) because HCY is released to the extracellular space (Huang et al. 2005).



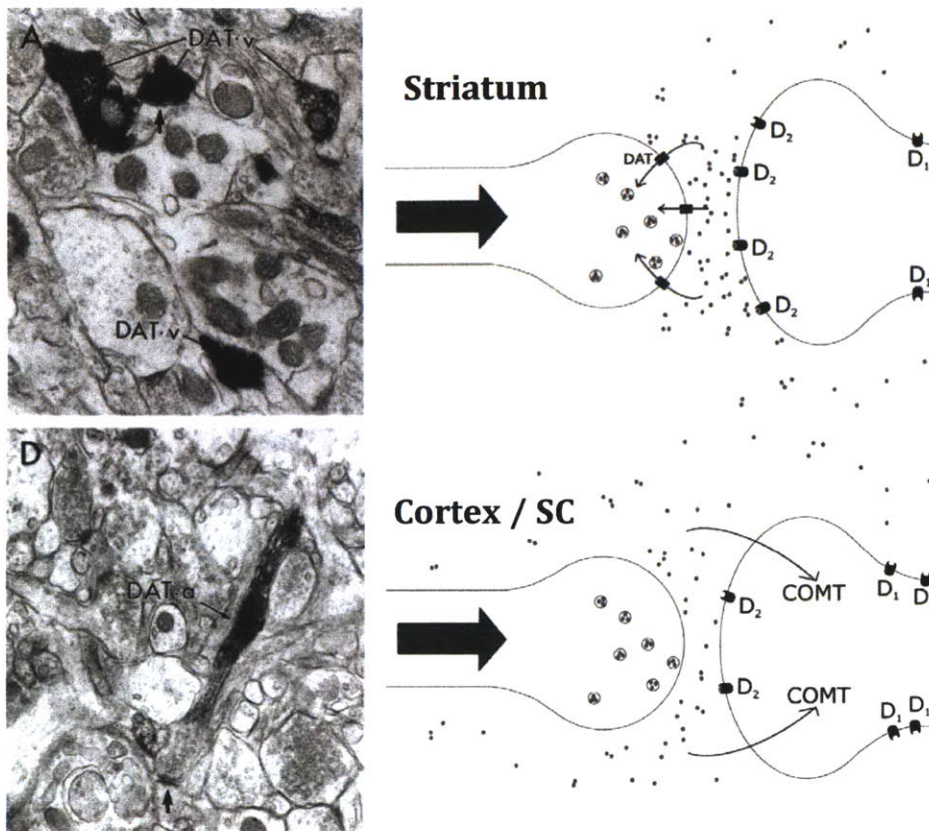


**FIGURE 1.12 – Method of dopamine clearance differs across the brain.** Electron micrographs from striatum (top) and prefrontal cortex (bottom) show immunogold particles attached to a DAT antibody. DAT is prominently expressed in the presynaptic terminal in the striatum; however, DAT is not present at the presynaptic terminal in cortex. Instead, DAT is expressed far away from the synapse on the axon shaft. It is thought that this DAT rounds up any dopamine that has escaped the synapse, and that COMT breaks down synaptic dopamine as a clearance mechanism. The SC expresses high levels of COMT, suggesting that the mechanism of dopamine clearance there is the same as in cortex (micrographs taken from Sesack et al. 1998, diagram modified from Tunbridge et al. 2006).

Recall that hyperactive polymorphisms of COMT and hypoactive polymorphisms in MTHFR, the protein that remethylates HCY for future COMT methylations, significantly interact to produce working memory deficits in schizophrenia patients (Roffman et al. 2008a). Oddly, Roffman et al. conclude that this interaction indicates that hypoactive MTHFR alleles exacerbate the dopamine deficiency in the PFC induced by hyperactive COMT. This argument is strange considering MTHFR has no role in dopamine production nor signaling. All MTHFR does is create folate derivatives that are required for methylation of HCY. The only

way COMT and MTHFR could interact is via HCY, a notion previously mentioned in the literature (Tunbridge et al. 2008).

Therefore, it is the hypothesis of this thesis that both dopamine **and** HCY contribute to working memory deficits observed in schizophrenia. D1 and D2 receptor linkage to PFC function is weak, and we argue that understanding dopamine's role in working memory requires the examination of other brain regions involved in spatial memory. Our region of choice is the SC because the current actions of a monkey during the memory guided saccade task (seeing, remembering, saccading) can **be directly read out from single SGI neurons in the SC**, pointing to a crucial role for the SC in a task that schizophrenia patients fail (Wurtz et al. 2001, Munoz and Wurtz 1995). Moreover, dopamine is also likely to play a role in the SC because the absolute level of SC persistent activity is modulated by expected reward (Ikeda and Hikosaka 2007, Ikeda and Hikosaka 2003, Felsen et al. 2012).

### **1.3 – Summarized Hypothesis:**

My primary goal was to understand the neural circuitry that mediates persistent neural activity. My hypothesis is that persistent neural activity may go awry in schizophrenia, giving rise to working memory deficits observed in the disease. At the level of cells and circuits, I posit that dopamine and its byproduct HCY, which is upregulated in schizophrenia, both contribute to working memory deficits via modulation of persistent activity. I focus on understanding how these dopaminergic molecules affect the NMDAR feedback model of working memory, which captures the major characteristics of persistent activity. Understanding working memory, one of the main endophenotypes of schizophrenia, could lead to an understanding of the more complex symptoms observed in the disorder and eventually pave the way to more effective treatments.

I originally proposed to study how the dopamine system, namely dopamine, its byproducts, and its receptors, affect the SC, an underappreciated structure in the field of working memory research. Before this dissertation began, two major

unknowns existed concerning how dopamine and HCY might impact NMDAR mediated feedback activity in the SC:

1) How does HCY, which is known to bind NMDARs, affect NMDAR currents?

Answering this question is vital because any molecule that can impact NMDAR currents should be able to alter NMDAR mediated excitatory feedback in the SC, and thereby SC persistent activity and working memory.

2) How is the dopamine system arranged within the SC? Does the SC contain dopamine receptors, and where are these receptors located within the SC circuit? Do they appear in the upper visual layers that receive retinal input or are they located in the memory-mediating SGI? Understanding how dopamine enters the SC, where it terminates, and how it signals once it arrives will shed light on how dopamine might influence persistent activity in the SC.

Chapter 2 describes our results concerning how HCY affects NMDAR currents. This chapter was published in the *Journal of Neurophysiology* (Bolton et al. 2013). HCY reduces NMDAR desensitization and alters peak amplitude of NMDAR currents based on the GluN2 subunit the receptor contains. This reduction of desensitization would be expected to influence the duration of persistent activity. Reasoning for this claim will be addressed in Chapter 4.

Chapter 3 contains a description of how the dopamine system is patterned in the SC. There is an elegant separation of dopamine receptors within the SC, where D1 receptors are enriched in the superficial visual layers and D2 receptors occupy the deeper layers, where feedback activity is generated. Moreover, dopamine strongly affects the electrophysiological properties of SC neurons. D2 neurons show a significant drop in resting potential when exposed to dopamine while SGS D1 cells show a strong AMPA current reduction in response to visual axon stimulation.

Chapter 4 summarizes the introduction in Chapter 1 and the results in Chapter 2 and 3, placing each result into the context of the NMDAR feedback model.

**CHAPTER 2:**

***Homocysteine reduces NMDAR desensitization and differentially modulates peak amplitude of NMDAR currents, depending on GluN2 subunit composition***

**\*\* This chapter has been published**

**Andrew D. Bolton, Marnie A. Phillips and Martha Constantine-Paton. *J Neurophysiol* 110:1567-1582, 2013**

## **2.1 - Introduction:**

The role of N-methyl-D-aspartate receptors (NMDARs) in coincidence detection is critical for neural plasticity (Bi and Poo 1998), activity-dependent development (Constantine-Paton et al. 1990; Phillips et al. 2011) and persistent neural activity related to working memory (Wang 2001; Seung et al. 2000; Lisman et al. 1998). NMDARs are also strongly linked to neurological disease. For example, the NMDAR hypothesis of schizophrenia has arisen because NMDAR antagonists like ketamine induce schizophrenia symptoms in healthy individuals (Newcomer and Krystal 2001). It is unclear, however, how dysregulation of endogenous neurotransmitters could give rise to a ketamine-like environment in the schizophrenic brain. One hint comes from a meta-analysis showing that homocysteine (HCY), an amino acid that acts on NMDARs (Lipton et al. 1997; Poddar et al. 2009), is abnormally high in the blood of schizophrenia patients (Muntjewerff et al. 2006).

In addition to its presence in the blood, HCY also arises in many brain areas after catechol-o-methyltransferase (COMT) methylates synaptically released dopamine (DA) and norepinephrine (NE) (Bigl et al. 1974; Broch Jr. and Fonnum 1972; Tunbridge et al. 2008; Huang et al. 2005). HCY is present in normal human cerebrospinal fluid (CSF), and schizophrenia patients show increased HCY in the CSF (Regland et al. 2004), but studies that have addressed the synaptic actions of extracellular HCY have produced complex results. Previous work has demonstrated that HCY induces calcium flux into cultured neurons through NMDARs, causing excitotoxicity that is blocked by NMDAR glutamate site antagonists (Lipton et al. 1997). Acutely applied HCY also mimics NMDA in reducing long-term potentiation (LTP) in hippocampal slices (Christie et al. 2009). However, while these and other studies suggest that HCY is a weak agonist at the NMDAR glutamate site (Poddar et al. 2009), HCY also shows characteristics that are *not* typical of glutamate site agonists (Lipton et al. 1997, Christie et al. 2009). For instance, when HCY concentrations are raised above 100  $\mu\text{M}$ , the effect of HCY on LTP reverses – now HCY significantly *enhances* NMDAR-dependent LTP, which does not occur when NMDA is applied (Christie et al. 2009). Moreover, HCY *inhibits* peak NMDA-induced calcium flux when glycine concentrations are sub-saturating in young cultured

neurons (Lipton et al. 1997). This is significant because the NMDAR glycine site may not be saturated *in vivo* by its co-agonists d-serine and glycine, the latter of which is shuttled away from synapses by glycine transporters (GlyTs) (Bergeron et al. 1998; Martina et al. 2003; Chen et al. 2003). Considering the complexity of previous HCY results, we sought to directly test how the schizophrenia-related molecule HCY influences the dynamics of NMDAR currents in cultured neurons, human embryonic kidney (HEK) cells transfected with NMDAR subunits, and acute brain slices.

One feature of NMDAR currents is their rapid and extensive desensitization in response to prolonged agonist exposure (Mayer et al. 2004). Channel desensitization is thought to play a role in shaping synaptic events and protecting the neuron from calcium toxicity during repeated receptor stimulation (Lukasiewicz et al. 1995; Tong et al. 1995). Three forms of NMDAR desensitization are believed to be working in concert. The glycine-dependent component of desensitization is occluded upon raising extracellular levels of glycine or d-serine (i.e. glycine and d-serine relieve, rather than cause, this form of desensitization: Mayer et al. 1989; Lerma et al. 1990; Vyklicky et al. 1990). Calcium-dependent desensitization is caused by calcium flux through the NMDAR, involves calmodulin and calcineurin, and is prevented by fast calcium chelation and low extracellular calcium (Zilberter et al. 1991; Legendre et al. 1993; Krupp et al. 1996; Ehlers et al. 1996; Tong et al. 1995). Glycine-independent desensitization is the component of desensitization that remains after glycine levels are saturated and calcium flux is prevented; the molecular motifs governing glycine-independent desensitization have been elegantly localized to the GluN2 N-terminal domain (Sather et al. 1990,1992; Villarroel et al. 1998).

In the present study, we examined how NMDARs responded to HCY during prolonged agonist application. Neurons and HEK cells transfected with NMDAR subunit cDNA (GluN1+GluN2A, GluN1+GluN2B, or GluN1+GluN2D) showed strongly reduced NMDAR desensitization in the presence of HCY. We demonstrate that HCY specifically reduces the glycine-dependent component of NMDAR desensitization, with pronounced effects at doses as low as 50  $\mu$ M. HCY maintained its desensitization reducing capabilities in hippocampal slices, where native glycine

and d-serine levels do not appear to saturate the NMDAR. HCY also affects peak amplitude of the NMDAR response depending on ambient glycine levels and GluN2 subunit composition. Our results are consistent with, and add to, previous literature describing HCY's effects on NMDAR currents and LTP.

It is known that GluN2A:GluN2B ratios vary with age and between excitatory and inhibitory neural populations (Flint et al. 1997; Townsend et al. 2003; van Zundert et al. 2004; Kinney et al. 2006). This suggests that HCY's effects will change with development and differ according to cell type within neural circuits. A change in HCY's effect with development is shown here and may be critical given the late adolescent / early adulthood onset of schizophrenia (Macdonald and Chaffee 2006).

## **2.2 - Materials and Methods:**

All experiments were carried out with the approval of the Committee on Animal Care at the Massachusetts Institute of Technology.

**2.2.1 - Primary Neuron Culture:** Cortical cultures were prepared from P0 Thy-1 GFP mice (Feng et al. 2000), while hippocampal cultures were from C57B6. Cells were plated on poly-D-lysine coated coverslips and grown glia-free in B27 supplemented Neurobasal A media (Invitrogen, Grand Island, NY). Older culture recordings (DIV30) were obtained from cultures expressing tdTomato in parvalbumin (PV) positive neurons; however, PV+ neurons were not targeted for patching.

**2.2.2 - NMDA receptor expression in HEK293T cells:** cDNAs for mouse GluN1-1a (P35438), GluN2A (P35436), and GluN2B (Q01097) (M Mishina, University of Tokyo, Japan) were previously cloned into DsRed2N1 (Clontech, Mountain View, CA), where the DsRed2 gene was replaced with an NMDAR subunit. All subunits were selected by full-length sequencing. The GluN2D (Q03391) construct was a gift from Dr. John Woodward (Medical University of South Carolina; Jin et al. 2008). HEK293T (HEK) cells (293tsA1609neo; ATCC, Rockville, MD) were plated onto uncoated glass coverslips in 1 ml DMEM +/- (DMEM + GlutaMAX

(Invitrogen Gibco 10569) + 10% FBS + 1% Pen/Strep). Cells were transfected 1 hour after plating with GluN1 and GluN2 subunits plus a pEGFP reporter to visualize transfected cells (1:1:1 ratio). For each reaction, cDNAs were added to 200  $\mu$ l Optimem (Invitrogen), incubated for 5 minutes after addition of 2  $\mu$ l Plus reagent (Invitrogen), then incubated for 25 minutes after adding 6  $\mu$ l Lipofectamine LTX (Invitrogen) for a total volume of 208  $\mu$ l. This solution was added to the 1 ml of DMEM+/+ on plated cells for 30-45 minutes of transfection. Transfection media was removed and cells were incubated in a medium containing DMEM +/+, 3 mM kynurenic acid (Sigma, St. Louis, MO), and 1 mM D,L-AP5 (Tocris, Minneapolis, MN) at 37° C, 5% CO<sub>2</sub>.

**2.2.3 - Electrophysiology Drugs Used / Prepared:** N-methyl-D-aspartate, glutamate (L-glutamic acid), D,L-homocysteine, D,L-homocysteine thiolactone, L-homocysteine thiolactone, D,L-homocystine, strychnine, and L-cysteine (free base) were obtained from Sigma. Dichlorokynurenic acid (DCKA), D,L-AP5, MNI-caged glutamate, NBQX, Gabazine, N-[3-([1,1-Biphenyl]-4-yloxy)-3-(4-fluorophenyl)propyl]-N-methylglycine (NFPS), and tetrodotoxin (TTX) were obtained from Tocris. Glycine was obtained from JT Baker (Pittsburgh, NJ). L-homocysteine, the form of homocysteine that is present in the brain, was synthesized from L-homocysteine thiolactone by opening the thiolactone ring. This method was generously communicated to us by Dr. Donald Jacobsen (Lerner Research Institute, Cleveland, OH). 154 mg L-homocysteine thiolactone was dissolved in 5M NaOH (.15 g/ml concentration) and incubated for 5 minutes at 37° C. A solution of 2 M HCl, .1 M TES (pH 7.4) and dH<sub>2</sub>O (1.9:1:1.1) was then mixed with the HCY/NaOH solution at a ratio of 4:1 and vortexed. Argon gas was bubbled through the solution. Maximal possible yield of L-HCY was 200 mM; this stock solution was diluted 1:100 for experiments leaving a possible 2 mM in experimental solutions for Figure 7.

We prepared L-homocysteine, D,L homocysteine, and all other drug solutions fresh on the day of recording. L-homocysteine effects were qualitatively identical to D,L – homocysteine (Figure 7). Commercially available D,L-homocysteine consists of



50% L-homocysteine and 50% D-homocysteine (personal communication with Sigma representative), and HCY quickly degrades in solution (Hogg 1999), so it is likely that effective doses of HCY are at most half of what is reported here.

**2.2.4 - Neuron and HEK Cell Electrophysiology:** DIV7-17 cultured cortical neurons (unless otherwise noted) or transfected HEK cells (14-24 hours after transfection), were transferred directly from culture media to extracellular solution before recording. Cells were patched and voltage clamped to -60mV (unless otherwise indicated) using pulled glass pipettes (3-8 M $\Omega$ ). Junction potentials were adjusted prior to break-in. Data were acquired using an Axopatch 1D patch clamp amplifier filtered at 5 kHz and sampled at 1 kHz using a Digidata 1320A and pClamp 8 software (Axon Instruments). Neuron experiments used an intracellular solution consisting of (in mM): 114.5 Cs-gluconate, 17.5 CsCl, 10 HEPES, .2 EGTA, 4 Mg-ATP, .4 Na-GTP, 7 Phosphocreatine-Na (pH to 7.23 w/CsOH). The intracellular solution used in HEK experiments contained (in mM): 140 CsCl, 5 BAPTA, 15 HEPES, and 4 Mg-ATP (pH to 7.3 w/ CsOH). To achieve fast solution exchange (10%-90% risetime = ~10 ms) for both neuron and HEK cell desensitization experiments, a gravity perfusion system equipped with computer-controlled Lee OEM solenoid valves (ALA Scientific Instruments VM-4, Farmingdale, NY) was used to apply drugs through an ALA MLF Millimanifold placed next to the patched cell. For low external calcium experiments on both neurons and HEK cells, cells were bathed and drugs were diluted in an extracellular solution (pH to 7.3 w/NaOH, ~300 mOsm) containing (in mM) 135 NaCl, 5.4 KCl, .2 CaCl<sub>2</sub>, 15 HEPES, 15 Glucose. 300 nM TTX was added only when neurons were used. For normal external calcium experiments in neurons, the extracellular solution used contained (in mM): 145 NaCl, 5 KCl, 2 CaCl<sub>2</sub>, 10 HEPES, 10 Glucose, and 300nM TTX. R<sub>a</sub> was continually monitored for all experiments throughout the recordings and cells with R<sub>a</sub> over 50 M $\Omega$  were rejected for analysis. To test deactivation kinetics, GluN1+GluN2A expressing HEK cells were patched and lifted to a 200  $\mu$ m OD theta perfusion tip for fast agonist application using a Burleigh PZ150M piezoelectric driver. Solutions were delivered through the theta tip using two Harvard Apparatus PHD2000 perfusion pumps.

For all culture experiments on desensitization, we accepted only cells that were tested for both conditions (drug on, drug off) and were flanked by equal amplitude recordings as a control. In other words, if an NMDA recording was followed by an NMDA+HCY recording, we required a second NMDA recording to follow with equal amplitude to the first NMDA trace. Because solution application was extremely fast, this assured that any changes noted were due to drug application and not degradation of seal quality due to the pressure of the stream. This control also assured that order of drug application (i.e. HCY first or control first) was not a contributing factor. For most cells, between 2 and 4 traces from each condition were averaged together to yield final traces for analysis.

Experiments on GluN2A, GluN2B, and GluN2D type NMDARs were always carried out on the same day with the same set of solutions. Recordings on cells expressing different subtypes were interleaved so duration after transfection and time-dependent effects on drug potency were ruled out. In figures, horizontal lines above current traces mean "NMDA On" or "Glutamate On" (except Figure 1D, where HCY is used as an agonist). Conditions are listed as agonist + HCY or HCY analog (red) or as agonist alone (black). The onset of HCY (or HCY analog) in each figure is noted with an arrow. For example, "NMDA+HCY" means that HCY was applied for 2 seconds before an NMDA+HCY stream was released at the step of the horizontal line above the current trace. In Figure 9 we show the NMDA + low NMDA trace as blue to emphasize that we are not testing HCY nor an HCY analog.

**2.2.5- Acute Hippocampal Slice Preparation:** Acute hippocampal slices were prepared from young (P10-P17) or older (P43-P58) mice. Mice used were from reporter lines driving the expression of tdTomato under the *Drd1a* or *Drd2* promoter that are phenotypically wild-type. These mice were used to assure patching in a region receiving dopamine / norepinephrine input which could produce HCY.

Young mice were anesthetized with isofluorane and decapitated. The brain was quickly removed and placed into ice-cold carbogenated artificial cerebrospinal fluid (ACSF) containing (in mM): 124 NaCl, 2.5 KCl, 1.2 NaH<sub>2</sub>PO<sub>4</sub>, 24 NaHCO<sub>3</sub>, 5

HEPES, 12.5 Glucose, 2 MgSO<sub>4</sub>, 2 CaCl<sub>2</sub>. Coronal or transverse hippocampal slices (200 μm) were cut in ice-cold ACSF using a Leica vibratome and placed in a chamber containing ACSF at 32° C. 15 minutes after slicing, the chamber was removed from the 32° incubator and allowed to recover at room temperature for 1 hour. For sectioning of older slices, animals were perfused through the heart with a modified ACSF containing (in mM): 93 N-Methyl-D-glucamine, 2.5 KCl, 1.2 NaH<sub>2</sub>PO<sub>4</sub>, 30 NaHCO<sub>3</sub>, 20 HEPES, 25 Glucose, 5 Na-Ascorbate, 2 Thiourea, 3 Na-Pyruvate, 10 MgSO<sub>4</sub>, .5 CaCl<sub>2</sub> adjusted to pH 7.3 with concentrated HCl. The same procedure used for young slice preparation was repeated for older slices except that the modified ACSF was used during cutting and 32° recovery. After 15 minutes of 32° incubation, slices were washed once in ACSF and then incubated in ACSF at room temperature for 1 hr.

**2.2.6 - Slice Electrophysiology and Glutamate Uncaging:** After recovery, slices were placed in a recording chamber and continuously perfused with warmed carbogenated ACSF (~32° C, 2 ml / min). Glass pipettes (5-8 MΩ) were filled with an internal solution containing (in mM): 105 Cs-Gluconate, 10 Na-phosphocreatine, .07 CaCl<sub>2</sub>, 4 EGTA, 10 HEPES, 4 Na-ATP, 1 Na-GTP, 3 MgCl<sub>2</sub>, brought to ~290 mOsm with sucrose and pH 7.3 with CsOH. Neurons in the CA1 region of the hippocampus were patched and held at -70 mV in voltage clamp. The patched neuron was next continuously perfused with Mg-free ACSF for 10 minutes. After Mg<sup>2+</sup> washout, MNI-caged glutamate (1 mM) was perfused onto the cell using an ALA millimanifold application pipette placed next to the cell and uncaged in the presence of 300 nM TTX, 10 μM NBQX, and 20 μM Gabazine to isolate NMDAR currents. Uncaging was accomplished using a Zeiss HBO 100 Arclamp filtered with a DAPI filter and temporally controlled using a UniBlitz shutter system. UV light (~16 mW) was flashed over the entire field of a 60x water immersion objective centered on the patched cell for two seconds to uncage glutamate both in the presence and absence of applied HCY.

**2.2.7 - Current Analysis and Statistics:** Using custom MATLAB software written by ADB, axon .abf files were imported and analyzed. Peak amplitude of each NMDAR current was recorded and the area under each trace was measured by simple integration after zeroing the baseline. Areas under the NMDAR current curves during agonist application are equal to total charge transfer during agonist application in microcoulombs ( $\mu\text{C}$ ).

We use “drug” in this text to mean HCY or HCY analog. “Agonist” means glutamate or NMDA. Peak amplitude and charge transfer were tested for significant differences using paired two-tailed t-tests because both agonist and agonist+drug treatments were always obtained from the same cell. Significance in these tests is indicated using a p-value, which we report for both significant and insignificant results. P-values equal to .05 or less were accepted as significant differences. One-tailed t-tests were used for studies on NMDAR antagonists AP5 and DCKA (5,7-dichlorokynurenic acid) because the actions of these drugs are known. One-tailed tests were also used in other instances when appropriate and are noted in the text. “N” in text and figure legends indicates number of cells recorded for the specified experiment, where each cell was exposed to multiple agonist and agonist+drug conditions.

The following statistics are illustrated in Figure 1E. Charge transfer ratios (CTR) and percentages reported reflect (charge transfer induced by agonist + drug) / (charge transfer induced by the same agonist with no drug). Peak amplitude ratios (PAR) and percentages reported reflect (peak amplitude of current induced by agonist + drug) / (peak amplitude with agonist alone). For example, if on a given cell the charge transfer after glutamate application was  $2 \mu\text{C}$  with a peak amplitude of  $500 \text{ pA}$ , and the charge transfer induced by glutamate with HCY preincubation was  $4 \mu\text{C}$  with a peak of  $400 \text{ pA}$ , the  $\text{CTR} = 4 \mu\text{C} / 2 \mu\text{C} = 2$  (a 100% increase) and the  $\text{PAR} = 400 \text{ pA} / 500 \text{ pA} = .8$  (a 20% decrease). However, HCY effects were complex. Increasing [HCY] altered the peak amplitude of the NMDAR response while simultaneously decreasing desensitization. Therefore we also report a normalized charge transfer ratio that compares charge transfer after peak amplitude of agonist and agonist+drug conditions have been scaled to the same size (see Figure 1E); this

measures effects on desensitization only. Distributions of these statistics from each cell tested were compiled. CTR, PAR, and normalized CTRs are not normally distributed, so averages reported for these statistics are median values. These ratios were compared across experiments (i.e. when comparing GluN2A vs. GluN2B charge transfer ratios) using Wilcoxon rank sum tests (a.k.a. Mann-Whitney-Wilcoxon tests) and p-values are reported. Plots display the median as a circle and the range between the 25<sup>th</sup> and 75<sup>th</sup> quartiles as a line behind the circle. If no line is present, the interquartile range is tightly contained within the bounds of the circle indicating the median. In addition, Figures 2.1, 2.8, and 2.12 show upper and lower thin lines representing the maximum and minimum values found. The thicker bars in these graphs represent the 25<sup>th</sup> to 75<sup>th</sup> quartile range.

## **2.3 - Results:**

***2.3.1 - HCY reduces NMDAR desensitization and peak amplitude in cultured neurons:*** We first determined the effects of HCY on NMDAR current dynamics at high temporal resolution using whole-cell voltage clamp and fast agonist application with the ALA-VM4 perfusion system. Two-second application of NMDA (100  $\mu$ M) to cultured cortical neurons in 200 nM glycine induced macroscopic NMDAR currents that strongly desensitized (Figure 1A). If HCY (1 mM) was applied to the same neuron two seconds prior to NMDA, desensitization was reduced, significantly enhancing total charge transfer by an average of 46% (N =6,  $p \leq .01$ ). HCY application also attenuated peak NMDAR current amplitude by 14% (N=6,  $p \leq .01$ ) (Figure 2.1A,B).

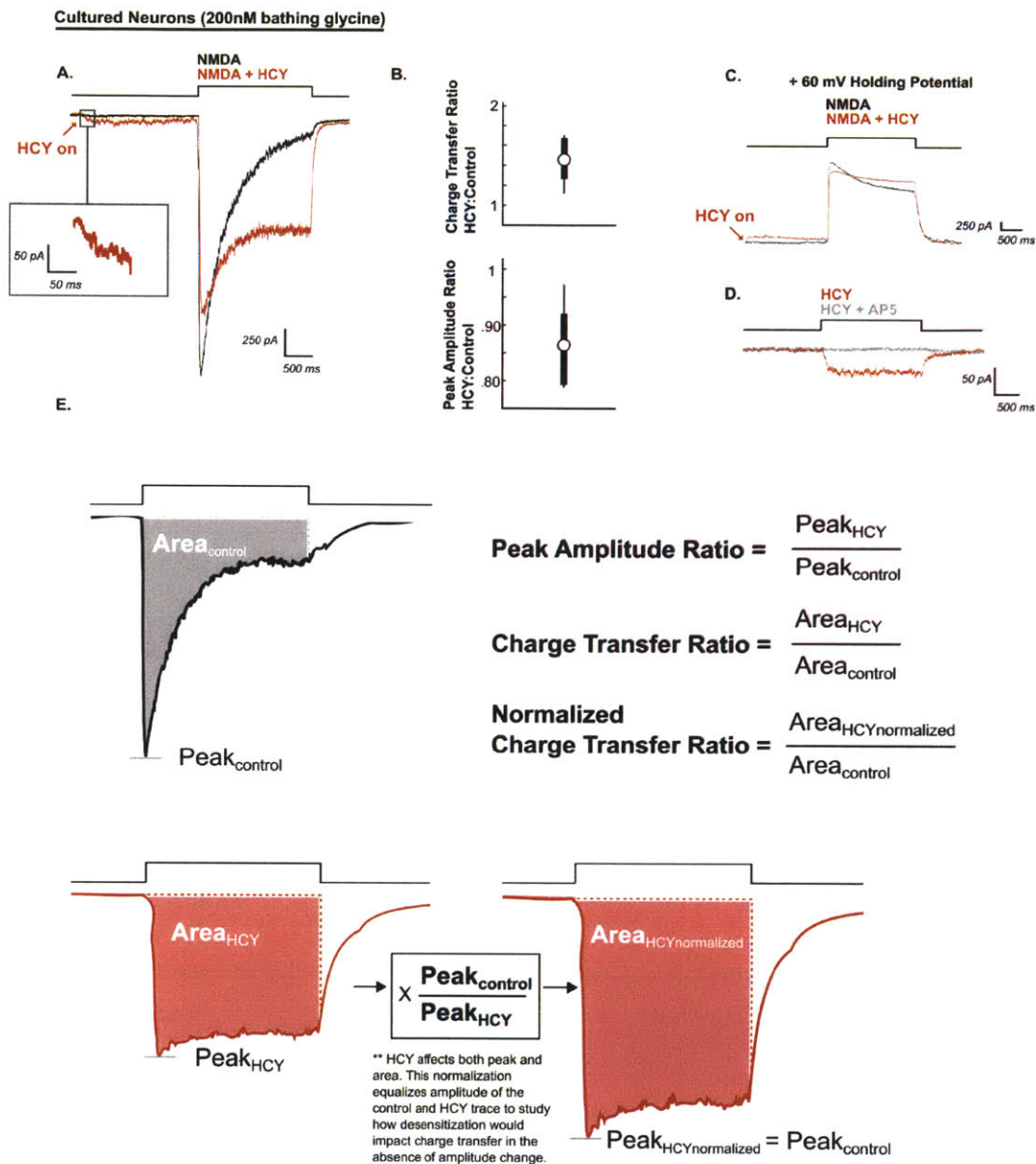


**FIGURE 2.1 - HCY induces a small depolarization in neurons and reduces desensitization of NMDAR currents.** A) Neurons voltage clamped at -60 mV were maintained in a 2 mM  $\text{Ca}^{2+}$  solution containing 200 nM glycine. NMDA (100  $\mu\text{M}$ ) applied for two seconds produced a strongly desensitizing NMDAR response. If HCY (1 mM = 500  $\mu\text{M}$  L-HCY isomer) was applied two seconds before NMDA (red arrow), it induced a low-amplitude current on its own. When NMDA + HCY was subsequently perfused onto the cell, desensitization was reduced, enhancing total charge transfer. The peak amplitude of the NMDAR response was also reduced. B) Box plot showing the distribution of charge transfer ratios and peak amplitude ratios for all neurons tested (N = 6) in 200 nM glycine, 2 mM  $\text{Ca}^{2+}$  bathing solution. C) When held at +60 mV, neurons still showed HCY-dependent desensitization reduction and peak amplitude reduction (N = 4). D) The small initial HCY-induced current was blockable with the NMDAR glutamate site antagonist AP5 (50  $\mu\text{M}$ ), (N = 4). E) Calculations of terms used throughout the text. Note: In this and subsequent figures, arrows indicate HCY onset, and red traces the presence of HCY (or HCY analog) before and during agonist application. “N” is the number of cells tested.

Importantly, HCY also induced a previously observed small current on its own (see arrow and box, Figure 2.1A, Lipton et al. 1997). Like NMDA currents, this HCY induced current reversed at positive holding potentials (Figure 1C, arrow) and was blocked with AP5 (50  $\mu$ M) a competitive antagonist at the NMDAR glutamate site (avg. 133 pA HCY, 3 pA HCY + AP5,  $p \leq .05$ ,  $N = 4$ , Figure 1D). This indicates that HCY is a weak agonist at the NMDAR glutamate site.

**2.3.2 - HCY effects are dose dependent and are occluded by saturating glycine:** As seen in Figure 2.1A, residual NMDAR desensitization remained even in the presence of HCY. There are at least three forms of NMDAR desensitization, one of which is caused by calcium flux into the cell (Zilberter et al. 1991; Legendre et al. 1993; Krupp et al. 1996; Ehlers et al. 1996; Tong et al. 1995). HCY reduced desensitization when neurons were held at +60 mV (Figure 1C) and in minimal calcium (0.2 mM, Figure 2.2) or zero extracellular calcium solutions. This suggests that HCY does not affect calcium-dependent desensitization resulting from calcium flux into the neuron.

Calcium inactivation of NMDARs can mask desensitization effects when recording whole-cell currents (Mayer et al. 1989). We therefore performed a [HCY] curve in minimal calcium (0.2 mM  $\text{Ca}^{2+}$ ) to study HCY desensitization effects in detail. NMDAR desensitization during 2 seconds of NMDA application in 200 nM glycine was reduced by 100  $\mu$ M ( $N=7$ ), 250  $\mu$ M ( $N=5$ ), and 1 mM HCY ( $N=10$ ) (Figure 2.2A), resulting in significant charge transfer enhancement at all concentrations tested ( $p \leq .001$  for all [HCY], Figure 2.2B). However, charge transfer enhancement through NMDARs was nonlinear with [HCY] because as HCY *enhances* charge transfer due to dose-dependent reduction of NMDAR desensitization, it simultaneously *reduces* charge transfer due to dose-dependent reduction of peak amplitude. Peak amplitude (Figure 2.2C) was not significantly reduced at low 100  $\mu$ M HCY ( $p = .11$ ), but showed a strong 22% reduction at 1 mM HCY ( $p \leq .001$ ).

Cultured Neurons (200 nM bathing glycine)

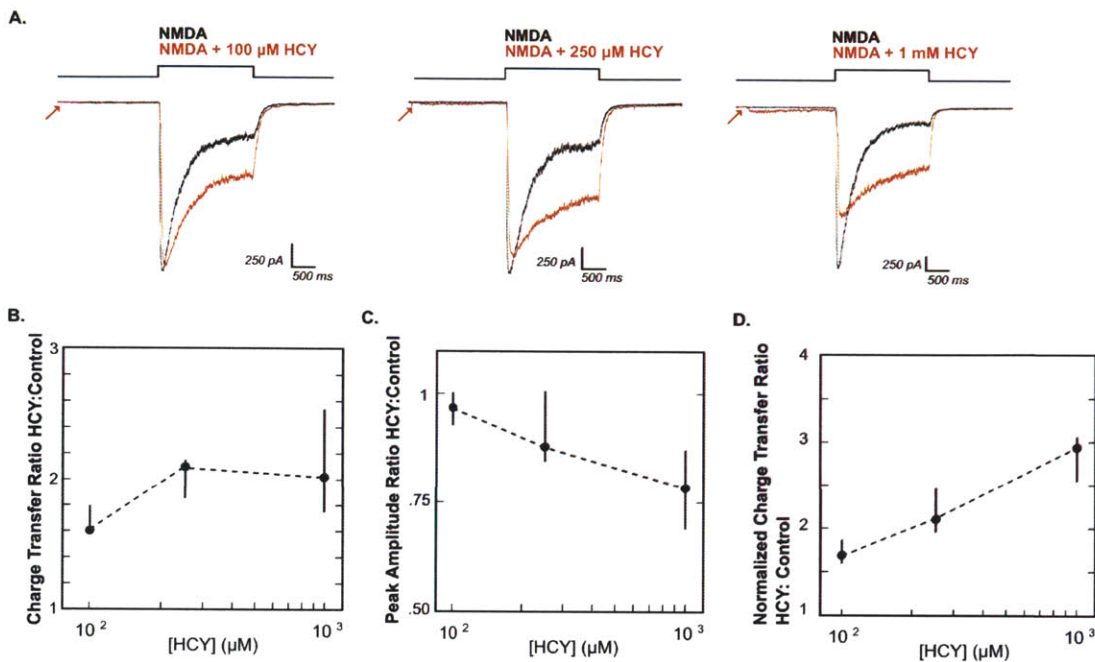


**FIGURE 2.2 - HCY effects on NMDAR current amplitude and desensitization are dose dependent.** A) Voltage clamped neurons were maintained in 200 nM glycine with low extracellular calcium (0.2 mM) to prevent masking of HCY effects by calcium dependent NMDAR desensitization. NMDA (100 μM) was applied for two seconds either with HCY or without HCY. Increasing HCY concentrations decreased peak NMDAR current amplitude (A,C) and reduced desensitization (A,D) dose dependently (i.e. HCY increased normalized charge transfer: see methods and Figure 1E). Notice that HCY still strongly reduced desensitization at one tenth of its maximal concentration (100 μM = 50 μM L-HCY isomer). There was no significant effect on amplitude at 100 μM but a significant amplitude reduction at 1 mM HCY. This resulted in a non-monotonic increase in charge transfer (B) because as desensitization reduction enhanced charge transfer, peak amplitude reduction decreased charge transfer (for [HCY] = 100 μM, 250 μM, 1 mM, N = 7,5,10).

Normalized charge transfer ratios isolate desensitization effects from changes in amplitude by scaling peak amplitudes of agonist and agonist+drug conditions to the same size (Figure 1E). This statistic therefore captures changes in charge transfer due only to altered desensitization. Increasing concentrations of HCY dose-dependently enhanced normalized charge transfer (i.e. decreased desensitization) by 69% (100 μM), 111% (250 μM), and 193% (1 mM) ( $p \leq .005$  for all [HCY], Figure 2.2D).



To determine if these dose-dependent HCY effects reflected a reduction in glycine-dependent desensitization, we increased extracellular glycine (GLY) in the bathing solution from 200 nM to 1  $\mu$ M or 10  $\mu$ M. At 1  $\mu$ M [GLY], 1 mM HCY showed a milder but significant enhancement of charge transfer (avg. 21% increase, N = 5,  $p \leq .05$ , Figure 2.3 A,B). Increasing [GLY] to saturating levels (10  $\mu$ M, Priestley et al. 1995) eliminated the HCY effect on charge transfer (2% avg. enhancement, N = 4,  $p = .16$ , Figure 2.3 A,B). These data indicate that HCY specifically reduces glycine-dependent NMDAR desensitization (Figure 3). Furthermore, at both moderate (1  $\mu$ M) and saturating (10  $\mu$ M) glycine levels, the HCY reduction of peak NMDAR current amplitude also disappeared (Figure 3C;  $p = .13$  for 1  $\mu$ M,  $p = .55$  for 10  $\mu$ M), suggesting that both of HCY's effects on NMDAR currents are fully occluded by saturating glycine. This is consistent with the result from Lipton et al. (1997) where HCY decreased calcium flux induced by brief NMDA application in low glycine, but not in saturating glycine. In addition, even when the glycine site is fully occupied, HCY continues to activate NMDARs on its own (Figure 2.3A, arrows), indicating that the glycine-dependent effects of HCY are separate from a weak agonist role of HCY at the glutamate site.

**2.3.3 - HCY reduces desensitization of all NMDAR subtypes, with effects on peak amplitude that are GluN2 subunit dependent:** Most NMDARs in the brain are a tetramer of two GluN1 subunits and two GluN2 subunits (GluN2A-2D). GluN1 subunits bind glycine and GluN2 subunits bind glutamate or NMDA. However, each GluN2 subunit confers different desensitization kinetics (Vicini et al. 1998) and a different glycine affinity to the receptor (Priestley et al. 1995; Ikeda et al. 1992). NMDARs with two GluN2A subunits have the lowest reported glycine affinity (saturated at 10  $\mu$ M [GLY]), NMDARs with two GluN2B subunits show an intermediate affinity (saturated at 3  $\mu$ M [GLY]), and NMDARs with two GluN2D subunits have the highest glycine affinity (saturated at 1  $\mu$ M [GLY]) (Priestley et al. 1995; Ikeda et al. 1992). Because cultured neuron results indicated that HCY effects were occluded by saturating extracellular glycine, we hypothesized that HCY could differentially impact the various NMDAR subtypes. We therefore transfected HEK

cells with constructs expressing GluN1 and one of the three GluN2 subtypes found in cortical neurons (GluN2A, GluN2B, GluN2D; Baron et al. 2010).

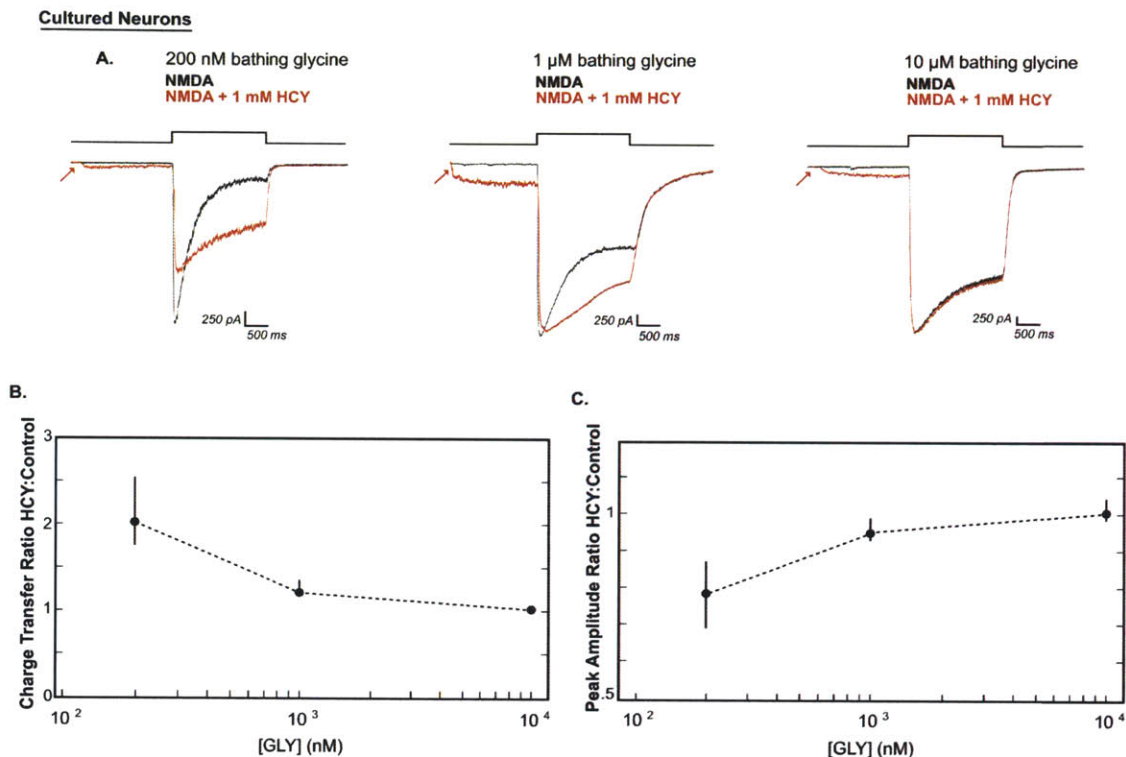


**FIGURE 2.3 - Increasing bathing glycine concentrations occlude HCY's desensitization effects.** A) Neurons were stimulated with 100  $\mu$ M NMDA with or without HCY (1 mM = 500  $\mu$ M L-HCY isomer). As extracellular glycine was raised, desensitization in the black control traces was reduced. HCY caused a modest enhancement of charge transfer at moderate (1  $\mu$ M) glycine levels and a non-significant reduction of peak amplitude. HCY no longer affected the amplitude of NMDAR responses (0% reduction) and did not provide additional enhancement of charge transfer when glycine was at a saturating 10  $\mu$ M (N=5 for 1  $\mu$ M glycine, N=4 for 10  $\mu$ M glycine). B,C) Charge transfer ratios and peak amplitude ratios plotted against extracellular glycine concentration shows that HCY lost its ability to modulate NMDA currents as glycine was raised (i.e. peak amplitude ratios and charge transfer ratios approach 1 at high [GLY]). These data suggest a common mode of action for glycine and HCY. (for [GLY] = 200 nM, 1  $\mu$ M, 10  $\mu$ M, N = 10, 5, 4

In 200 nM bathing glycine, 1 mM HCY significantly enhanced charge transfer by glutamate (100  $\mu$ M) for each NMDAR subtype tested (375% enhancement for GluN2A, N = 17,  $p \leq .00001$ ; 68% enhancement for GluN2B, N = 17,  $p \leq .001$ ; 38% enhancement for GluN2D, N = 8,  $p \leq .01$ ; Figure 2.4A,B). Charge transfer ratios were significantly more enhanced through GluN2A type receptors than GluN2B and GluN2D ( $p \leq .0001$  for GluN2A vs. GluN2B and GluN2A vs. GluN2D, Wilcoxon rank

sum test on charge transfer ratios). This was due to the large increase in peak amplitude caused by HCY on GluN2A containing receptors (Figure 2.4A,C). The average GluN2A peak amplitude increase was 59% (N = 17,  $p \leq .0001$ ), while GluN2B showed the same peak amplitude decrease by HCY that we observed in neurons (31% reduction in peak amplitude, N = 17,  $p \leq .000001$ ). GluN2D amplitude remained unchanged (peak amplitude ratio = 1.03, N = 8,  $p = .31$ ). We also tested lower concentrations of HCY (100  $\mu\text{M}$  and 250  $\mu\text{M}$ ). Both the charge transfer enhancement and peak amplitude changes were dose dependent, with GluN2A peak amplitude increasing as [HCY] was raised and GluN2B peak amplitude decreasing as [HCY] was raised (Figure 2.4B,C). Critically, charge transfer and normalized charge transfer were enhanced for every cell tested for all three GluN2 subtypes at 100  $\mu\text{M}$  ( $p \leq .001$ , N = 15) and 250  $\mu\text{M}$  HCY ( $p \leq .001$ , N = 13) (Figure 2.4B,D), indicating that relatively low doses of HCY could reduce the desensitization of diheteromeric GluN2A, GluN2B, and GluN2D NMDARs in the brain.

When bathing glycine concentrations were raised from 200 nM to 1  $\mu\text{M}$  (Figure 2.5), HEK cell recordings resembled neurons in that HCY lost its ability to reduce GluN2B peak amplitude (1 mM HCY; avg. peak amp ratio = 1.02,  $p = .42$ , N=5 for GluN2B) and retained statistically insignificant amplitude effects on GluN2A (avg. peak amp ratio = 1.28,  $p = .11$ , N=4). Moreover, although all GluN2A and GluN2B expressing HEK cells tested showed charge transfer enhancement by HCY at this higher [GLY] (GluN2A avg. 142% charge transfer ratio, N = 4,  $p \leq .05$ ; GluN2B avg. 21% charge transfer ratio, N=5,  $p \leq .05$ ; Figure 5), GluN2D was fully saturated at 1  $\mu\text{M}$  [GLY] and did not desensitize in control conditions. Therefore, reduction of desensitization by HCY was fully occluded by 1  $\mu\text{M}$  glycine for only GluN2D (avg. charge transfer ratio = 1.00, N=5,  $p = .51$ ), although as expected the small HCY-dependent depolarization via the glutamate site remained. The HEK cell system also allowed us to lift patched cells to a theta perfusion pipette to study HCY's effect on deactivation kinetics independently of desensitized receptor states. Synaptic-like 1 ms pulses of 1 mM glutamate in 1  $\mu\text{M}$  bathing glycine were delivered to lifted GluN1+GluN2A HEK cells using a piezo-electric driver to briefly bump the glutamate stream onto the cell. Using this system, desensitization and deactivation of NMDAR

currents could be studied on the same cell. 1 mM HCY did not significantly alter weighted decay time NMDAR currents after a 1 ms pulse of glutamate (avg. 76 ms control, avg. 59 ms HCY,  $p = .19$ , Figure 5B top). However, on these same cells, bathing 1 mM HCY significantly reduced desensitization during 1.5 second exposure to the glutamate stream ( $p \leq .05$ ,  $N = 4$ , Figure 5B bottom). This indicates that HCY reduces desensitization by affecting transitions of the NMDAR to or from desensitized states without prolonging deactivation of the channel.

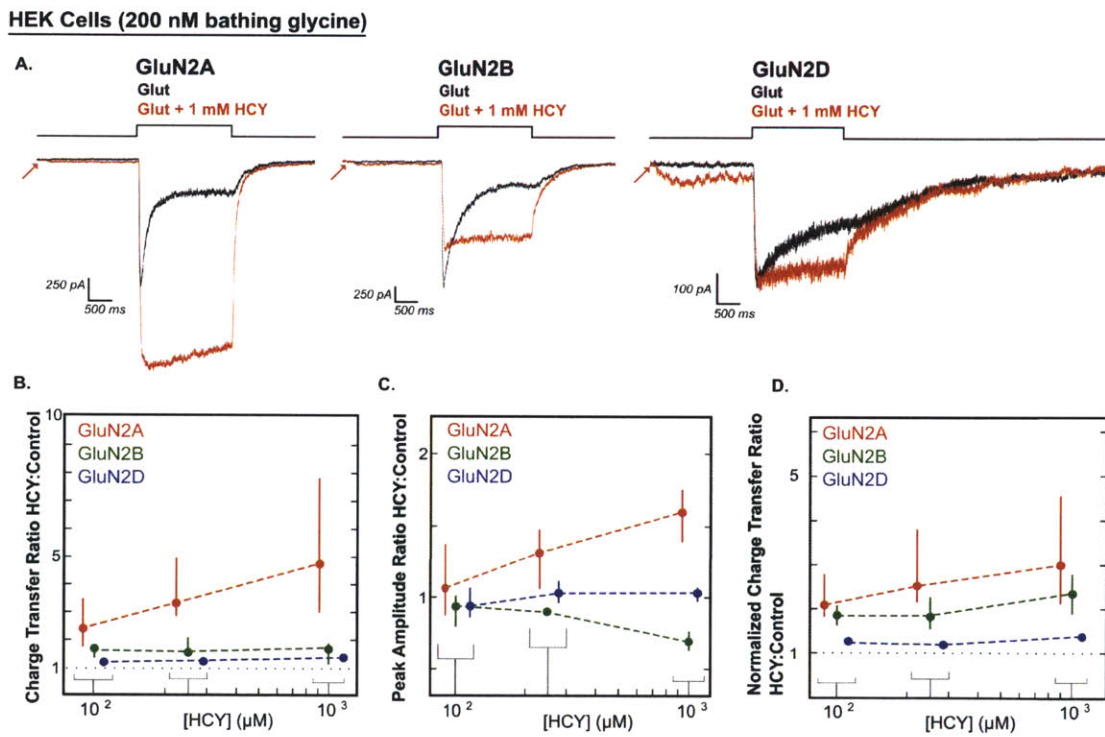


**FIGURE 2.4 - HCY effect on NMDAR currents depends on GluN2 subunit composition.** HCY reduced desensitization of all three NMDAR subtypes tested in HEK cells in a dose dependent manner (A,D). GluN2A showed the greatest enhancement in charge transfer ratio with HCY present, followed by GluN2B and GluN2D (B). The amplitude of GluN2A responses to glutamate was *enhanced* by the presence of HCY (A,C), again in a dose dependent manner. GluN2B, similar to NMDARs in young cultured neurons, showed dose dependent amplitude reduction by HCY (A,C). GluN2D showed no change in peak amplitude at any HCY concentration. [N for each [HCY] (100  $\mu\text{M}$  = 50  $\mu\text{M}$  L-HCY isomer, 250  $\mu\text{M}$  = 125  $\mu\text{M}$  L-HCY isomer, 1mM = 500  $\mu\text{M}$  L-HCY isomer): GluN2A N = 4, 5, 17; GluN2B N = 5, 5, 17 ; GluN2D N = 6, 3, 8].

HEK Cells (moderate 1  $\mu$ M bathing glycine)

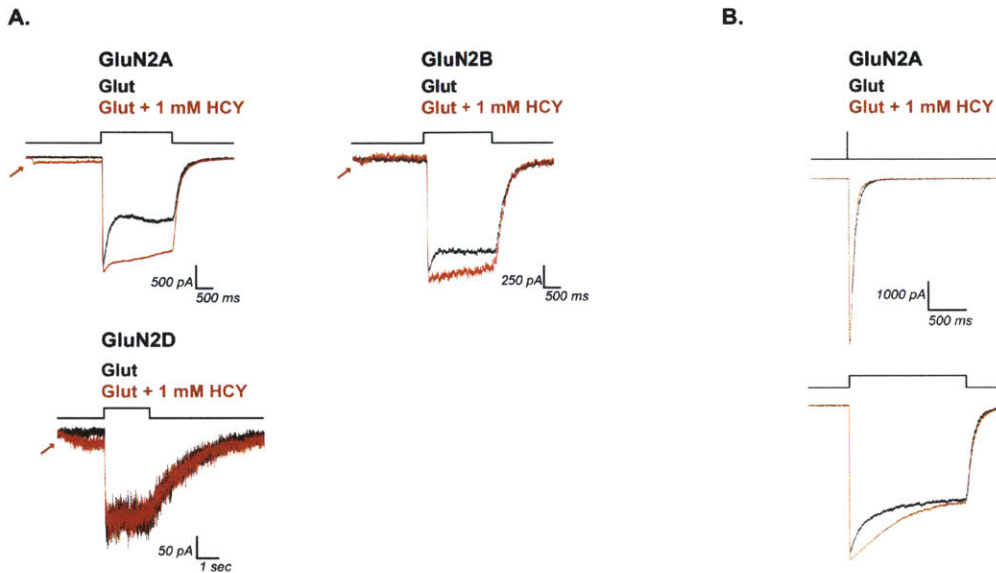


**FIGURE 2.5 - HCY reduces desensitization of GluN2A and GluN2B, but not GluN2D NMDAR currents, at 1  $\mu$ M glycine without affecting NMDAR decay kinetics.** A) Raising the ambient glycine concentration from 200 nM to 1  $\mu$ M prevented HCY from modulating peak amplitude of GluN2A and GluN2B mediated currents in HEK cells (N = 4, 5). However, HCY continued to enhance charge transfer through GluN2A and GluN2B containing receptors in 1  $\mu$ M glycine. GluN2D (N = 5) is completely saturated at 1  $\mu$ M glycine. B) Although HCY was effective in reducing desensitization in GluN2A HEK cells, it did not alter deactivation kinetics after 1 ms pulses of glutamate, indicating an effect on desensitized states only.

**2.3.4 - HCY effects in DIV30 cultured neurons:** That the charge transfer enhancement and peak amplitude suppression by HCY were similar in GluN2B type NMDARs and young cultured neurons was not unexpected. Cortical neuron cultures are highly enriched for GluN2B at DIV7 (~20:1 GluN2B:GluN2A), while GluN2A begins to express strongly at DIV21 (~3:1 GluN2B:GluN2A, Zhong et al. 1994). GluN2A is expressed at a ~10:1 ratio with respect to GluN2D in young cultured neurons, indicating that GluN2A and GluN2B are the main subunits at this stage and should dictate whole cell NMDAR kinetics (GluN2C is not expressed at any age tested in cortical neurons; Baron et al. 2010). We therefore predicted that as GluN2A expression increases and balances GluN2B with age, the effects of HCY on

neuron NMDAR currents should look less like GluN2B-expressing HEK cells and begin to resemble a hybrid between GluN2A and GluN2B responses. Specifically, because GluN2B peak amplitude is decreased by HCY while GluN2A is enhanced by HCY in HEK cells (Figure 2.4C), a whole cell response in older neurons where GluN2B to GluN2A ratios are ~1:1 should show little or no amplitude change. Our recordings in old (DIV30) cortical neuron cultures supported this prediction. 1 mM HCY did not significantly reduce peak amplitude in DIV30 cultures (avg 2% peak enhancement, N=4,  $p = .96$ , Figure 2.6). Meanwhile, every cell previously tested in our DIV7-8 culture experiments showed a peak amplitude reduction by 1 mM HCY (N = 10, avg. reduction of 22%,  $p \leq .001$  Figure 2.2A,C). Consequently, the average charge transfer ratio per cell was 3.33 in old cultures (N = 4,  $p \leq .05$ ) versus 2.02 in young cultures, consistent with the addition of the GluN2A subunit, which showed strongly enhanced charge transfer in response to HCY in HEK cells (Figure 2.4A,B).

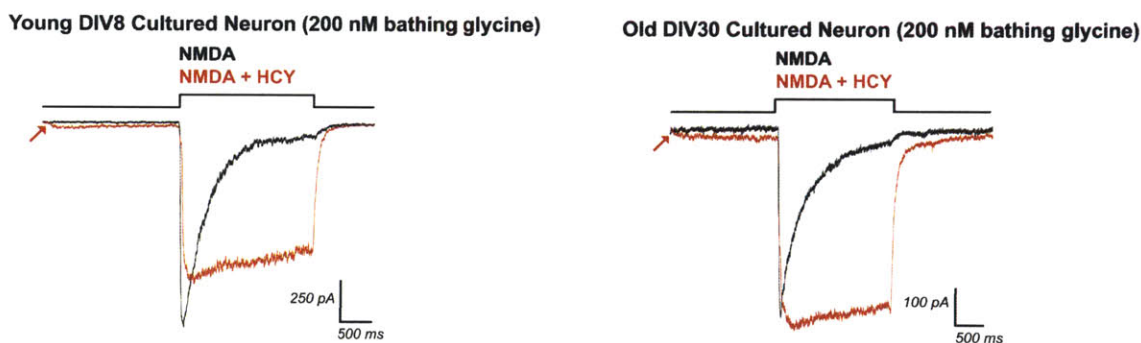


**FIGURE 2.6 - HCY does not reduce peak amplitude in old neuronal cultures.** Neurons recorded at DIV7 and DIV8 are highly enriched for GluN2B and showed strong peak amplitude reduction by HCY (upper trace, DIV8 1mM HCY = 500  $\mu$ M L-HCY, N = 10). This mirrored the HCY effect on GluN2B expressing HEK cells. However, HCY produced no significant change in peak amplitude in older cultured neurons (lower trace, DIV30, 1mM HCY = 500  $\mu$ M L-HCY, N = 4), reflecting the addition of GluN2A subunits as the cells mature.

**2.3.5- A free sulphur group is critical for HCY's effects on NMDARs:** We next tested whether other HCY-resembling chemicals could mimic HCY effects on NMDAR current amplitude and desensitization. We used both 2 and 8 second preincubation of these chemicals in case their binding dynamics differed from HCY. All experiments were performed in 200 nM [GLY]. Homocysteine, a dimer of

homocysteine linked by disulphide bonds, did not enhance charge transfer by glutamate through NMDARs in any transfected HEK cells tested (N=4 [2 GluN2A, 2 GluN2B],  $p = .97$ , one tailed paired t-test for enhancement, data not shown). Homocysteine thiolactone, a cyclized form of HCY with its sulphur bound in a thiol ring, also showed insignificant charge transfer enhancement (N = 5 [3 GluN2A, 2 GluN2B],  $p = .07$ , Figure 2.7A) without affecting current amplitude (avg. peak amp ratio = .99 for GluN2A, .93 for GluN2B). We subsequently used the procedure of Poddar et al. (2009, communicated by Dr. Donald Jacobsen, Lerner Research Institute, Cleveland, OH) to open the thiol ring of L-homocysteine thiolactone. This method liberates the free sulphur-group containing molecule L-homocysteine (L-HCY – final concentration dependent on efficacy of ring removal reaction, max possible = 2 mM), the isomer of HCY that is present in the brain. Both the amplitude and desensitization effects we observed with D,L HCY (Figure 4) were qualitatively identical to effects found with the L-HCY isomer (Figure 2.7B). GluN2A containing receptors showed a significant increase in charge transfer (avg. 178% increase, N = 3,  $p \leq .05$ ) and peak amplitude (24% increase, N = 3,  $p \leq .05$ ) when L-HCY was present. L-HCY significantly reduced peak amplitude of GluN2B receptors (avg. 23% reduction, N=3,  $p \leq .05$ ), mirroring the amplitude reduction in neurons and GluN2B expressing HEK cells by D,L HCY, while reducing desensitization in all cells tested (avg. normalized charge transfer enhancement of 40%).

As mentioned earlier, the *in vivo* isomer L-HCY is present at a 1:1 ratio with the D-HCY isomer, which is not present in the brain, in commercially available D,L-HCY (see Methods). Considering that L-HCY replicated D,L HCY's effects, it is likely that L-HCY is the only active isomer in our studies using the racemic D,L HCY. Therefore, effective doses of HCY are likely half of what is reported in this paper (i.e. 100  $\mu\text{M}$  D,L HCY = 50  $\mu\text{M}$  L-HCY). D-homocysteine thiolactone was not available for purchase.

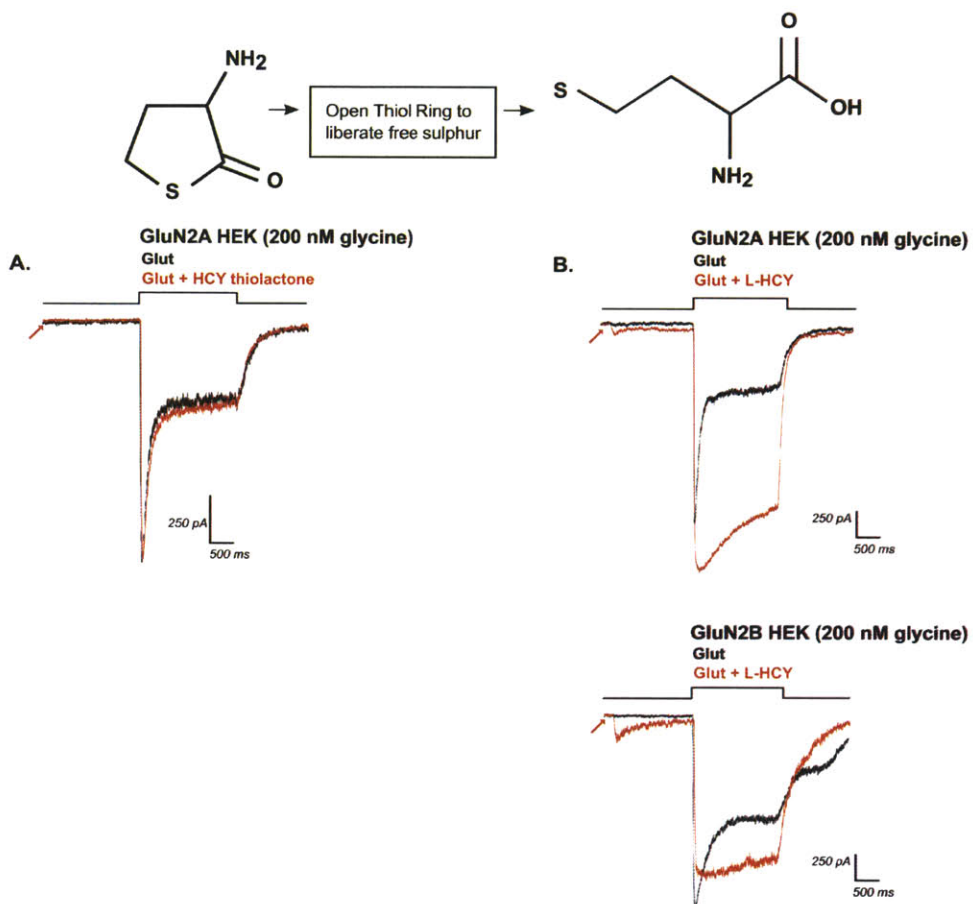


**FIGURE 2.7 - Opening the thiol ring of HCY-thiolactone creates L-HCY, which reproduces D,L HCY effects.** Top left: structure of HCY-thiolactone, with its sulphur group bound in a thiol ring. A) Application of HCY-thiolactone (1 mM) did not significantly enhance charge transfer through NMDARs by glutamate (N = 5). B) Opening the thiol ring of HCY-thiolactone creates L-HCY (see top right for structure). L-HCY showed effects that were qualitatively identical to D,L HCY. L-HCY activated a small current on its own (see arrows), reduced desensitization, and enhanced peak amplitude of currents in GluN2A-transfected HEK cells (N = 3) while reducing peak amplitude and reducing desensitization of currents in GluN2B-transfected HEK cells (N = 3).

L-cysteine (1 mM) was the last HCY analog tested. The name “homocysteine” is derived from “homolog of cysteine”. Unlike homocystine dimers, which are disulphide bonded, and homocysteine thiolactone, which has its sulphur bound in a thiol ring, cysteine possesses a free sulphur group. L-cysteine mimicked the desensitization related effects of HCY. In cultured neurons, it significantly enhanced NMDAR charge transfer (N = 5,  $p \leq .01$ , avg. 109% increase, Figure 2.8A,B). However, L-cysteine did not cause significant changes in peak amplitude (avg peak amp ratio = 1.11, N = 5,  $p = .30$ ) at the young age where GluN2B:GluN2A ratios are ~8:1 (DIV9). These results paralleled L-cysteine’s effects on GluN2A and GluN2B



expressing HEK cells (Figure 2.8). L-cysteine applied with glutamate to GluN2A-expressing HEK cells greatly enhanced peak amplitude by an average of 73% ( $p \leq .001$ ,  $N = 7$ ) and strongly enhanced charge transfer by an average of 223% ( $N = 7$ ,  $p \leq .005$ ). L-cysteine also increased charge transfer through GluN2B type receptors ( $N = 8$ ,  $p \leq .005$ , 29% increase). As with HCY, L-cysteine's charge transfer enhancing effects on GluN2B expressing HEK cells were significantly less than on GluN2A expressing HEK cells ( $p \leq .0005$ , Wilcoxon rank sum test on GluN2B vs. GluN2A charge transfer ratios). Peak amplitude reduction of GluN2B NMDAR currents with L-cysteine was more subtle than HCY's effects. Though L-cysteine did consistently reduce peak amplitude of GluN2B currents (avg 9% reduction,  $N = 8$ ,  $p \leq .05$ ), the average reduction of only 9% was significantly less than the peak reduction of 31% produced by HCY ( $p \leq .0005$  Wilcoxon rank sum test, avg. 31% vs. 9% reduction). This likely explains why DIV9 neurons, which have high GluN2B:GluN2A ratios, did not show significant amplitude reduction in response to L-cysteine. The reduction of NMDAR desensitization by cysteine that spares GluN2B NMDARs from strong peak depression may explain why all concentrations of cysteine, unlike HCY, enhance LTP in hippocampal slices (Christie et al. 2009).

Finally, because HCY is a weak NMDAR glutamate-site agonist (Figure 2.1D and see Lipton et al. 1997), we tested the hypothesis that low-dose NMDA itself might recapitulate the effects of HCY on charge transfer and peak amplitude. We found that 2  $\mu\text{M}$  NMDA induced small currents that were similar in amplitude to currents evoked by HCY alone (Figure 2.9). However, 2  $\mu\text{M}$  NMDA application two seconds before high-dose (100  $\mu\text{M}$ ) NMDA application never enhanced charge transfer (avg. charge transfer ratio = .98,  $N=4$ ,  $p = .99$  for enhancement by 2  $\mu\text{M}$  NMDA). This experiment provided an additional indication that the glutamate-site related and glycine-site related effects of HCY are independent of each other.

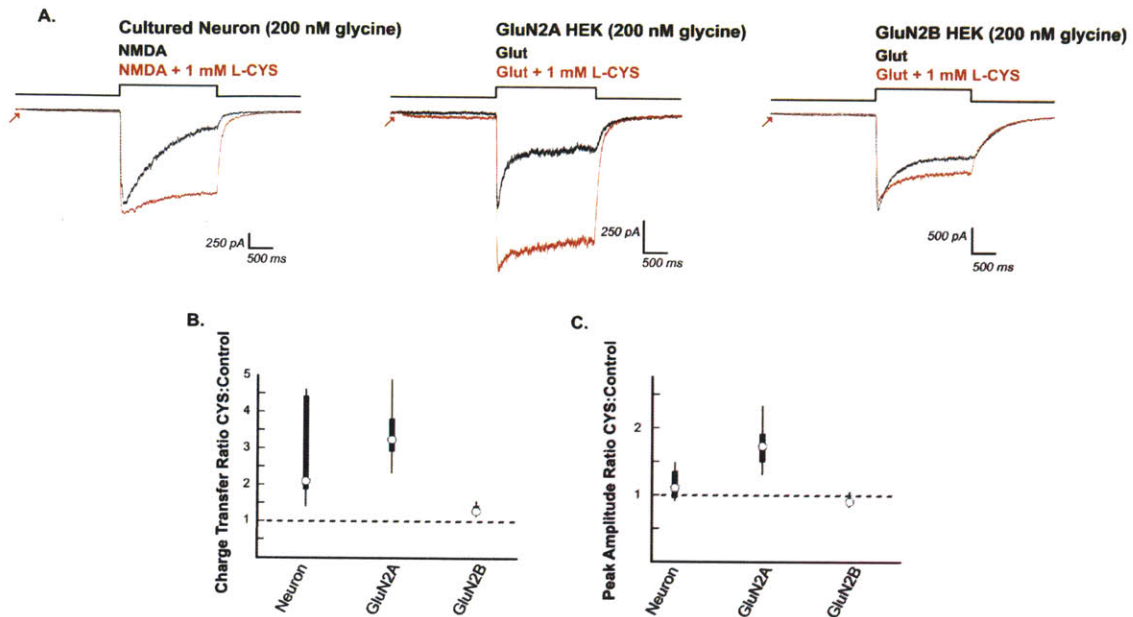


**FIGURE 2.8 - Cysteine enhances NMDAR charge transfer through neurons and GluN2A and GluN2B expressing HEK cells.** A) 2-second preincubation of neurons with L-cysteine (1 mM) mimicked HCY in reducing NMDAR desensitization, which significantly enhanced charge transfer (N=5, DIV9, 2 mM  $Ca^{2+}$ , 200 nM [GLY] in bath). However, there was no significant effect of L-cysteine on peak amplitude in these neurons. L-cysteine (1 mM) enhanced charge transfer in HEK cells transfected with GluN2A (N = 7) and GluN2B (N = 8) containing NMDARs. Peak amplitudes of GluN2A responses were significantly enhanced while peak amplitudes of GluN2B NMDAR currents were only slightly reduced. B,C) Boxplots show that the neuron response is a hybrid between GluN2A and GluN2B expressing HEK cells.

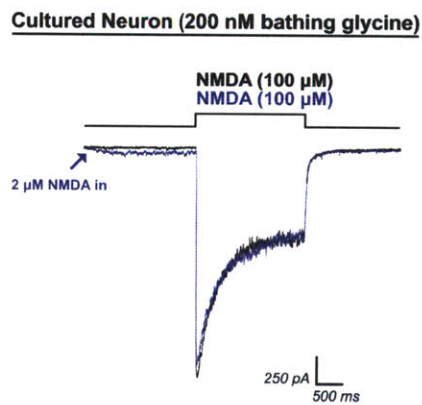


**FIGURE 2.9 - Low dose NMDA application does not recapitulate HCY induced reduction of desensitization.** Because HCY was capable of inducing small AP5-blockable currents, we tested the hypothesis that doses of NMDA that induce current amplitudes similar to those produced by HCY could recapitulate HCY's effects on desensitization. Initial application of 2  $\mu$ M NMDA to neurons (blue trace, 200 nM glycine) induced an NMDAR current similar in amplitude to HCY application (compare to Figure 1). However, when 100  $\mu$ M NMDA was then applied, desensitization was not reduced (N = 4) and charge transfer was never enhanced.

**2.3.6- Is HCY acting at the NMDAR glycine site?:** 2  $\mu$ M NMDA was not effective at reducing desensitization (Figure 2.9); instead, desensitization reduction by HCY resembled and was occluded by saturating glycine (Figure 2.3). This led us to ask if the NMDAR glycine site antagonist dichlorokynurenic acid (DCKA) could prevent HCY from reducing NMDAR desensitization. In control experiments in non-saturating (200 nM) bathing glycine with no HCY, NMDA application was preceded by ten seconds of 1  $\mu$ M DCKA. As expected, DCKA reduced NMDAR current amplitude by an average of 82% (Figure 2.10A2 vs. 2.10A1, N=5 DIV7 neurons,  $p \leq .001$ ) and promoted further glycine-dependent desensitization of the NMDAR response (16% less normalized charge transfer with DCKA present,  $p \leq .05$ , Figure 10A3). We repeated this experiment with 1 mM HCY present in the bath, preincubation (1  $\mu$ M DCKA + 1 mM HCY) and stimulating solutions (1  $\mu$ M DCKA + 1 mM HCY + 100  $\mu$ M NMDA). We hypothesized that if HCY was blocking desensitization independently of the glycine site, then DCKA would have no effect on desensitization in the presence of HCY. However, if HCY was acting at the glycine site, we expected DCKA to have a stronger desensitization enhancing effect in the presence of HCY, as DCKA would be blocking both the effects of HCY *and* glycine on desensitization versus that of glycine alone. The latter was the case, as can be seen by comparing the normalized traces in Figure 2.10A3 to 2.10B3. DCKA promoted even further desensitization of the NMDAR response to NMDA application during HCY exposure (46% reduction of normalized charge transfer, N=4,  $p \leq .05$ ; Wilcoxon rank sum HCY+DCKA vs. DCKA only,  $p \leq .01$ , 46% vs. 16%). Thus, antagonism of the glycine site appears to prevent HCY's desensitization effects. Peak amplitude was also strongly reduced by DCKA in the presence of HCY at an average of 79% per cell. This was not significantly different than trials without HCY [ $p = .90$ , Wilcoxon rank sum test on peak amp ratios with (.21) and without (.18) HCY].

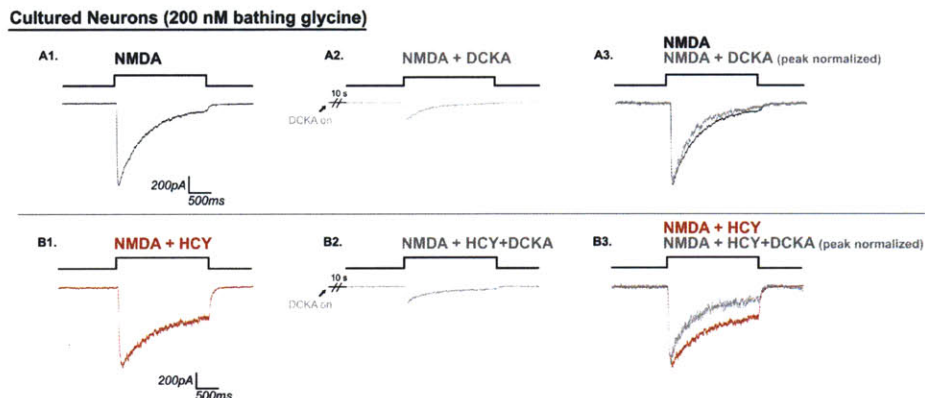


**FIGURE 2.10 - HCY does not rescue effects of partially blocking the glycine site with DCKA.** DCKA (1  $\mu$ M, 10s preincubation) inhibited peak NMDAR current amplitude by  $\sim$ 80% in the presence (B2 vs. B1) and absence (A2 vs. A1) of bathing 1 mM HCY. DCKA largely prevented the ability of HCY to reduce glycine-dependent desensitization. It is as if HCY was not even present when DCKA was preincubated because HCY+NMDA+DCKA currents desensitize similarly to NMDA+DCKA (see normalized superimposed traces A3 and B3), indicating that DCKA blocks both the effects of HCY and glycine on desensitization [N = 5 for DCKA alone, N = 4 for DCKA + HCY].

**2.3.7 - Are NMDARs in the brain susceptible to HCY?:** Because HCY's desensitization effects are occluded at high [GLY] and are blocked by the glycine site antagonist DCKA, NMDAR susceptibility to HCY in real neural circuits relies on whether the NMDAR glycine site is saturated at synapses in the brain. Data-based modeling experiments have presumed that the synaptic glycine concentration in glycine transporter (GlyT) expressing brain areas is below 150 nM (Attwell et al. 1993; Roux and Supplisson 2000), which, by design, resembles the concentration used in our culture experiments. D-serine, a second *in vivo* co-agonist of the NMDAR glycine site, is strongly expressed in the forebrain (Schell et al. 1997; Wolosker 2006 for review), and may be the primary NMDAR co-agonist at some synapses (Papouin et al. 2012). Nonetheless, adding extracellular glycine or d-serine to forebrain slice preparations, or blocking GlyT to allow accumulation of synaptic glycine, enhances evoked NMDAR currents in brain slices (Chen et al. 2003; Bergeron et al. 1998; Martina et al. 2003), indicating that the combination of d-serine and glycine does not fully activate the NMDAR co-agonist site. In fact, in the CA1 region of the hippocampus, GlyT block plus glycine supplementation (10  $\mu$ M) enhances postsynaptic currents by up to 100% (Bergeron et al. 1998). Glycine-dependent

NMDAR desensitization has not been shown in a slice preparation, but the subsaturation of the NMDAR glycine site should allow this phenomenon to occur. We therefore sought to induce NMDAR desensitization with caged glutamate in CA1 to see if it could be reduced by HCY. As proof of principle, uncaging of 1 mM MNI-caged glutamate with a two-second ultraviolet (UV) light flash was extremely effective at inducing glycine-dependent desensitization in cultured hippocampal neurons. This desensitization was strongly reduced by HCY (Figure 11). Because GluN2A subunits express significantly earlier in the hippocampus than in other brain regions (Monyer et al. 1994), we did not expect, and did not observe, amplitude effects in hippocampal neurons. Homocysteic acid (10  $\mu$ M), an NMDAR-active derivative of HCY that is produced by an unknown metabolic pathway in the brain (Benz et al. 2004, Kruger 2001), strongly damped responses to glutamate uncaging and did not resemble HCY in its actions (Figure 2.11); therefore the results below are unlikely to be due to conversion of HCY to homocysteic acid in the intact circuit of the hippocampal slice.

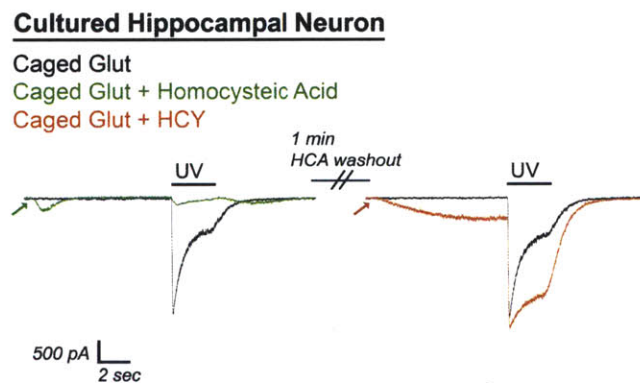


**FIGURE 2.11 - Caged glutamate induces HCY-reducible desensitization in hippocampal cultures.** UV uncaging of 1 mM MNI-caged glutamate strongly desensitized NMDAR currents in DIV11 cultured hippocampal neurons (200 nM bathing glycine). 10  $\mu$ M homocysteic acid (HCA), an active agent at the NMDAR glutamate site, induced NMDAR currents of similar amplitude to 1 mM HCY. However, instead of enhancing charge transfer, HCA greatly damped the response to glutamate uncaging (91% reduction of charge transfer,  $p \leq .05$ ,  $N = 3$ ). Washout of HCA lead to restoration of a desensitizing response to glutamate uncaging. Desensitization was in turn strongly reduced by 1 mM HCY on the same cell (49% enhancement of norm. charge transfer,  $p \leq .05$ ). Therefore the effects of HCY and HCA are separate and it is unlikely that metabolic conversion of HCY to HCA that could occur in hippocampal slices is a source of HCY's charge transfer enhancement.

We next applied 1 mM MNI-caged glutamate (+ 300 nM TTX, 10  $\mu$ M NBQX, 20  $\mu$ M Gabazine to isolate NMDAR currents) to voltage clamped CA1 neurons in acute hippocampal slices (-70 mV, 2 mM  $\text{Ca}^{2+}$ , Mg-Free ACSF) and uncaged using 2 second UV flashes. Most cells tested (6/6 cells from P10-P17 mice, 6/8 from old P43-P58 mice) showed immediate NMDAR desensitization upon glutamate uncaging (Figure 12). To each desensitizing neuron, we subsequently applied caged glutamate + HCY (1 mM D,L HCY) for 30 seconds, then uncaged again for 2 seconds. As can be seen in Figure 2.12A, the initial application of HCY induced a small NMDAR current, as seen in our culture studies, that did not appear if the cell was held at -70 mV in Mg-containing ACSF. Also, as in our culture experiments, HCY reduced glutamate-induced NMDAR desensitization on every cell tested by an average of 10% (N = 12,  $p \leq .0005$ , Figure 2.12C; also  $p \leq .005$ , average 10% increase in charge transfer ratio). If CA1 neurons in P14 or P15 slices were preincubated with glycine (10  $\mu$ M) and the GlyT antagonist NFPS (100 nM), HCY only reduced desensitization by an average of 3%, which was significantly less than with HCY alone (N = 3, Figure 2.12B, 2.12C; Wilcoxon rank sum test on HCY vs. HCY + GLY + NFPS,  $p \leq .01$ , 10% vs. 3% avg normalized charge transfer enhancement). This indicates that neurons in CA1 of the hippocampus do show glycine-dependent desensitization that is reducible by HCY.

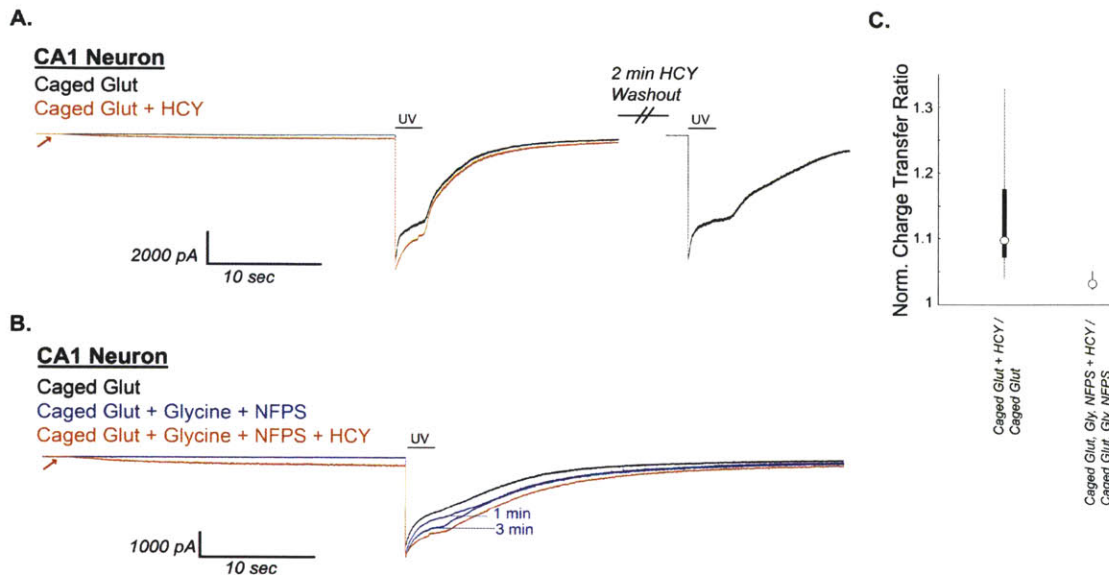


**FIGURE 2.12 - HCY induces a small initial depolarization and reduces glycine-dependent NMDAR desensitization in neurons from acute CA1 slices during uncaging of 1 mM MNI-caged glutamate.** A) CA1 neurons in acute hippocampal slices (N = 6 from P10-P17 mice, N = 6 from P43-P58 mice) were voltage clamped in the presence of 300 nM TTX, 10  $\mu$ M NBQX, and 20  $\mu$ M Gabazine. Under these conditions, Schaffer collateral axon stimulation (200  $\mu$ s) consistently evoked currents at +40 mV but not at -70 mV holding, indicating the isolation of NMDAR currents. After Mg-washout, MNI-caged glutamate (1 mM) was perfused onto the neuron and a two second flash of UV light was used to uncage glutamate. This induced an NMDAR current with pronounced desensitization. If HCY (1 mM D,L HCY = 500  $\mu$ M L-HCY) was washed onto the slice 30s before UV-uncaging, HCY induced a small NMDAR current on its own and reduced desensitization of the NMDAR response to glutamate. When HCY was washed out (washout peak normalized to initial control), sharp desensitization returned. B) When glycine (10  $\mu$ M) and the GlyT antagonist NFPS (100 nM) were washed onto CA1, desensitization was progressively reduced in 3 of 4 cells tested. HCY had a strongly reduced effect in the presence of glycine and NFPS (Note 1  $\mu$ M strychnine is present to avoid glycine receptor activation by exogenously applied glycine). C) Boxplots showing distributions of normalized charge transfer ratios in the presence and absence of glycine and NFPS.

## 2.4 - Discussion:

In this report, we use recordings from cultured neurons (Figure 2.1), transfected HEK cells (Figure 2.4), and acute hippocampal slices (Figure 2.12) to show that HCY, a byproduct of catecholamine breakdown, modulates peak amplitude and reduces desensitization of NMDAR currents. These effects are dose-dependent (Figures 2.2, 2.4), and peak amplitude changes depend on GluN2 subunit composition of the receptor (Figure 2.4). Desensitization reductions are present in all NMDAR subtypes

tested in HEK cells (GluN2A, GluN2B, GluN2D; Figure 2.4) and are occluded by raising ambient glycine (Figures 2.3, 2.5), but not by reducing or eliminating extracellular calcium. This is consistent with a specific HCY reduction of the glycine-dependent component of NMDAR desensitization (Mayer et al. 1989; Vyklicky et al. 1990; Lerma et al. 1990). The relevance of this report to NMDAR currents *in vivo* is therefore contingent upon the NMDAR glycine site being unsaturated in brain tissue. Non-saturation of the NMDAR glycine site *in vivo* has been suggested previously (Martina et al. 2003; Martina et al. 2004; Bergeron et al. 1998; Chen et al. 2003; Wilcox et al. 1996) despite the fact that glycine and the other NMDAR co-agonist d-serine are both present in some brain regions (Schell et al. 1997; Papouin et al. 2012; Rosenberg et al. 2013). Using glutamate uncaging in acute hippocampal slices, we find that the NMDAR responses from CA1 neurons show desensitization upon glutamate uncaging that is significantly reduced by exposure to HCY. Thus, native concentrations of glycine and d-serine are not high enough to abolish HCY desensitization reductions in the relatively intact environment of the slice (Figure 12).

**2.4.1 - Site of HCY's action:** Previous reports concerning HCY effects on NMDARs are complex (Lipton et al. 1997, Christie et al. 2009). Our finding that HCY reduces the peak amplitude of GluN2B currents at low (200 nM) glycine is consistent with previous work showing that in young GluN2B-enriched cortical neurons, HCY reduces calcium flux during brief applications of NMDA in low but not saturating glycine levels (Lipton et al. 1997). We also show that HCY shares some characteristics with the NMDAR co-agonist glycine. First, HCY, like glycine, reduces glycine-dependent desensitization (Figure 2.3). Also like glycine, HCY dose-dependently enhances the peak amplitude of GluN2A-type NMDAR currents in response to glutamate (Figure 2.4, Priestley et al. 1995). Lastly, HCY loses its ability to reduce desensitization if the NMDAR glycine site is blocked by DCKA (Figure 2.10). Future work may reveal why HCY decreases peak amplitude of GluN2B NMDAR responses while continuing to reduce desensitization. It may be that HCY resembles partial glycine site agonists such as L-alanine, which reduce glycine-



dependent NMDAR desensitization but decrease receptor opening probability relative to full agonists (Benveniste et al. 1990; Kussius and Popescu 2009).

Unlike glycine application, the initial response of neurons and transfected HEK cells to HCY alone is a small depolarization (Figures 2.1, 2.4, 2.12 and Lipton et al. 1997). This current is blocked with AP5, a competitive antagonist at the NMDAR glutamate site (Figure 2.1D), and resembles currents induced by 2  $\mu$ M NMDA in amplitude (Figure 2.9), suggesting that in addition to its glycine-like properties, HCY is a low affinity agonist at the glutamate site (Lipton et al. 1997). This may be critical if HCY is elevated during pregnancy or childhood considering that low chronic NMDAR activation that is not correlated with pre-synaptic input causes functional depression and synapse elimination in the developing brain (Debski et al. 1990; Colonnese et al. 2006). We also show in Figure 2.9 that preceding exposure of neurons to low levels of NMDA (2 $\mu$ M) does not enhance 100 $\mu$ M NMDA induced charge transfer, indicating that HCY activation of the glutamate site is not likely to be responsible for its desensitization reducing effects. Therefore, *HCY has two separate and unique effects on NMDARs* that are likely to work in concert: HCY can resemble both glycine and glutamate. This may provide a basis for understanding why low HCY depresses hippocampal LTP while higher HCY enhances LTP, characteristics of glutamate and glycine respectively (Christie et al. 2009).

**2.4.2- HCY and NMDAR Gating:** When bound by glutamate and glycine during synaptic transmission, NMDARs show a slow rising ( $\sim$ 10 ms) and biphasically decaying EPSC. Patch-clamping electrophysiologists have used single channel recordings to describe the complicated nature of NMDAR activation states governing channel opening and closing (Lester and Jahr 1992; Popescu and Auerbach 2003; Banke and Traynelis 2003). These studies reveal complex gating that entails multiple closed, open, and long-lived desensitized states. Indeed, there appears to be a “modal” gating of NMDARs where, in the continual presence of agonists, the receptor will enter three or more activity “modes” defined by the mean time between closed and open states (Popescu and Auerbach 2003; reviewed in Magleby 2004). The comprehensive models in these reports precisely predict the

kinetics of the NMDAR EPSC and provide a basis for understanding the different molecular arrangements that the receptor can adopt. It will be interesting to determine the states or modes HCY modifies and how these could affect glutamatergic transmission in the brain. However, a recent single channel study has shown that NMDAR desensitization is unlikely to affect the decay time of the NMDAR EPSC, which is accurately predicted using modal gating models that do not incorporate desensitized states (Zhang et al. 2008). This result is consistent with our finding that NMDAR decay time is not affected by HCY (Figure 2.5B), which is therefore likely to only impact transitions to or from desensitized states. These data suggest that HCY may not affect single EPSCs but instead enhance NMDAR currents by reducing NMDAR transitions to desensitized states during high frequency presynaptic firing. Transitions to desensitized states are likely also important during LTP, which is induced by a high frequency tetanus expected to repeatedly activate the same set of NMDARs; this may explain why HCY shows strong enhancement of LTP at concentrations that reduce glycine-dependent NMDAR desensitization (Christie et al. 2009). This idea is supported by the finding that synaptic rises in glycine induced by blocking the glycine transporter (GlyT), which would reduce glycine dependent desensitization (Figure 2.3), also enhance LTP (Martina et al. 2004).

**2.4.3 - HCY effects are age dependent:** A developmental turnover of GluN2B- to GluN2A-containing NMDARs is a common feature of cortical neuron cultures and many areas in the intact brain (Zhong et al. 1994; Flint et al. 1997; van Zundert et al. 2004; Townsend et al. 2003). NMDAR currents in young GluN2B-enriched neurons and in GluN2B-expressing HEK cells showed significant peak amplitude reductions when exposed to HCY (1 mM D,L HCY = 500  $\mu$ M L-HCY, Figures 2.1, 2.2, 2.4). Conversely, NMDAR currents in GluN2A-expressing HEK cells showed strongly enhanced peak amplitudes in response to the same HCY application (Figure 2.4). Older cultured neurons did not show a change in peak amplitude, reflecting a hybrid GluN2B/GluN2A response as GluN2A is added to NMDARs during development (Zhong et al. 1994; Baron et al. 2009). Thus, HCY

effects on NMDARs are likely to change with maturity as synapses in the brain incorporate GluN2A subunits and receptors composed of two GluN2B subunits relocate to extrasynaptic sites (van Zundert et al. 2004).

**2.4.4 - Relevance to disease:** This report shows that low micromolar doses of HCY (50  $\mu\text{M}$  L-HCY) strikingly enhance NMDAR charge transfer by 69% in neurons ( $p \leq .001$ ) and in every transfected HEK cell tested ( $p \leq .001$ ) (68% in GluN2B-transfected HEK cells, and 141% enhancement in GluN2A-transfected HEK cells; Figures 2.2, 2.4). Higher doses of HCY (500  $\mu\text{M}$  L-HCY) caused even stronger charge transfer enhancement in all tested systems (Figures 2.2, 2.4, 2.11, 2.12). We will argue that these HCY levels are likely to be involved in disease states where HCY is upregulated, first outlining current clinical data.

There has been debate concerning the relevance of high HCY in the blood of schizophrenia patients to the disease itself. These observed levels nearly double the  $\sim 10$   $\mu\text{M}$  level observed in controls ( $\sim 15$ - $20$   $\mu\text{M}$ , Levine et al. 2002; Applebaum et al. 2004), and a 5  $\mu\text{M}$  increase of HCY in the blood is known to increase schizophrenia susceptibility by 70% (Muntjewerff et al. 2006). Consistent with the fact that CSF HCY levels are also increased in schizophrenia (Regland et al. 2004), studies on HCY injected rats have shown that increasing HCY levels in the blood causes heightened HCY in the brain that alters NMDAR dependent plasticity (Algaidi et al. 2006). In addition, the same schizophrenia-linked molecules that produce and metabolize HCY in the blood (COMT, methyl-tetrahydrofolate reductase (MTHFR)) also do so in brain regions where COMT is the primary clearance mechanism for synaptic dopamine and norepinephrine (i.e. cortex, hippocampus, superior colliculus; not the striatum; Tunbridge et al. 2006; Bigl et al. 1974; Tunbridge et al. 2008; Roffman et al. 2008; Muntjewerff et al. 2006). This suggests that the heightened levels of blood HCY could reflect dysregulated HCY production and metabolism at many dopamine and norepinephrine synapses in the central nervous system (Tunbridge et al. 2006; Tunbridge et al. 2008).

HCY doses used in this study could thus affect NMDARs in brain disorders like schizophrenia, where HCY levels average 20  $\mu\text{M}$  HCY in blood and  $\sim 1$   $\mu\text{M}$  HCY is

observed in some patients' CSF (Levine et al. 2002; Regland et al. 2004). Hyperhomocysteinemia and fibromyalgia, both associated with cognitive dysfunction, also show increased HCY (Hyperhomocysteinemia:  $\sim 150 \mu\text{M}$  plasma HCY levels with low micromolar CSF levels, Blom et al. 1993; Surtees et al. 1997. Fibromyalgia:  $\sim 1 \mu\text{M}$  CSF, Regland 2005). It is also possible that HCY has a role in brains of normal humans, as controls show  $\sim 8 \mu\text{M}$  HCY in blood and  $\sim .2 \mu\text{M}$  in CSF. These control levels of CSF HCY are higher than normal CSF levels of dopamine (Levine et al. 2002; Regland et al. 2004; Gjerris et al. 1987).

Although HCY CSF levels are somewhat lower than we use in this study, synaptic concentrations of neurotransmitters are not often reflected in total CSF or blood preparations. This occurs for two reasons: **1)** Transporters surrounding synapses (DAT for dopamine or EAATs for glutamate) clear neurotransmitters from the extracellular space within milliseconds (Garris et al. 1994; Clements et al. 1992). **2)** Synaptically released neurotransmitters reach high concentrations due to the miniscule volume of the synaptic cleft, but after escaping the synapse, they are no longer confined to a small volume, lowering their absolute concentration. For example, the documented concentration of dopamine in the synaptic cleft after single vesicle release is  $1.6 \text{ mM}$  (Garris et al. 1994). However, even with dopamine transporters blocked, the local extrasynaptic dopamine rise due to a single vesicle is only  $.25 \mu\text{M}$  (Garris et al. 1994), and the CSF concentration of dopamine is only  $40 \text{ nM}$  (Gjerris et al. 1987). Glutamate also reaches millimolar ( $1.1 \text{ mM}$ ) concentrations at synapses but is only found at  $1.1 \mu\text{M}$  in the CSF (Clements et al. 1992; Yamamoto et al. 1999).

Like these neurotransmitters, HCY is released to the extracellular space. This occurs after dopamine breakdown by COMT in astrocytes (Huang et al. 2005). HCY is also quickly cleared from the extracellular space by an as yet uncharacterized neuronal transporter (Huang et al. 2005). If HCY is released from astrocytes into the synaptic cleft, it could reach glutamate or dopamine-like concentrations ( $\sim 1 \text{ mM}$ ). This idea is substantiated by the growing list of "gliotransmitters" that participate in synaptic signaling (Halassa et al. 2007). Clearly, the hypothesis that HCY is a gliotransmitter should be tested experimentally; however, if HCY reaches even 5%

(50  $\mu$ M) of the synaptic glutamate or dopamine concentration at synapses, it is likely to produce the striking effects on NMDAR desensitization found in this study (Figures 2.2, 2.4).

An additional factor in the interpretation of the present experiments is that HCY molecules quickly dimerize in solution via their free sulphur groups, which we consistently noticed (Hogg 1999). We report in this text that dimerized HCY (homocystine) fails to reduce NMDAR desensitization; this is a significant finding because after only 4 hours in solution, 50% of HCY has dimerized to homocystine (Hogg 1999). It is therefore possible that much of our data underestimates the potency of HCY on NMDARs: a substantial amount of data were obtained 4+ hours after the beginning of recording sessions, and we only compensated our solutions for the slight decay that occurred between making solutions and the start of recording sessions.

An important question that arises from these HCY findings is whether the association of HCY with schizophrenia is due to its induction of a brain environment similar to that caused by drugs like ketamine and PCP. These NMDAR interacting drugs produce temporary schizophrenia-like symptoms in normal subjects. Ketamine and PCP, however, are NMDAR open channel blockers. Our work does not support a ketamine or PCP-like antagonist role for HCY at the level of the NMDAR itself. Nonetheless, despite initial expectations that ketamine would depress activity in neural circuits due to antagonism of NMDARs, it is now generally accepted that ketamine produces psychotic symptoms by *enhancing* circuit activity through preferential inhibition of NMDARs on inhibitory interneurons (Seamans 2008; Homayoun and Moghaddam 2007). HCY may also have emergent effects on neural circuits *in vivo*. Indeed, the dynamic effects of HCY on desensitization and amplitude that vary according to GluN2 composition and glycine concentration suggest an extremely complex role for HCY in the nervous system. Considering the growing list of brain molecules that can reduce NMDAR desensitization (eg. spermine, glycine, d-serine, PSD-95) it may even be the case that NMDAR desensitization itself is a critical under-explored feature *in vivo* (Mayer et al. 1992; Sornarajah et al. 2008).

**CHAPTER 3:**

***D1 and D2 dopamine receptors segregate to behaviorally relevant zones in the SC: an anatomical and electrophysiological characterization***

\*\* This section will be submitted as an article to the Journal of Neuroscience in 6/2014

**3.1 – Introduction:** The mammalian superior colliculus (SC), known as the optic tectum in birds, reptiles, amphibians, and fish, is a phylogenetically old structure originally studied in the context of eye movements. Recent work, however, has revealed that the SC has a far more complex role than originally believed. The SC is now known to participate in a variety of diverse behaviors including sensorimotor integration (Hall and Mochavakis 2004), covert spatial attention (Muller et al. 2005, Lovejoy and Krauzlis 2010, Katyal et al. 2010), short-term memory (Wurtz et al. 2001, Felsen and Mainen 2012), behavioral target selection, and decision making (Felsen and Mainen 2008, Horwitz and Newsome 1999, Krauzlis et al. 2004). Removal of the SC causes profound behavioral deficits that reflect its critical role in brain function. Monkeys with collicular removal become mute with expressionless faces and lose their characteristic social behaviors (Denny Brown 1962). They stare aimlessly into space, stop grooming, and return to apathy immediately after stimulation from the environment. The only reported SC lesion in a human rendered the patient expressionless, un-reactive to the environment, and resigned to staring into space (Denny Brown 1962).

Like its non-mammalian predecessor, the SC is divided into multiple layers that are functionally (Northmore et al. 1988), electrophysiologically (Isa and Hall 2009), and molecularly distinct (Illing 1996). The superficial layers of the SC are primarily visual: the dorsal-most SC layer, the stratum griesium superficialae (SGS), receives converging topographic visual input from retinal ganglion cells and feedback visual input from V1 (Phillips et al. 2011). These visual axons enter the SC via the stratum opticum (SO), which like the SGS is considered part of the superficial SC. In contrast to the purely visual superficial layers, the intermediate SC layers [stratum griesium intermediale (SGI) and stratum album intermediale (SAI)] are multimodal, receiving auditory, tactile, and visual input. The intermediate SC layers also contain a “motor map”, meaning that stimulating neurons in these layers evokes movements of the eyes and head (Robinson 1972, Schiller and Stryker 1972), or shifts in covert attention (Muller et al. 2005, Lovejoy and Krauzlis 2010), to prescribed locations in space. Critically, this motor map is in direct register with the visuotopic map above it in the SGS; cells in the SGS project directly downward

and excite premotor neurons in the deeper SC layers (Isa and Hall 2009). This means that salient visual input from the environment can trigger movements to the location of that input in only two synapses. The deepest layers of the SC are also arranged in a motor map; these layers have larger visual receptive fields than the SGI and receive the largest relative auditory input in the SC (Sparks and Harwich-Young 1989).

Electrical stimulation of the different SC layers causes a wide range of behavioral effects. For instance, SGS/SO stimulation can induce freezing behaviors in Syrian hamsters while SGI stimulation induces orienting turning movements (Northmore et al. 1988). In rats, even more complex behaviors can be evoked with electrical stimulation of the SC, ranging from turning and running to biting (Dean et al. 1986). Stimulating the intermediate layers of the frog tectum induces striking behavior to prescribed locations in space, mimicking prey capture (Ewert 1984).

Finally, frogs, rats, and monkeys all use the intermediate layers of the SC to store the intent of future orienting directions; this is observed neurally as a preparatory persistent neural activity that is locked to a particular location in space within the SC motor map (Ingle 1975, Felsen and Mainen 2012, Munoz and Wurtz 1995, Wurtz et al. 2001). Interestingly, this preparatory activity is modulated by the expectation of reward in both rats and monkeys (Felsen et al. 2012, Basso and Wurtz 1998, Ikeda and Hikosaka 2007, 2003). The dopamine system is consistently implicated in the coding of reward prediction error (for review, see Schultz 2007) and in the modulation of persistent neural activity (Goldman-Rakic et al. 2001, Wang et al. 2004). Moreover, like the SC, dopamine is known to be heavily involved in attention. Ritalin, the main treatment for ADHD, targets catecholamine transporters and modulates levels of synaptic dopamine. D1 dopamine receptor haplotypes have known linkage to ADHD heritability (Misener et al. 2003; Bobb et al. 2005; Luca et al. 2007). However, dopamine's role in the SC is currently unknown despite the fact that there is more dopamine in the SC than the hippocampus or frontal cortex (Versteeg et al. 1976).

Previous literature has also shown that the intermediate and deeper layers of the SC send a strong excitatory projection to the substantia nigra, which can activate



dopamine neurons at short latency (Comoli et al. 2003, Coizet et al. 2006, Coizet et al. 2003). However, the projection of dopamine neurons back to the superior colliculus has only been sparsely studied (Campbell et al. 1991, Takada et al. 1988)

Considering the distinct roles of the various SC layers in not only controlling behavior but remembering which behaviors are to be executed, our results here concerning the location of dopamine receptors within the SC are critical. We report a mosaic pattern of D1 and D2 dopamine receptors that segregates according to collicular layer. We characterize both the D1+ and D2+ population of SC cells extensively using anatomical, immunohistochemical, and electrophysiological methods. We find that the A13 cell group of the zona incerta is the primary TH+ source to the SC that does not express dopamine beta hydroxylase (DBH). Dopamine in the SC induces clear and reversible electrophysiological effects that vary according to dopamine receptor expression. On the whole our results suggest that dopamine inputs to the SC dampen the SC circuit and would reduce the tendency of an animal to respond to salient visual stimuli during natural behavior or SC dependent tasks like working memory.

### **3.2 - Materials and Methods:**

All experiments were carried out with the approval of the Committee on Animal Care at the Massachusetts Institute of Technology.

**3.2.1 - Animals:** Mice listed as WT in this manuscript are C57B6/J. Strains from GENSAT include: D1-Cre (FK150); D2-Cre (ER44); and D2-EGFP (S118). D2-EGFP were back-crossed to C57B6/J after arriving on a Swiss Webster background. Strains from Jackson Labs include: D1-tdTomato (#016204); floxed-tdTomato (B6.Cg-Gt(ROSA)26Sortm14(CAG-tdTomato)Hze/J. #007914); DAT-Cre (#006660), and TH-Cre (#008601). VGAT-Venus mice were generously given to us by Janice Naegele via Yuchio Yanagawa (Wang et al. 2009). Venus was developed by Dr. Atsushi Miyawaki at RIKEN, Wako, Japan.

***3.2.2 - RNA Sequencing:*** Total RNA from the 3 week old rat superior colliculus was extracted using Qiazol® (Qiagen #79306) reagent following the manufacturers instructions. Total RNA was cleaned up using the RNeasy MinElute cleanup kit (Qiagen #74204) and stored at -80°. The purity of RNA was assayed using a NanoDrop spectrophotometer and samples with 260/280 ratios less than 1.8 or 260/230 ratios less than 2.0 were subjected to a second round of cleanup and discarded if they were still not pure after the second cleanup. Samples were run on the Agilent 2100 Bioanalyzer and samples with RIN numbers less than 9 were discarded. Samples were stored at -80° until library creation.

DNA libraries for paired-end sequencing on the Illumina Genome Analyzer II were prepared following the Illumina protocol (#1004898 Rev. D) with a few alterations. The resulting product was PCR amplified for 10 cycles using primers against the Illumina adaptors. The final library was run on an Agilent Bioanalyzer to confirm proper size selection. Samples were submitted to the BioMicro Center at MIT for sequencing on the Illumina Genome Analyzer II with 36 base pair paired-end reads.

We processed the RNA-sequencing data using the best practice RNA-seq pipeline implemented in version 0.7.9a of the bcbio-nextgen framework. Briefly, we trimmed off poor quality ends with AlienTrimmer (2) version 0.3.2, using a cutoff of phred score of 5 or less and trimmed portions of reads and anything after it matching the first 13 bases of the Illumina universal adapter sequence to remove read-through contamination caused by the read length being longer than the insert size for a fragment. We also trimmed polyA and polyT homopolymer sequences from the 5' ends of reads. Reads were aligned using the STAR (1) aligner version 2.3.14z against the *rattus norvegicus* genome build rn5 and Ensembl release 74 of the gene annotation. Counts of reads mapping to genes in the Ensembl annotation were calculated using FeatureCounts (3) version 1.4.4 and FPKM expression was estimated using Cufflinks (4) version 2.1.1.

***3.2.3 - Animal Surgery:*** Young mice (P10-P16) were anesthetized with isoflurane and immobilized in a stereotaxic frame. The skin overlying the skull was

incised and a dental drill was used to burr a hole through the skull above the SC. Glass pipettes (Drummond) were pulled and ~2  $\mu$ L of injectable was loaded into the pipette tip using a Drummond Nanoject. Injectables included latex microspheres (Retrobeads IX, Lumafluor Inc: green beads injected at 100%, red beads injected at 25% beads:PBS) or adeno-associated virus carrying FLEX-AAV-EGFP or FLEX-Channelrhodopsin2. Loaded pipettes were lowered under stereotaxic guidance into the SC. Microspheres or virus were injected (~45-100 nL total), and five minutes later the pipette was slowly retracted. Animals were sutured and returned to their home cages for 2 weeks (microspheres, AAV-GFP) or 6 weeks (AAV-ChR) before perfusion. In some cases P0-P3 mice were injected under cold anesthesia using a “through-the-skull” injection method requiring no other surgery.

*3.2.4- Anatomy and Histology:* Animals were perfused through the heart with 15 mL PBS followed by 15 mL 4% paraformaldehyde in PBS under isoflurane anesthesia. Brains were extracted and post-fixed in 4% paraformaldehyde at 4° C overnight. After post-fixing, brains were transferred to 30% sucrose in PBS for cryoprotection at 4°. Slices were cut at 75-90  $\mu$ M using a Leica freezing microtome or a Leica cryostat using OCT as a freezing medium. For immunohistochemistry experiments, free-floating slices were incubated for 2+ hours at room temperature in a blocking buffer containing 1% TritonX and 5% Goat or Donkey serum in PBS. Slices were then incubated on a shaker overnight at 4° in blocking buffer containing primary antibody. Primary antibodies used included rabbit anti-tyrosine hydroxylase (Millipore AB152; 1:1000), rat anti-DAT (MAB369; 1:1000), rabbit anti-RFP (MBL PM005; 1:2000), chicken anti-GFP (AbCam ab13970; 1:10000), mouse anti-NeuN (Millipore MAB377; 1:3000). After primary antibody incubation, slices were washed in PBS for 15 minutes three times. Slices were then incubated in Alexa Conjugated IgG (1:500 or 1:1000) directed to the species of the primary antibody in blocking buffer at RT for 2 hrs. After a second round of three 15 minute PBS washes, slices were mounted with Fluoromount. All samples were imaged using a Nikon C2 confocal system equipped with 488 nM, 561 nM, and 647 nM lasers.

**3.2.5- Cell Counting:** Custom software for counting and assigning coordinates to fluorescent neurons was written in Python by ADB. This software with instructions is freely available at ADB's Github address (<https://github.com/LarryLegend33>). Heatmap histograms were created using the Python Matplotlib library's "hexbin" function with a minimum count of 1 (i.e. bins with 0 counts appear as white). Hexagonal binned images were smoothed in Adobe Photoshop and overlaid with Paxinos Atlas Figures 59 (Rostral), 64 (Middle), and 68 (Caudal). Samples chosen for cell counting came from 3 coronal planes of the SC. Caudal samples were approximately the first sample of caudal SC where the SC was significantly larger than the inferior colliculus. Rostral samples were approximately the last slices that contained full-size SGS (i.e. before disappearance of the SGS at the rostral pole). Middle slices were halfway between the chosen caudal and rostral slices.

**3.2.6 - Slice Electrophysiology:** P20-P45 mice were anesthetized in a bell jar using isoflurane and decapitated. The brain was quickly removed and submerged in an ice cold sucrose cutting solution containing (in mM): 206 Sucrose, 2.5 KCl, 1.2 NaH<sub>2</sub>PO<sub>4</sub>, 24 NaHCO<sub>3</sub>, 5 HEPES, 12.5 Glucose, .4 Sodium Ascorbate, 10 MgSO<sub>4</sub>, .5 CaCl<sub>2</sub>. After 1 minute of cooling, the brain was mounted on a Leica vibratome and submerged in sucrose solution. Sagittal SC slices were prepared at 280  $\mu$ m. Slices were then incubated at 32° for 15 minutes in a carbogenated slice chamber filled with artificial cerebrospinal fluid (ACSF) composed of (in mM): 124 NaCl, 2.5 KCl, 1.2 NaH<sub>2</sub>PO<sub>4</sub>, 24 NaHCO<sub>3</sub>, 5 HEPES, 12.5 Glucose, .4 Sodium Ascorbate, 2 MgSO<sub>4</sub>, 2 CaCl<sub>2</sub>. The chamber was then removed from the 32° water bath and allowed to return to RT. Slices recovered for 1 hour+ before being added to a recording chamber under continuous perfusion of ACSF (~2 mL/min). For voltage clamp experiments, pipettes were filled with a solution containing (in mM): 105 Cs-Gluconate, 10 Phosphocreatine (Na), .07 CaCl<sub>2</sub>, 4 EGTA, 10 HEPES, 4 Na-ATP, 1 Na-GTP, 3 MgCl<sub>2</sub>, brought to osmolarity of ~290 mOsm with sucrose. In some experiments, sucrose was omitted and neurobiotin (0.5%) was used. Current clamp internal solution was identical except 105 K-Gluconate replaced Cs-Gluconate. Cells

were patched with glass pipettes (Sutter) pulled to 3-7 M $\Omega$  using a Multiclamp 700B with pClamp10 software. Fast bath exchange (~10 sec) was performed using an ALA VM-4 perfusion system with a Millimanifold attached directly to the bathing chamber, with the bath kept at ~30-32°. Neurons were visualized before patching with an Arclamp and identified as D1+ or D2+. For experiments stimulating the stratum opticum, a concentric bipolar electrode (FHC) driven by a World Precision Instruments IsoStim 320 was placed in the SO axons at the rostral pole of the SC. Stimulating intensities were raised until spikes were driven in the post-synaptic neuron. Typical current applied was ~.1 mA.

### **3.3 Results:**

**3.3.1 - RNA Seq:** An ongoing study in our laboratory characterized expression levels of every RNA read within the superficial and intermediate layers of the 3-week old rat SC (Kirchner et al., in prep). RNA transcript levels were averaged across 3 lanes of RNAseq, each containing 3-4 colliculi cut from the rat according to Figure 3.1a. Figure 3.1b shows the average expression level of transcripts related to the dopamine system in the SC. Notably, there were high RNA levels of only two dopamine receptor subtypes in the SC: *Drd1a*, which codes for the D1 dopamine receptor, and *Drd2*, which codes for the D2 dopamine receptor (15.9 FPKM and 48.9 FPKM respectively; Figure 3.1b – see Legend for FPKM explanation). *Drd3* transcripts were detected at miniscule amounts in the SC (0.89 FPKM; 1:55 *Drd3*:*Drd2*), *Drd4* transcripts were undetectable in the SC (zero reads), and only a small amount of *Drd5* was present (~1:7 *D5*:*D2*). *COMT*, which initiates the catabolism of dopamine via *o*-methylation (Tunbridge et al. 2006), is strongly expressed in the SC, as is the enzyme *MTHFR*, which contributes to the remethylation of the NMDAR active dopamine breakdown product homocysteine (Bolton et al. 2013). Two common NMDA receptor subtypes are included for comparison, indicating that *Drd1a* and *Drd2* expression in the SC is on the same order as the genes coding two of the most common excitatory receptors in the brain.

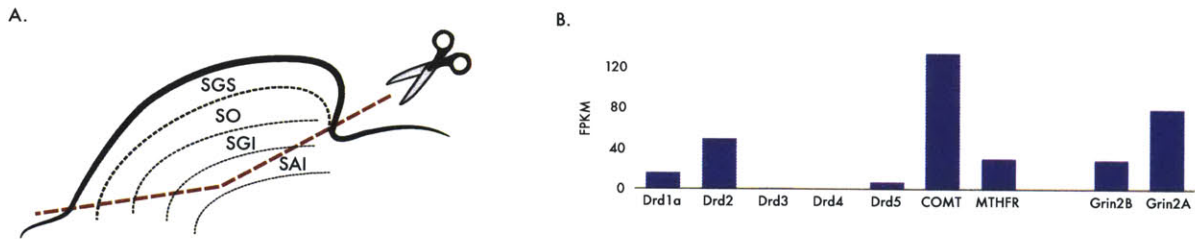


**FIGURE 3.1: RNA sequencing of dopamine system related genes in the SC. A.** Crowns of the superior colliculus were dissected from P21 rats according to the diagram. These tissue samples contained the superficial SC along with the intermediate gray (SGI) and part of the intermediate white (SAI) layers. **B.** The only dopamine receptor genes that showed strong expression in these samples were Drd1a and Drd2, which code for the D1 and D2 dopamine receptor. Values for each gene are reported in Fragments Per Kilobase per Million Reads. This statistic normalizes the amount of reads observed in the RNAseq experiment to the length of the gene, preventing large genes from being over-represented in the analysis and small genes from being under-represented. Drd3 and Drd4 were miniscule or absent from the SC while Drd5 showed low expression. Two of the enzymes involved in dopamine metabolism, COMT and MTHFR, are both strongly expressed in the SC. Grin2B and Grin2A, which code for the common NMDA receptor subunits GluN2B and GluN2A respectively, are expressed on the order of Drd1a and Drd2, indicating that D1 and D2 dopamine receptors are nearly as abundant in the SC as two of the most ubiquitous glutamate receptors in the brain.

*3.3.2 - D1+ and D2+ cells are spatially segregated in the SC:* Considering that Drd1a and Drd2 appeared to be the major dopamine receptor subtypes in our RNAseq experiment, we sought to characterize the electrophysiological effects of dopamine on neurons expressing D1 or D2 receptors in the SC. To visualize these neurons for targeted patch clamping, mice expressing Cre under the Drd1a promoter (D1-Cre) and mice expressing Cre under the Drd2 promoter (D2-Cre) were crossed to a floxed-tdTomato reporter line. Surprisingly, we immediately noticed a striking pattern of dopamine receptor expression within the laminar SC structure. In the D1-Cre animal, tdTomato was enriched in the neuropil and cell bodies of the superficial visual layers (SGS) of the SC while D2 expression was sparse in this area (Figure 3.2). D2 reporter expression was instead enriched ventral to the SGS in the SO and intermediate SC.



**FIGURE 3.2: D1-Cre and D2-Cre positive cell populations segregate to different SC layers.**

Cre positive neurons in both images appear in red after crossing both lines to the floxed-tdTomato line. D1-Cre (left) is expressed most strongly in the superficial superior colliculus (SGS), which receives visual input from the retina and visual cortex. D2-Cre expression (right), on the other hand, is sparse in the superficial layers and is more highly expressed in the SO and multimodal intermediate layers.

*3.3.3 – Characterizing the location, overlap, and inhibitory / excitatory identity of D1 and D2 neuron populations:* We next performed experiments to characterize the locations of D1+ and D2+ neurons relative to each other, the percent overlap of the D1+ and D2+ populations, and the inhibitory / excitatory identity of both cell groups. Identification of excitatory / inhibitory identity is critical to understanding how D1+ and D2+ cells operate within the SC circuit.

To identify percent overlap of D1+ and D2+ neurons, a mouse line expressing tdTomato under direct control of the *Drd1a* promoter (D1-tdTomato) was crossed to a second line expressing EGFP under direct control of the *Drd2* promoter (D2-EGFP). To query whether D1+ and D2+ cells were GABAergic, D1-tdTomato and D2-tdTomato (D2-Cre x floxed-tdTomato) mice were crossed to a line expressing the yellow fluorescent protein Venus under control of the VGAT promoter (Wang et al. 2009). SC slices from three rostro-caudal planes (rostral, middle, caudal – see Methods) were prepared from each of these double-labeled transgenic lines. Three animals were used for each condition. Fluorescent cells were counted using custom Python software written by ADB and counts are provided in Table 3.1.

**3.3.3a - Total Neuron Counts and Rostro-Caudal Quantification:** Box1 contains the figure legends for Figures 3.3-3.5. In the SC of D1-tdTomato x D2-EGFP mice, it was clear that the segregation of D1 and D2 receptors was nearly identical to the D1-Cre and D2-Cre reporters (Figure 3.3). This indicates that the segregation is not due to an artifact in the Cre lines.

Slices of D1-tdTomato x D2-EGFP double transgenic mice were stained with an antibody for NeuN to count all SC neurons (Figure 3.3, NeuN panels). Of the 29,343 total neurons labeled with NeuN in our D1-tdTom x D2-EGFP samples, 11.3% were D1+ and 9.4% were D2+. Only 1.2% of SC neurons were both D1+ and D2+ (Table 3.1 for counts). D1+ neurons outnumbered D2+ in the middle and caudal planes, but in rostral sections D2+ neurons were more numerous (878 D2+ vs. 783 D1+). D1+D2 double labeled cells dropped in number along the caudo-rostral axis (140 caudal, 118 middle, 91 rostral), making up less than 1% of NeuN+ cells in the rostral plane.

	<i>D1-tdTom x D2-EGFP</i>				<i>D1-tdTom x VGAT-Venus</i>		<i>D2-tdTom x VGAT Venus</i>	
	<u>D1</u>	<u>D2</u>	<u>D1+D2</u>	<u>NeuN</u>	<u>D1+ VGAT+</u>	<u>D1+ VGAT-</u>	<u>D2+ VGAT+</u>	<u>D2+ VGAT-</u>
<i>Rostral</i>	783	878	91	10787	524	520	381	604
<i>Middle</i>	186	787	118	11018	726	443	608	952
<i>Caudal</i>	1036	737	140	7538	547	330	503	960
<b>TOTAL</b>	3005	2402	349	29343	1797	1293	1492	2516

**TABLE 3.1 – Total neuron counts for D1,D2 overlap and D1 VGAT, D2 VGAT experiments.** Three animals were used for each condition, with total neuron counts summing across the three mice. Average age for mice: D1 x D2 = P32, D1 x VGAT = P38, D2 x VGAT = P33.

Overall, D1+ cells expressed VGAT at a 58% rate (1797/3090). The specific distribution of these cells will be addressed in our layer by layer analysis in section 3.3.3b. Interestingly, D1 neurons are less likely to be GABAergic in the rostral SC



(Figure 3.5, Rostral SC, Table 3.1). This may be due to the fact that the SGS shrinks in the rostral SC, which is where D1 neurons primarily co-localize with VGAT in the middle and caudal planes.

In total, 63% of D2+ neurons were VGAT- while 37% were VGAT+ (Table 3.1, Figure 3.5). This overlap was not different across the rostro-caudal axis (39% VGAT+ rostral, 39% VGAT+ middle, 34% VGAT+ caudal – Table 3.1). However, there was an interesting laminar pattern of D2+ VGAT+ vs. D2+ VGAT- cells that will be addressed in section 3.3.3b.

*3.3.3b - Distribution of D1+ and D2+ cells within the SC layered structure:* To further analyze the spatial distribution of D1+ and D2+ subtypes in the SC, two dimensional histograms were prepared from all D1-tdTom x D2-EGFP (Figure 3.3), D1-tdTom x VGAT Venus (Figure 3.4) and D2-tdTom x VGAT Venus (Figure 3.5) animals in all three coronal planes (rostral, middle, caudal; see Box 1 for legends and method for generating histograms). X,Y coordinates of each neuron were stored in Numpy Arrays during cell counting and are available for download ([github.com/LarryLegend33](https://github.com/LarryLegend33)).

The density of D1+ and D2+ neurons, along with D1+ VGAT-, D1+ VGAT+, D2+ VGAT+, and D2+ VGAT- subtypes, was calculated according to recorded x,y coordinates in the layered structure of the SC. Histograms were plotted after the SC was divided into bins, each covering a hexagonal region 30 microns wide. These histograms (Figure 3.3) clearly show that D1+ density is the highest in the superficial SGS in the rostral, middle, and caudal planes. With regard to VGAT overlap, 3 of every 4 D1+ cells was VGAT positive (73%) in the SGS (< 400 um deep). This is clearly shown in Figure 3.4, where the majority of D1+ neurons in the SGS are yellow and the bulk of D1+ VGAT+ density is in the SGS in rostral, middle, and caudal sections. Figure 3.6a shows a high magnification image of the D1-tdTom x VGAT Venus SGS, where nearly every D1+ cell imaged is VGAT+. Interestingly, an almost exactly equal portion of D1+ cells in the deeper layers (> 400 um deep) are VGAT+ and VGAT- (50%/50%), as shown by the wide spread of D1+ VGAT- high density bins in Figure 3.5 across all rostro-caudal sections.

D2+ cell density was always the greatest in the SGI intermediate layer, especially laterally in the middle and rostral coronal planes. D2 also showed high density bins in the medial SO in all planes. Amazingly, the highest density D2+ bins always overlapped with the highest density D2+ VGAT negative bins, indicating that lateral SGI D2+ neurons and medial SO D2+ are non-GABAergic. Medial SO D2+ neurons are shown at high magnification in Figure 3.6b, where a mosaic overlap with VGAT is noted. In the SO, almost every D2+ neuron is non-GABAergic, while just beneath the SO in the medial SGI, D2+ cells are GABAergic. This can also be seen in Figure 3.5 where high density D2+ VGAT+ bins are always found in the medial SGI. The conclusion with regards to D2 overlap with VGAT are that medial SO and lateral SGI, which are the regions of highest D2+ density in general, are primarily non-GABAergic. Meanwhile, SGI D2+ neurons underneath the large nonGABAergic D2+ SO neurons are GABAergic.

The only major difference in distribution of D2+ cells in general across the rostro-caudal axis was the presence of “D2+ islands” unique to the rostro-medial SC pole (Figure 3.7). D2 islands lie directly within the SC commissure, where the deeper SC layers join at the midline. Note the high density D2+ bins in the deep rostral SC at the midline in Figure 3.3 (Rostral SC, D2+ panel) and the arrow in Figure 3.6. Upon further inspection, these islands were clusters of approximately 50 D2+ neurons that also appeared in D2-tdTom animals, showing up as VGAT negative. The functional identity of these neurons will be addressed in the Discussion section, as they may represent a set of “fixation” cells that, when activated, prevent orienting movements (Hall and Moschavakis 2004).

D1+D2 cells were sparse in all planes and never appeared to show any sort of location specificity besides a relatively consistent spattering of high density bins in the SGI (Figure 3.3, D1+D2 panels).

**BOX 1:** Rostral, Middle, and Caudal SC sections were imaged and quantified for three D1 tdTom x D2 EGFP, D1 tdTom x VGAT Venus, and D2 tdTom x VGAT Venus animals. Raw images of each plane are included in the large panel figures to follow (Figures 3.3 – 3.5), along with the monochrome images of each channel. Fluorescent cells were counted using custom Python software written by ADB after confirmation of NeuN identity. Two-dimensional histograms binning the SC into 30 micron-wide hexagonal regions were compiled using the Python Matplotlib hexbin() function for each rostro-caudal plane of section. In each histogram, white bins had zero neuron counts across 3 animals (i.e. mincnt = 1 in hexbin()). Red bins had the maximal number of counts. Between dark blue and red, neuron counts per bin increase (neuron counts: dark blue < blue < bluegreen < green < yellow < orange < red).

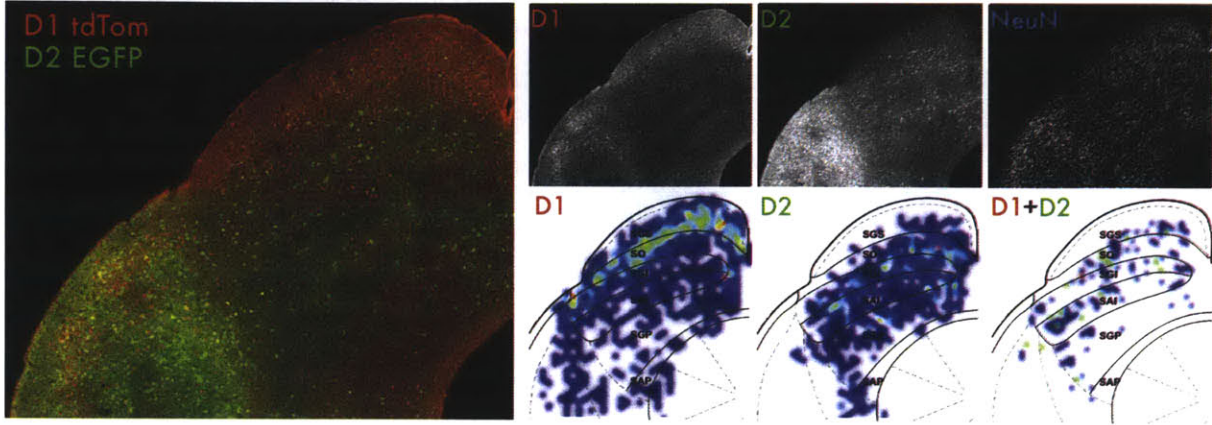
**LEGENDS FOR LARGE PANEL IMAGES:**

**FIGURE 3.3 – D1 tdTomato neurons are enriched in the SGS while D2 EGFP neurons avoid the SGS and are concentrated in the SO and SGI.** Layered segregation of D1 and D2 receptors is maintained rostro-caudally. D1+ neurons were always enriched in the SGS, while D2 showed strong expression in the medial SO and the SGI, especially laterally in the middle and rostral planes. D2+ neurons showed high density near the midline in rostral slices – these D2 islands that lie on the SC commissure will be addressed in Figure 3.7.

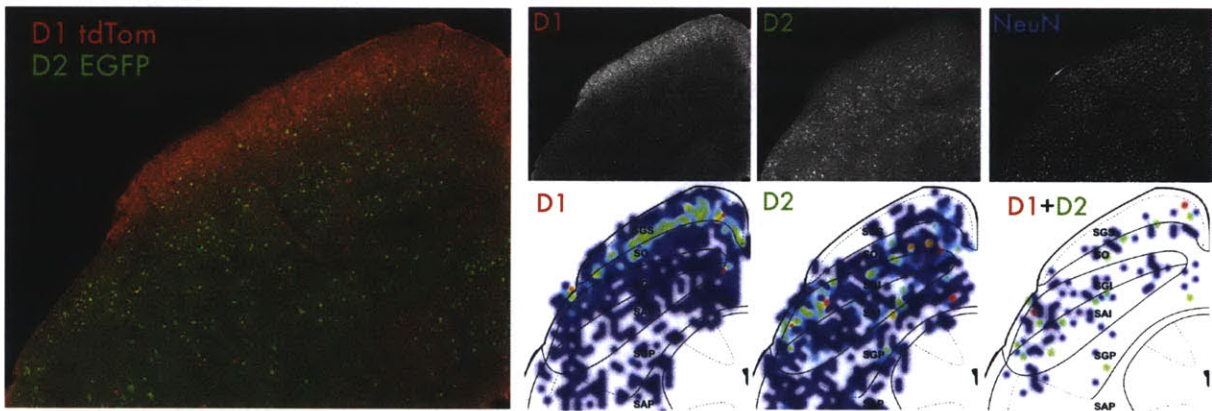
**FIGURE 3.4 – D1 tdTom x VGAT Venus mice show strong overlap between D1 and Venus in the SGS.** D1 neurons co-localize strongly with VGAT in all rostro-caudal planes in the SGS. Outside the SGS, D1+ neurons are equally VGAT+ and VGAT-. D1+ VGAT- neurons do not appear to specifically segregate to any particular layer.

# FIGURE 3.3

## Caudal SC



## Middle SC



## Rostral SC

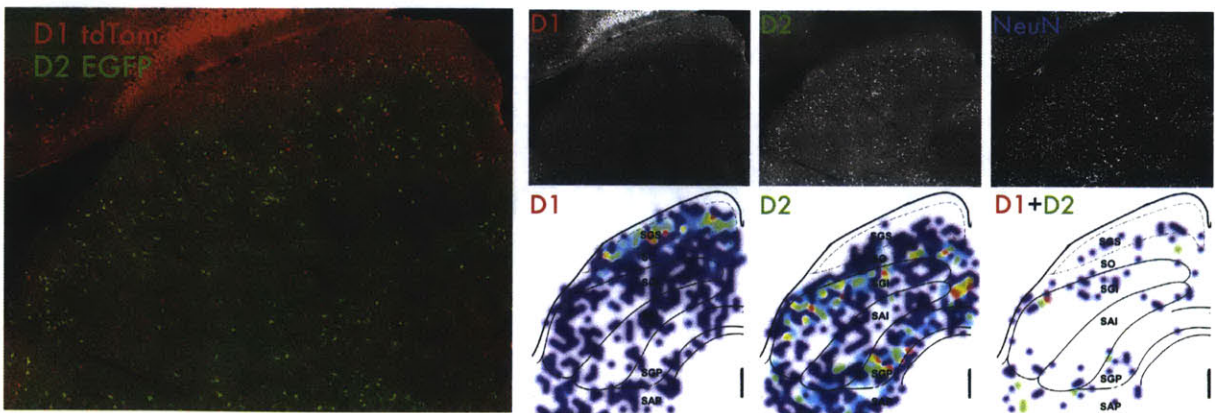
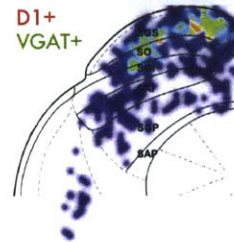
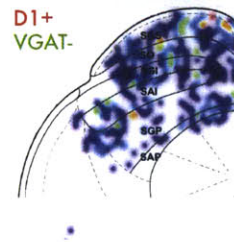
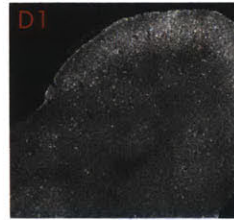
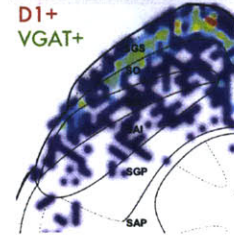
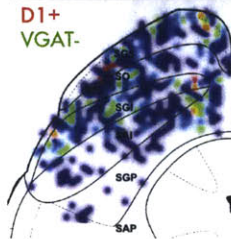
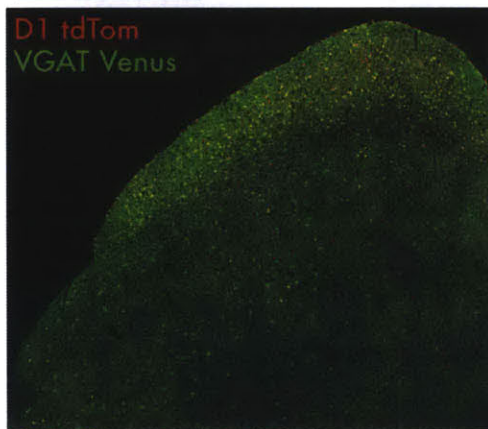


# FIGURE 3.4

## Caudal SC



## Middle SC



## Rostral SC

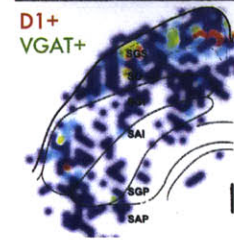
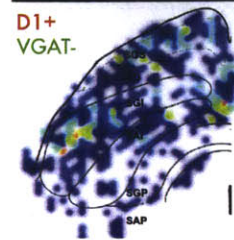
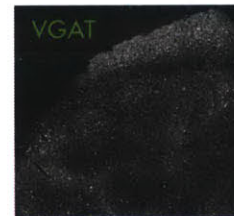
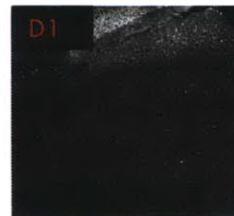
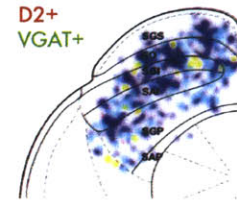
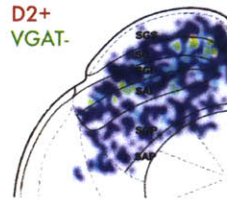
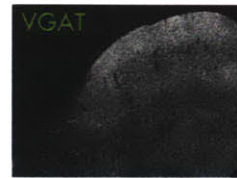
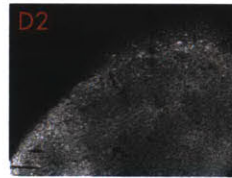
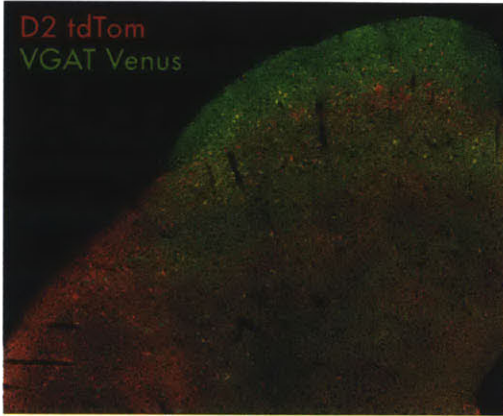
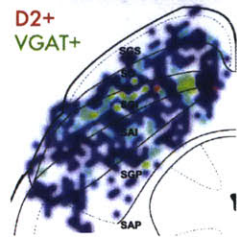
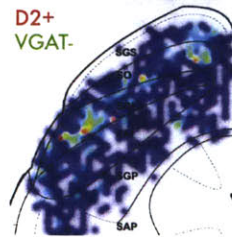
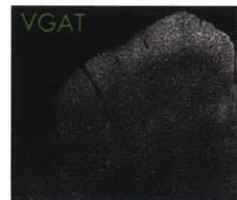
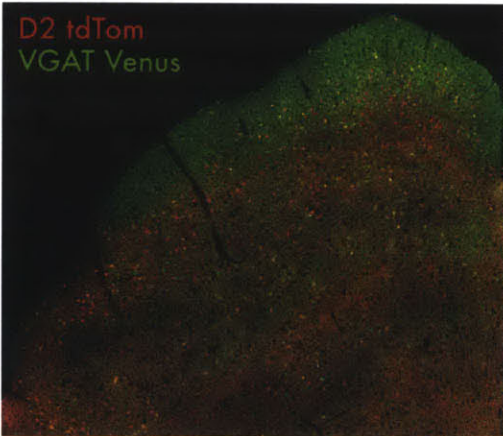


# FIGURE 3.5

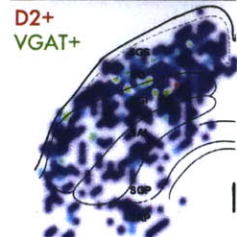
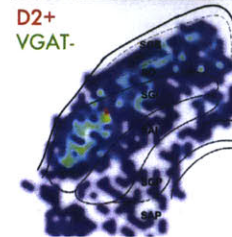
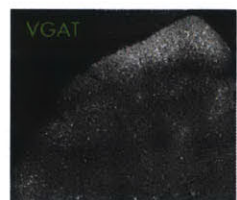
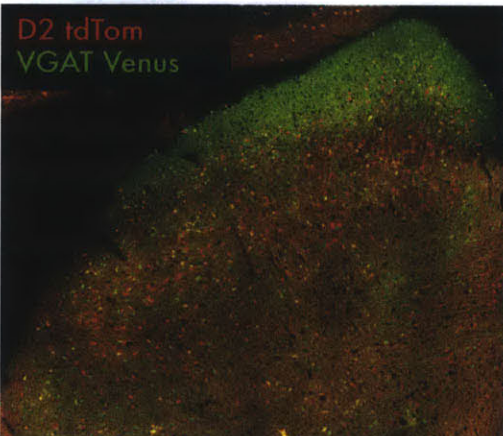
## Caudal SC



## Middle SC



## Rostral SC



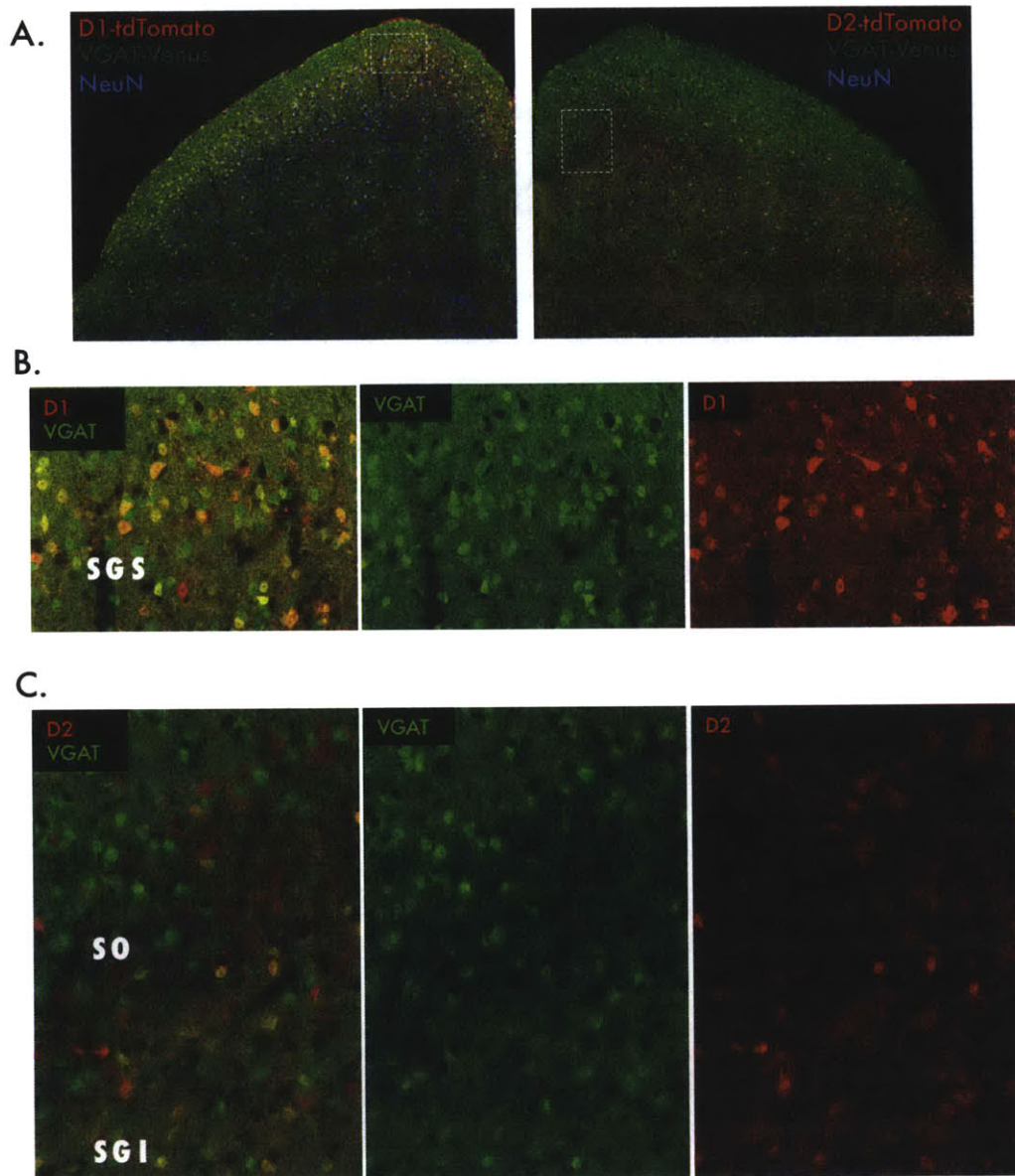


**FIGURE 3.6 – D1 SGS cells are primarily GABAergic while most D2 SO neurons are VGAT-**

A. D1 tdTom x VGAT Venus mice show strong co-localization between D1+ and VGAT+ cells in the SGS, while D2 tdTom x VGAT Venus mice show a lack of D2 / VGAT overlap in the medial SO. We zoomed in on these regions (dashed lines in A.) and confirm that D1+ cells are largely inhibitory in the SGS (B). Meanwhile, D2+ cells in the SO do tend to avoid VGAT. However, directly underneath the SO in the SGI, D2 and VGAT overlap, revealing a mosaic pattern of D2 VGAT co-localization.

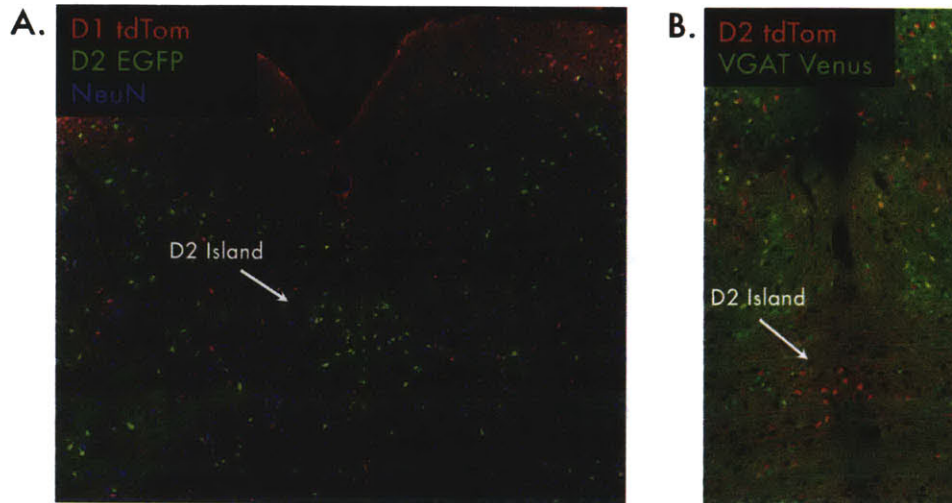


**FIGURE 3.7 – D2 “Islands” are present where the SC fuses at the SC commissure.**

D2 islands are seen in D2 EGFP mice (A) and in D2 tdTom mice crossed to the VGAT Venus line (B). Lack of VGAT co-localization indicates that D2 islands are likely excitatory. These cells may represent a commonly recorded set of “fixation” neurons in the rostro-medial pole. This will be addressed in Discussion.

3.3.4 – Dopamine source to the SC is DAT negative: Now that mRNA for dopamine receptors has been found (Figure 3.1) and the distribution of D1 and D2 receptors has been described, it is important to identify the source of SC dopamine. Dopamine is actually present in the SC at a higher concentration than frontal cortex or hippocampus (Versteeg et al. 1976). Previous studies suggested that dopamine neurons coexpressing GABA in the substantia nigra parts reticulata (SNr) project to the rat SC (Takada et al. 1988, Campbell et al. 1991). We sought to confirm this projection in order to understand how dopamine reaches the D1+ and D2+ neurons in the SC.

First, the SC localization of tyrosine hydroxylase (TH) was inspected using immunohistochemistry. TH catalyzes the conversion of tyrosine to the required dopamine precursor L-DOPA; therefore, only neurons expressing TH can create dopamine. TH+ axons were densely present in the SC (Figure 3.8c), with no preferential targeting to specific SC layers. This means that terminals capable of producing dopamine do terminate in the SC, which has been observed in hamsters (Arce et al. 1994) and chickens (Metzger et al. 2006).



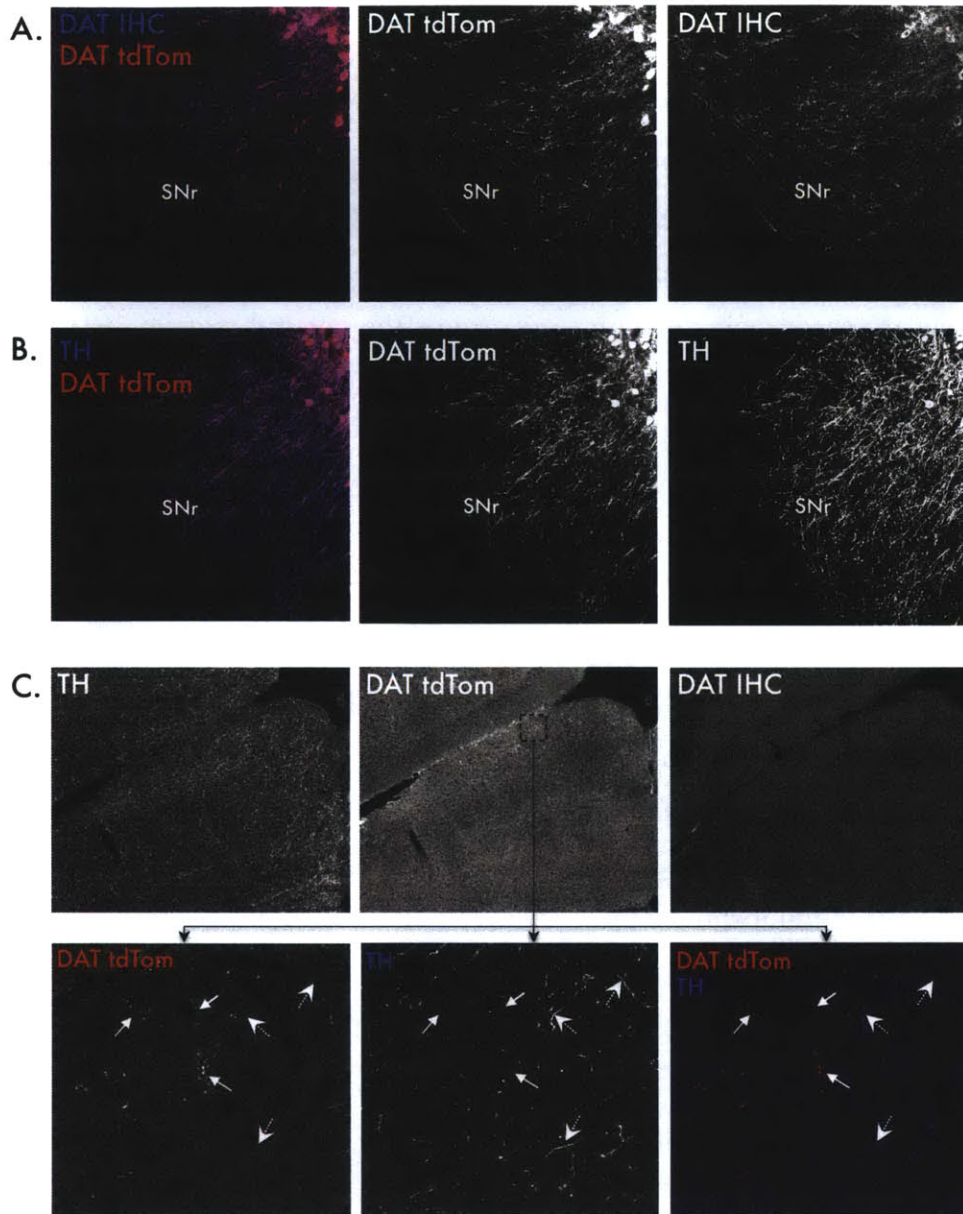


**FIGURE 3.8 – TH axons in the SC are DAT negative.** Our TH antibody strongly stained axons that co-express DAT in the substantia nigra pars reticulata (SNr). This was observed using both DAT IHC (A) and DAT-IRES-Cre x floxed tdTomato (DAT tdTom) as a reporter (B). Although TH was ubiquitously expressed in the SC (C, left panel), DAT-tdTom expression was sparse and localized only to the SGS (C, middle top). DAT IHC was typically undetectable in the SC (C, top right panel). TH+ axons hardly ever co-localized with DAT-tdTom positive terminals (C, bottom: small flathead arrows: DAT+, TH-. Pointed dashed arrows: DAT-,TH+); entire SC slices were typically void of TH and DAT-tdTom co-localization.

However, in TH+ neurons, dopamine may be converted to norepinephrine or epinephrine via dopamine beta hydroxylase (DBH), which in conjunction with TH demarks norepinephrine and epinephrine neurons [eg. in the locus coeruleus (LC)]. All DBH+TH expressing noradrenergic cell groups (LC, A1-A7) and epinephrine cell groups (C1-C3) are located caudal to the midbrain (see Mejias-Aponte et al. 2009). Conversely, the three main dopamine cell groups, the retrorubral field (A8), the substantia nigra (A9), and the ventral tegmental area (A10), are all located in the midbrain. And unlike the A1-A7 and C1-C3 cell groups, the vast majority of midbrain TH+ neurons co-express the dopamine transporter (DAT). DAT is thought to demark dopamine-releasing neurons; DAT co-localizes with TH at almost 100% in the midbrain, which is confirmed by the fact that stimulating DAT-Cre axons expressing channelrhodopsin induces dopamine transients in electrochemistry experiments (Fu et al. 2011, Trisch et al. 2012, Tecuapetla et al. 2011).

To uncover whether any of the TH+ axons in the SC were from traditional DAT-expressing midbrain dopaminergic zones, we obtained SC slices from a DAT-IRES-Cre knock-in mouse crossed to the floxed-tdTomato reporter line (DAT-tdTomato). We immunostained these slices with our TH antibody and an antibody targeting the DAT protein. Both TH and DAT immunostaining showed nearly 100% co-localization with DAT-tdTomato axons in the substantia nigra pars reticulata (SNr, Figure 3.8 a,b). However, in the exact same slices where SNr was robustly stained, neither the DAT antibody nor DAT-tdTomato showed dense dopamine terminals in the SC. In fact, the DAT antibody, despite showing strong expression and co-localization with TH+ axons and DAT-tdTomato axons in the SNr, (Figure 3.8c, right panel), did not show staining at all in most SC slices. DAT-tdTomato axons were consistently restricted to the superficial SC (Figure 3.8c, top middle panel and bottom panels), but these axons hardly ever co-localized with TH, indicating that they come from a set of neurons that do not create dopamine at the age tested (Figure 3.8c, bottom panels). We therefore conclude that the primary source of dopamine to the SC is not from typical DAT-expressing midbrain dopamine centers (A8, A9, A10).

3.3.5 - Retrobead Injections to the SC reveal A13 as a dopaminergic input: To determine the source of dopamine to the SC, mice were injected with latex microspheres (“Retrobeads”) known to enter axon terminals and transport retrogradely to cell bodies of efferent fibers. Two DAT-tdTomato mice and five C57B6 WT animals were injected into the SC during the second postnatal week and perfused approximately two weeks later. Brain slices were prepared and immunostained for TH and DAT.

As suspected from SC immunostaining in section 3.3.4, DAT+, TH+ neurons in the main dopamine centers of the midbrain (A8, A9, A10) were not labeled with retrobeads in any injected animal. A previous report described a projection from a GABAergic subset of SNr dopamine neurons to the SC (Campbell et al. 1991, Takada et al. 1988). Retrobeads *were* consistently observed in the substantia nigra pars reticulata, which is a main source of tonic GABAergic inhibition to the SC (Hikosaka and Wurtz 1985), but these retrogradely labeled neurons were never TH+ or DAT+ (Figure 3.9a). Moreover, the previously mentioned studies detailing a SNr-SC dopamine connection from GABAergic SNr dopamine cells are unlikely to be correct because VGAT+ co-localization with DAT antibody or DAT-tdTomato neurons was never observed in the SNr in this study (2 DAT-tdTomato x VGAT-Venus mice; see Figure 3.9b).

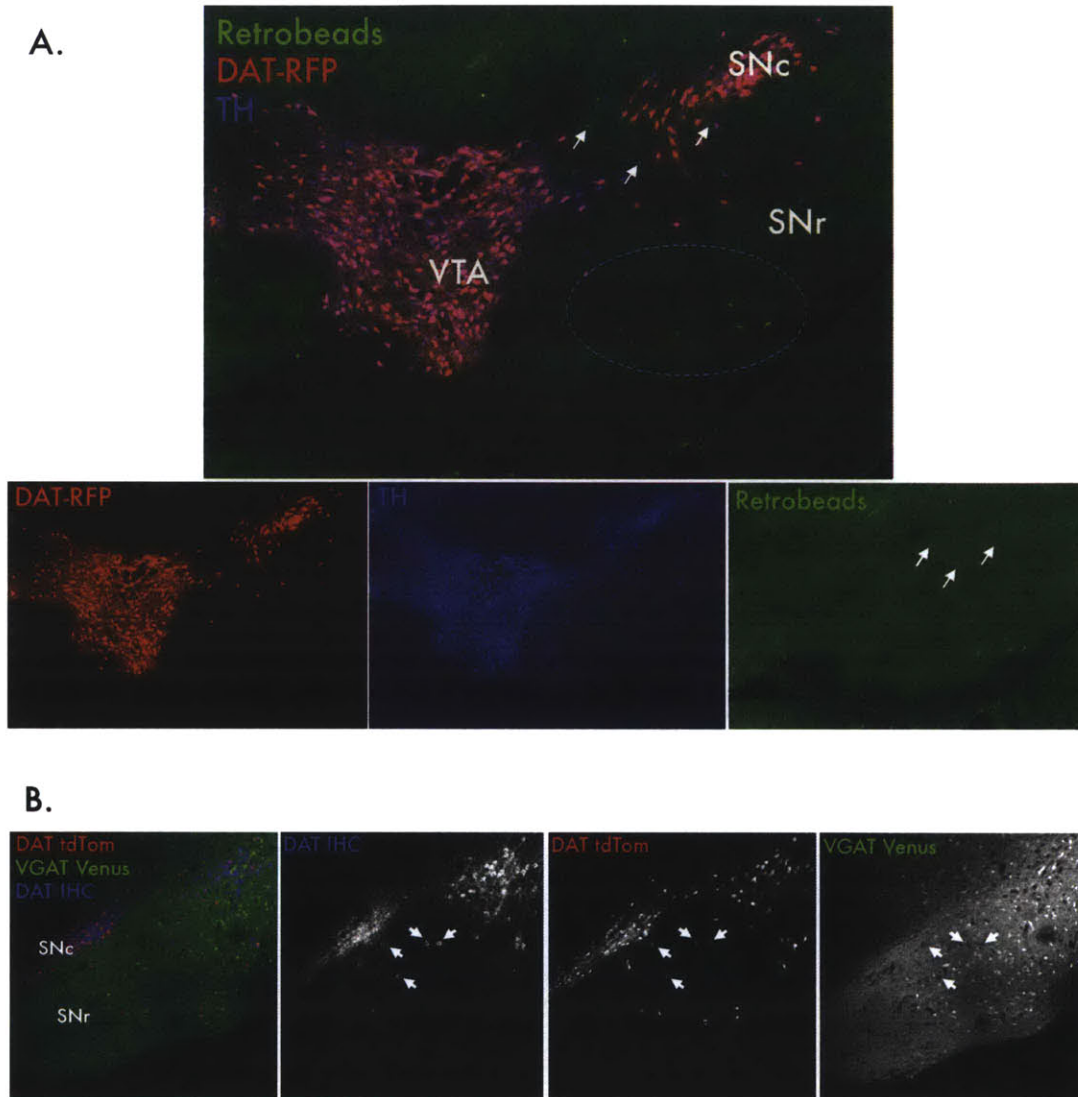


**FIGURE 3.9 – Retrobeads do not label SNr dopamine neurons and SNr dopamine neurons do not express VGAT.** Green retrobeads were injected into the SC of DAT tdTom and WT mice. Retrograde labeling of the SNr was always observed (A, top panel). However, we never noted any co-localization between SN dopamine neurons and retrobeads (see arrows that represent the only retrobead labeling in DAT/TH+ regions – they do not fill dopamine cells). SNr cells do sometimes express TH and DAT; however, in addition to never receiving retrograde label in our studies, we never noted overlap between DAT and VGAT (see arrows indicating DAT+ neurons that localize to VGAT negative holes), making a previous suggestion that GABAergic SNr cells project dopamine to the SC unlikely. (\*This injection covered all layers of the SC).

Although midbrain dopamine neurons were void of retrobeads in all animals studied, two TH+ cell groups were consistently hit with retrograde label. The first group is the locus coeruleus, a noradrenergic hindbrain region previously shown to project strongly to the superficial SC (Arce et al. 1994; Figure 3.10 b). This cell group has been recently shown in numerous reports to co-release dopamine and norepinephrine, which provides a possible basis for dopamine receptor activation in the SC (Devoto et al. 2005a, Devoto et al. 2005b).

The second retrogradely labeled TH+ region that was not previously known to project to the SC is the A13 cell group of the zona incerta. This cell group is known as the only completely DAT negative, TH positive dopamine group in the brain (Tritsch et al. 2012). All seven injections showed retrograde labeling of A13, which never stained positive for DAT antibody nor showed DAT-tdTomato expression (Figure 3.10 c).

We also managed to identify why there was a small subset of DAT-tdTomato positive axons in the superficial SC that did not stain for TH (Figure 3.8). Although TH+ DAT-tdTomato cells were completely absent of retrobeads in the midbrain (Figure 3.9), a small packet of hindbrain neurons lying just underneath the 4<sup>th</sup> ventricle was retrogradely labeled in both injected DAT-tdTomato mice. These neurons were void of TH (Figure 3.11) and also were not stained by the DAT antibody, indicating a lack of dopaminergic identity in the adult animal. Due to the DAT reporter being an IRES-Cre, DAT was, in fact, expressed in this cell population at some point during development. Whether this population ever expressed TH or provided dopamine to the SC is unknown.

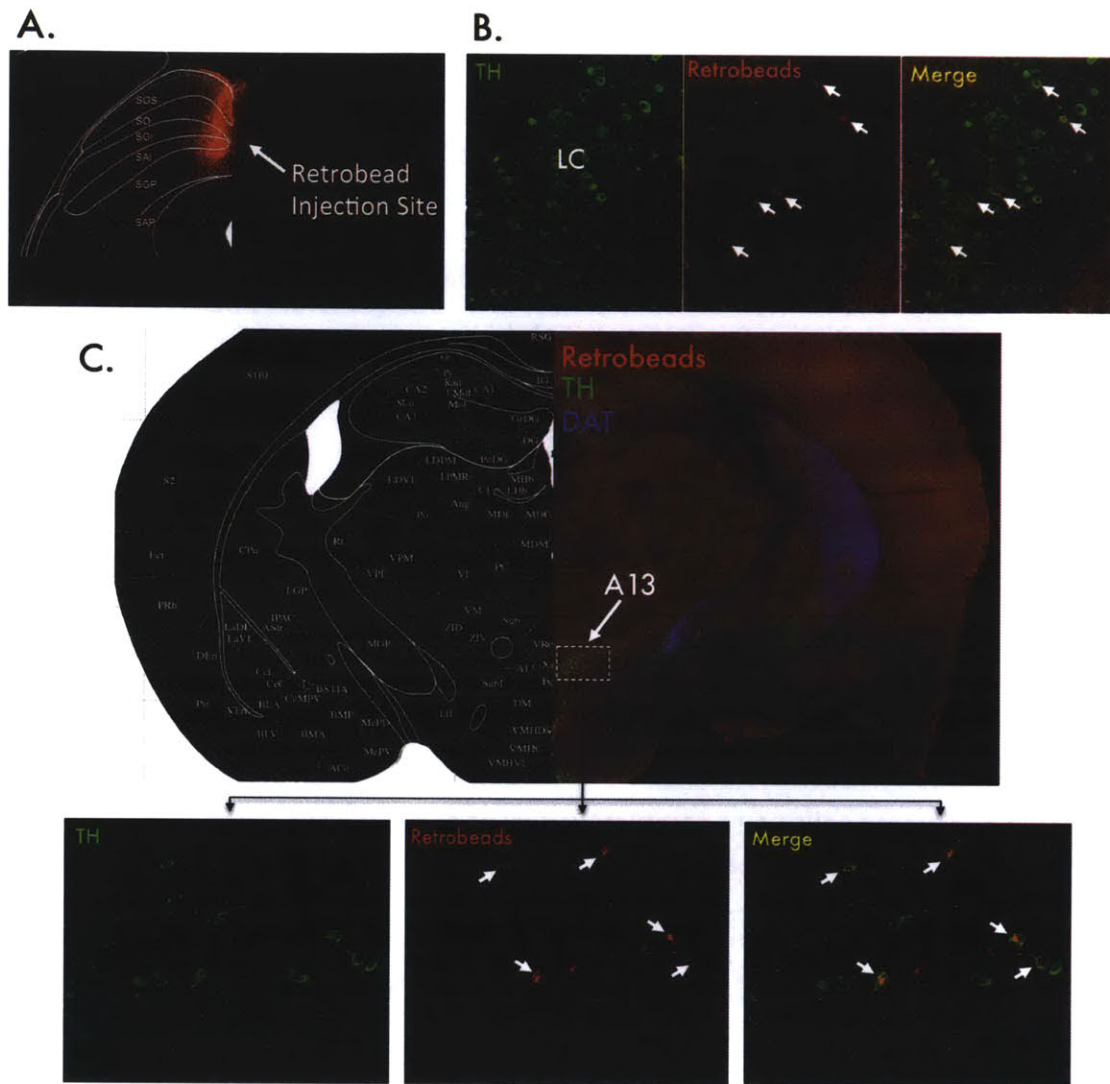


**FIGURE 3.10 – Retrobead injection into the SC labels the locus coeruleus and A13.** A) Injection site hits the superficial SC, intermediate SC, and deep gray layer of the SC. B) Retrobeads are found in TH+ neurons of the locus coeruleus. C) A13 is located in the zona incerta near the midline in the diencephalon. It does not stain positive for DAT despite the fact that the DAT antibody strongly labels axons in the vicinity of A13. TH+ neurons in A13 were retrogradely labeled with retrobeads in all seven injections.

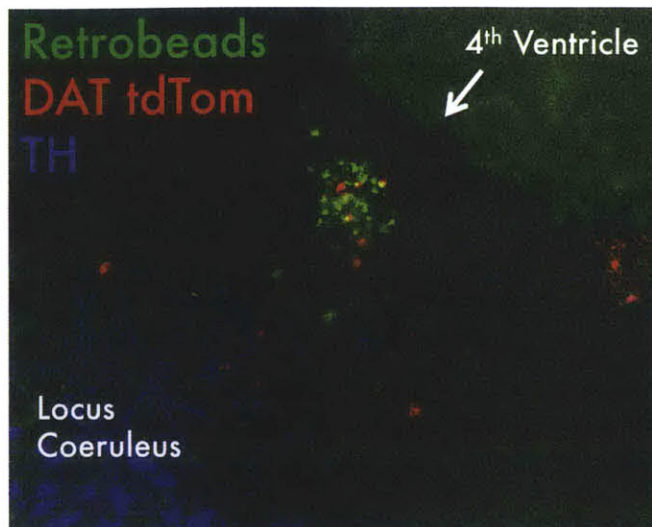


**FIGURE 3.11 – DAT tdTom +, TH- neurons in the dorsal hindbrain project to the SC.**

Retrobead injection into the SC labels a small population of DAT tdTom + neurons in the dorsal hindbrain, just ventral to the 4<sup>th</sup> ventricle near the locus coeruleus. These neurons never stained for TH+ and were retrogradely labeled in both DAT tdTomato mice. They likely represent the source of DAT tdTom+, TH negative axons in the superficial SC that also do not stain positive for DAT (Figure 3.8).

*3.3.6 - Dopamine alters electrophysiology of D1 and D2 neurons:* Once dopamine arrives from its zona incerta or locus coeruleus source, it likely acts on D1 and D2 receptors in the SC. Patch clamp electrophysiology was used in sagittal SC slices to determine how D1+ and D2+ cells respond to dopamine. D1+ neurons in the superficial SC were current clamped while the axons in the optic layer were electrically stimulated every 5 seconds. This was meant to mimic visual input via stimulation of retinal ganglion and visual cortex terminals. Stimulation intensity was increased until consistent spikes in the postsynaptic D1+ cell were evoked. When dopamine (50  $\mu$ mol) was washed onto the slice, we observed a severe and reversible elimination of spiking (Figure 3.12). This effect was sometimes, but not always, coupled to a negative shift in resting potential, and the drop in resting potential was not required to eliminate spiking (Figure 3.12a). Multiple possibilities could explain how dopamine is reducing D1+ neuron firing in response to visual input. First we tested if the excitatory currents evoked by SO stimulation were modified by dopamine. This was the case.

In voltage clamp, D1+ neurons were held at -70 mV in  $Mg^{2+}$  containing ACSF with 20  $\mu M$  gabazine. This setup isolates AMPA currents in response to visual input. AMPA currents dropped an average 67% when dopamine was added to the bath ( $p < .005$ ,  $n = 9$ , Figure 3.12b).

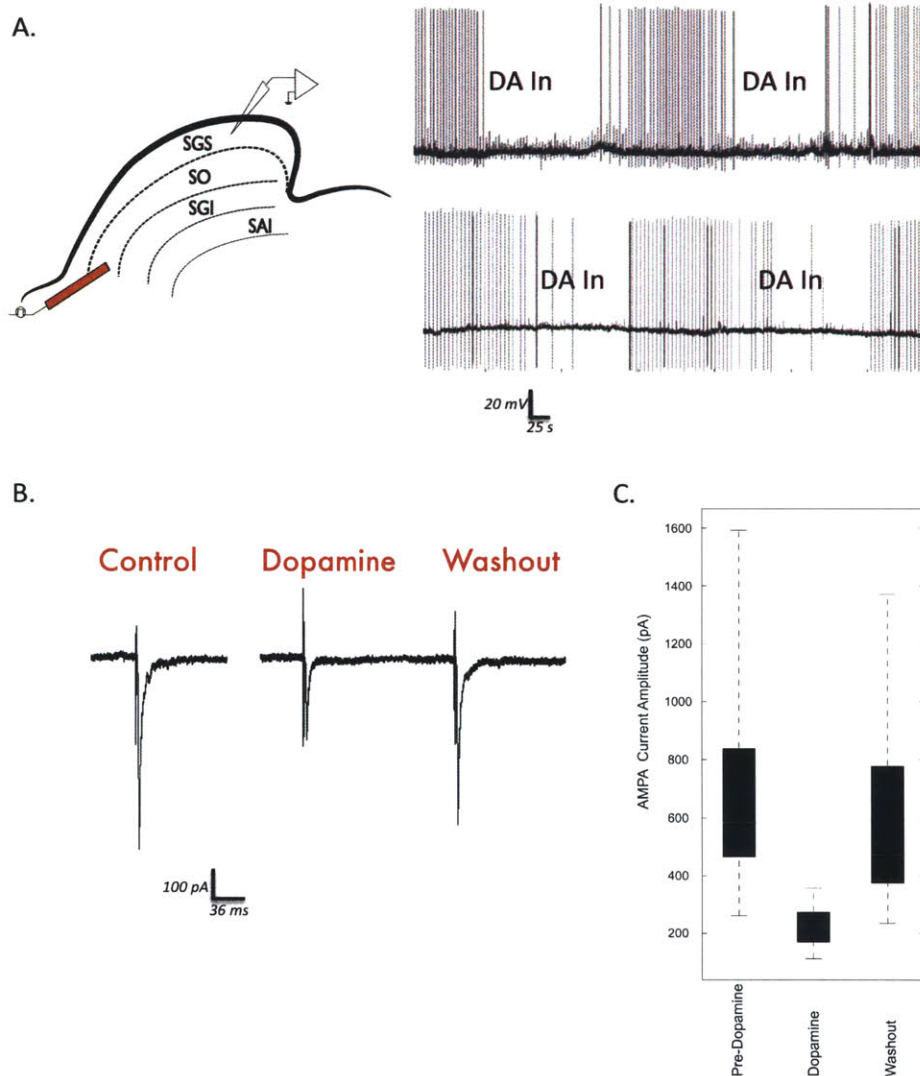


**FIGURE 3.12: D1 expressing neurons respond to dopamine with reduced spiking and decreased AMPA currents.** D1+ neurons were patched in the SGS and driven to spike threshold by SO electrical stimulation. When dopamine was washed onto the slice (50  $\mu M$ ), spiking was reversibly eliminated, often times in the absence of a resting voltage shift (A). In voltage clamp, in the presence of gabazine and magnesium, AMPA EPSCs induced by SO stimulation were reversibly decreased by dopamine, providing a basis for understanding the reduced spiking to visual input.



D2+ neurons were also current clamped to read out resting membrane potential. This resting potential dropped, sometimes severely (see Figure 3.13), when dopamine (50  $\mu\text{M}$ ) was washed into the bath. Resting voltage dropped by an average of 5.28 mV upon dopamine washin ( $p \leq .001$ ), an effect that was also reversible upon dopamine washout.

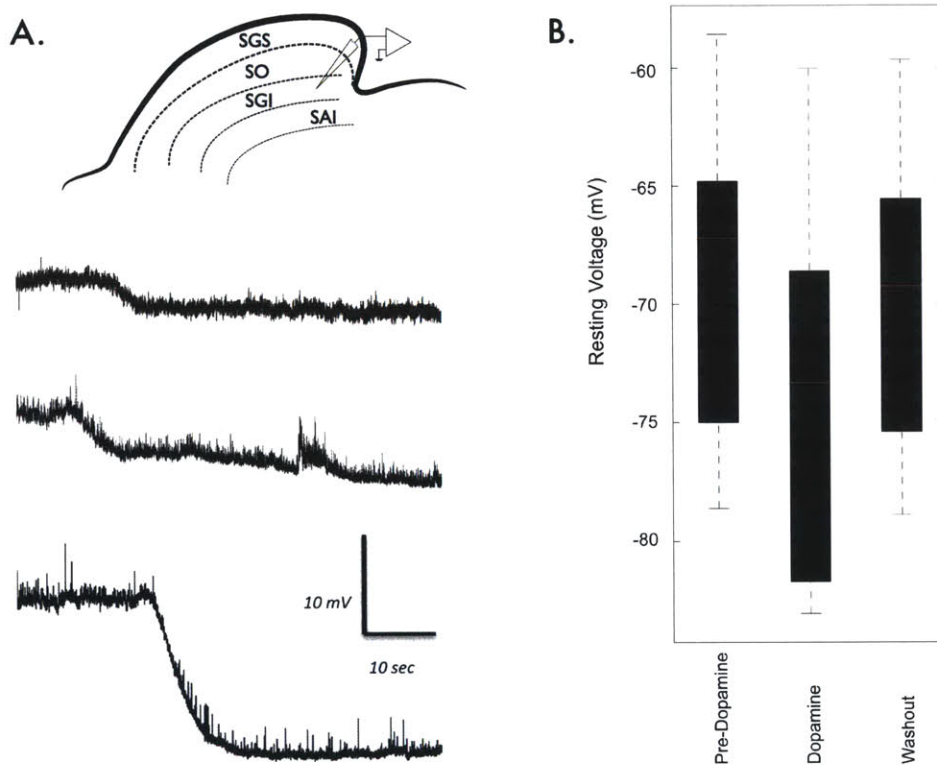


**FIGURE 3.13 – D2 neurons respond to dopamine with resting voltage hyperpolarization.** D2+ cells were recorded in the intermediate SC in current clamp. Resting voltages were typically between -65 mV and -75 mV (B). When dopamine was added to the bath (50  $\mu\text{M}$ ), all neurons tested showed a reversible drop in resting voltage. Some resting drops were severe (A, bottom trace = 15 mV shift).

### **3.4 -Discussion:**

Two major findings were uncovered in this chapter. First, dopamine receptors are organized in an interesting pattern in the mouse SC, with D1 enriched in the SGS and D2 showing the highest density in the deeper SC layers. This means that D1 lies in the visuotopic map of the SC while D2 is enriched in the multisensory SC that is also arranged in a motor map. Second, the source of dopamine to the SC is likely the LC and/or A13, not the midbrain retrorubral field, SN, or VTA. The SC likely responds to this input with two forms of depression: AMPA current reduction on D1 neurons and resting voltage hyperpolarization on D2 neurons.

We began this study by showing that transcripts encoding two dopamine receptors, D1 and D2, are strongly expressed in the SC (Figure 3.1). Reporter mice that indicate the location of D1+ and D2+ expressing neurons show that D1+ cells in the SC are preferentially enriched in the superficial SGS layer of the SC while D2+ cells are found throughout the deeper layers, especially in the medial SO and intermediate layers (Figure 3.2, 3.3). The only difference in the rostro-caudal patterning of these receptors was the presence of “D2 islands” in the rostromedial deep SC. These islands correlate well with the location of “fixation” neurons from the saccade literature which upon stimulation prevent saccades (Hall and Moschavakis 2004). The discovery of these cells lead to the “moving hill hypothesis” of SC orientation. The idea is that the amplitude of orientation movements an SC neuron will induce can be read out neurally by how far away it is from a fixation cell. Once a “moving hill” of activity is initiated, activity proceeds down the caudo-rostral axis of the SC until it arrives at SC fixation cells, which stop the movement. If D2 receptors can modulate these cells, they would be in a unique position to influence the amplitude of orienting movements (see Hall and Moschavakis book, 2004).

With regards to the inhibitory / excitatory nature of D1+ and D2+ populations, D1+ neurons in the superficial SC were primarily GABAergic (73%; Figure 3.4) while D2+ neurons tended to overlap with VGAT negative neurons (63% VGAT-). It is possible that this arrangement means that dopamine inhibition of GABAergic cells in the SGS would enhance visual input, while hyperpolarization by dopamine of excitatory D2+ neurons could reduce orienting movements.

As noted, dopamine is present in the SC at a higher concentration than frontal cortex or hippocampus (Versteeg et al. 1976) and TH+ axons were densely present in the mouse SC, showing no discrimination according to SC layer (Figure 3.8). Moreover, the COMT-generated dopamine breakdown product 3-MT, which does not arise after norepinephrine or epinephrine COMT-methylation, is strongly expressed in the SC (~1:5 SC to striatum; Weller et al. 1987). These results indicate that endogenous dopamine likely activates the D1 and D2 populations described in this study. The fact that 3-MT is highly expressed in the SC is not surprising considering our result that COMT transcripts are highly expressed in the SC (Figure 3.1). The dopamine transporter DAT clears dopamine from synapses for reuse and does not generate 3-MT: antibody binding to the dopamine transporter was absent in the SC (Figure 3.8c) and mRNA expression of *Slc6a3*, the gene encoding DAT, was also completely absent of reads in our RNAseq experiment. This is not the case in the striatum where DAT antibody binding is abundant at dopamine terminals (Ciliax et al. 1995; personal observations). The fact that DAT mRNA and DAT immunostaining were undetectable in the SC was the first hint that the main DAT+ midbrain dopamine centers (retrosubstantia nigra, ventral tegmental area, substantia nigra) were not the primary source of dopamine to D1+ and D2+ SC neuron populations.

DAT-IRES-Cre x floxed-tdTomato mice (DAT-tdTomato) showed dense axon labeling across the brain from DAT-Cre+ neurons. However, DAT-tdTomato axons were rarely present in the D2+ neuron zones of the SC (Figure 3.8). DAT-tdTomato expression was observed in a thin region of the superficial SC (Figure 3.8). However, these DAT-tdTomato terminals did not co-localize with TH and likely arose from a population of TH-, DAT-, DAT-tdTomato + cell bodies lining the 4<sup>th</sup> ventricle in the hindbrain (Figure 3.11). It is possible that since this population expresses a DAT-IRES-Cre, it previously delivered dopamine to the SGS at an early developmental timepoint, eventually losing its dopaminergic identity in adulthood.

The lack of robust DAT+ axons in the SC was supported by retrograde labeling experiments. Injections of retrobeads into the SC consistently labeled only two TH+ cell groups: the locus coeruleus group of norepinephrine neurons and the A13 zona incerta group of dopamine neurons (Figure 3.10). These areas were void

of DAT immunostain or DAT-tdTomato label in our studies. We could not confirm a previously described projection from dopaminergic neurons co-expressing GABA in the SNr to the rat SC (Campbell et al. 1991). We did find labeling in the SNr in all brains injected with retrobeads into the SC (Figure 3.9); however, these were likely the oft-described GABAergic cells that tonically inhibit the SC (Hikosaka and Wurtz 1995; Basso and Wurtz 2002) as they never co-localized with TH in our study (Figure 3.9). Moreover, we never found co-localization of DAT antibody nor DAT-tdtomato with VGAT+ neurons in the VGAT Venus mouse (Figure 3.9b). It is possible that our retrobead injections were simply not uptaken by terminals described by Takada and Campbell. The methods used to identify GABAergic cells and TH+ cells were also different, and it is possible that the rat's SC does receive this input but the mouse does not.

TH+ axons in the superficial hamster SC were previously shown to co-localize with DBH, the norepinephrine-producing enzyme, at a 92% rate. This previous study determined the locus coeruleus as the primary source of the DBH+, TH+ projection to the superficial SC (Arce et al. 1994). We surmise that the remaining 8% of TH+, DBH- axons in the SC are from the dopamine cell group A13, the only other consistently labeled TH+ cell group found in our retrobead experiments. Additionally, it is possible that the locus coeruleus delivers both dopamine and norepinephrine to the SC. As noted in section 3.3, TH produces dopamine first, which is eventually converted to norepinephrine. Therefore, if TH is present in terminals, dopamine is present until DBH conversion of dopamine to other catecholamines. A recent line of research has found that this intermediate dopamine is co-released with norepinephrine from locus coeruleus terminals (Devoto et al. 2005a, Devoto et al. 2005b). Moreover, a second line of new research describes the promiscuity of dopamine receptors regarding which catecholamine activates them. Norepinephrine, for example, can activate D2 receptors, which modulates HCN currents (Arencibia Albite et al. 2007). Dopamine is also known to strongly activate norepinephrine receptors in the entorhinal cortex (Cilz et al. 2013), indicating that the nomenclature of dopamine and norepinephrine receptors may be better well served if changed to "catecholamine receptors". If these receptors are as

promiscuous as described in recent literature, it will be interesting to uncover why the brain uses both neurotransmitters and both receptor subtypes (eg. noradrenergic and dopamine receptors). It may be possible that the locus coeruleus does only release norepinephrine from its TH+ SC terminals, but that this norepinephrine can activate the D1+ and D2+ neuron populations in the SC.

Dopamine always induced a drop in resting potential in every D2+ neuron tested. These effects were often severe (sometimes reaching 15mV drops; Figure 3.13) and under such conditions would practically shut down D2+ SC neurons. Coupled to the strong reduction of EPSCs in D1+ neurons (Figure 3.12), it appears that dopamine is primarily inhibitory to SC neurons. However, considering both populations' propensity to co-localize with VGAT to some degree, the results on neural circuit function are likely complex and require a more thorough investigation. Moreover, to understand how dopamine influences the SC, it is critical to discover how A13 responds during tasks typically thought to require dopamine; A13 may also be involved in tasks not normally related to dopamine. Linking behaviorally relevant dopamine neuron activity in A13 to dopamine release and D1+ / D2+ cell modulation in the SC should be the primary goal of future research on SC dopamine. Considering dopamine's significant electrophysiological effects on the SC, it is possible that A13 is in a position to modulate the "state" of the SC. With its ability to hyperpolarize the very neurons that induce orienting movements in the intermediate SC (Northmore et al. 1988), dopamine release in the SC via A13 could modulate how animals attend and interact with their spatial environment.

**CHAPTER 4:**

***Conclusions and Future Directions***

**4.1 – Introduction:** This thesis originally sought to establish a research program that bridged the behavioral, neurophysiological, and genetic perspectives on schizophrenia. No doubt, there have been many wonderful research angles not considered here. For example, I once had a talk with Mike Merzenich where he told me, in as much, that he could cure schizophrenia patients with the right battery of computer-based cognitive “exercises”. James Watson once called schizophrenia a “learning disorder”, which I admittedly don’t quite understand and certainly did not address. I also did not address that the outcomes of patients with the exact same treatment patterns (i.e. using dopamine receptor based drugs) are often wildly variable, and that trying to pin down one neural system to the disorder might be a fruitless endeavor.

I never touched upon some of the more unique symptoms of schizophrenia that may provide insight into how the brain is affected in the disease. One facet of schizophrenia pathology that always amazes me is the patient’s fear of being watched or controlled. What are the voices the patients hear and why are these voices so negative? My wife, who runs a first episode psychosis clinic at Mclean Hospital, comes home with a new fantastical story every night about the complexity of schizophrenia symptoms. The disease appears to be as variable as human personality because it *is a disorder of the personality*. One might argue that reducing schizophrenia to an upregulation of one chemical or a defect in one brain area is at best short-sighted and at worst delusional, because a properly working personality likely requires almost every brain region and every neurochemical system. Is this really the case though? In my experience with schizophrenia patients through my wife’s charitable work, it seems like they can see, hear, talk, have ideas, desires, etc. Schizophrenia patients call my house constantly, and they always have very relatable problems like a broken air conditioner or feeling sad that a person they love doesn’t love them back. One patient posts videos about his psychosis on Youtube. Can a person with a totally defective brain understand the concepts of video recording, much less have the wherewithal to post them to the internet?

There are certain symptoms of schizophrenia, like auditory hallucinations, disorganized or delusional speech patterns, and working memory deficits that do

appear to be relatively consistent. Personally, though, at the end of 6 ½ years of graduate school, I believe that the most worthwhile pursuit in the face of severe neurological disorders is to understand how the brain computes, not how its computing power breaks when we perform broad interventions. We have to ask questions in the spirit of David Marr's "Vision". Questions like: what is a voice to the brain and how is it represented and manipulated? What algorithm is the brain using to distinguish "real" from "simulated" voices and how does the brain in general distinguish reality from its own inner workings (i.e. where is the "reality filter"?). This is not the same as asking "which brain areas light up when a voice is heard" or "does the subject stop hearing threatening voices if I remove his/her amygdala?" Observing and breaking don't hold much water without a clear model of the computations being performed.

This thesis didn't answer any profound questions about the brain, but there is science here and it is certainly worth criticizing. To me, spatial working memory is one of the brain's incredible accomplishments. I am still constantly amazed at how my brain knows exactly where my beer is on the table at this very moment so I don't kick it over when I shift my feet. Rory Kirchner and I originally intended this project to contain a behavioral working memory component to compliment the anatomy and electrophysiological work. We tried to mimic the delayed saccade task in mice using automated eye tracking coupled with computer-controlled reward delivery. The technology we built was actually quite successful, but it turned out that mice actually do not saccade very often, and when they do, the saccades are very small in amplitude. Although we were beginning to increase the frequency of saccades to a water reward, it was clear that developing an entirely new behavioral paradigm in the rodent could have been a thesis in itself and my committee suggested I abandon the project to focus on physiology and anatomy. I'm glad because these aspects of the project took 6 ½ years.

Despite the lack of a behavioral correlate, I do think that the data presented herein may provide insight into how the SC stores working memories. Whether this is important for understanding schizophrenia pathology is certainly debatable. I also think that my data have broad implications concerning how dopamine and its



byproduct homocysteine might affect many aspects of brain function and brain development. These ideas will be shared here along with criticisms and future directions.

**4.1.1 – Issues and future directions concerning the homocysteine project:** The main takehome from the homocysteine chapter (Chapter 2) is that an amino acid that is upregulated in many schizophrenia patients can strongly influence NMDAR currents. HCY's role in reducing NMDAR desensitization was studied using fast application of agonist to patch clamped neurons and transfected HEK cells. This method is excellent for identifying properties of neurotransmitters on single receptor types and we would not have been able to isolate the specific roles of GluN2A and GluN2B without the HEK cell preparation. However, flooding a cell with agonist for seconds may not be a good model for synaptic transmission in the brain. The scenario during which this sort of constant neurotransmitter binding would occur is sustained, seconds long, high frequency firing of one neuron onto another. This would hypothetically keep postsynaptic NMDA receptors saturated with glutamate for long durations. We think that this could occur during persistent activity, when excitatory feedback synapses receive glutamatergic input at upwards of 40 Hz (Goldman Rakic et al. 1996, Romo et al. 1998, Wurtz et al. 2001) for seconds long durations. This assumption might be a leap. There are high fidelity clearance mechanisms for glutamate that may allow resensitization of receptors during inter-spike intervals (Clements et al. 1992). Moreover, it is unclear whether the exact same synapses are stimulated on every pass through a recurrent excitatory loop as described in Chapter 1 (Figure 1.7a). Lastly, there is likely short-term presynaptic depression or enhancement occurring (Zucker and Regehr 2002) that may play an even more important role than channel desensitization in shaping glutamatergic responses during high frequency firing.

Another important question is whether HCY is even present at synapses. HCY is found in the CSF (Regland 2004) and it is known to be released from glia (Huang et al. 2005), but no studies have ever localized HCY to synapses in an intact fixed brain. There is an HCY antibody available and it could be gold-conjugated in order to

perform immunogold experiments followed by electron microscopy. If I were going forward with this project, this is the first thing I would do. If HCY is bound to synaptic receptors in the brain, especially in regions that express COMT but no DAT at dopaminergic terminals (and would therefore be prone to dopamine breakdown / HCY production instead of dopamine uptake), a role for HCY in synaptic modulation would be more likely. Measuring density of the gold particles at synapses could reveal whether the concentrations used in this study could be achieved *in vivo*.

Developing a realistic method for evoking HCY release in the brain is also an important next step. Washing HCY onto slices or cultured cells produced myriad effects. However, the brain is not floating in 500  $\mu\text{mol}$  of HCY. What is the mechanism by which HCY leaves glia in the brain? Is HCY in vesicles that are actively released like homocysteic acid (Benz et al. 2004)? The immunogold study would go a long way to answering this question, but the next functional step is evoking HCY release onto synapses and recording how this release affects NMDAR currents in a more intact preparation.

The temporal dynamics of dopamine to HCY conversion are also important to uncover. For example, when dopamine neurons fire phasically as they do during Wolfram Schultz-like reward learning paradigms, it would be interesting to find out whether synaptic rises in dopamine are followed by immediate synaptic rises in HCY. The temporal relationship between dopamine neuron firing, dopamine release, and subsequent production of neuroactive dopamine byproducts like HCY must be understood. Figuring out the timecourse of these effects could provide better insight into how dopamine neuron firing influences behavior via its afferent projection targets.

At the end of chapter 2, we reported use of caged glutamate to induce NMDAR desensitization in brain slices. To our knowledge, this was the first illustration of channel desensitization in a slice. HCY reduced caged glutamate-induced desensitization in all cells tested. If HCY is truly involved in schizophrenia pathology, and desensitization reduction of NMDARs is its primary role, then other molecules and genes involved in schizophrenia may affect NMDAR desensitization.

It would be interesting to try the caged glutamate experiment on slices from well-accepted model mice with “schizophrenia-like” phenotypes. It may be that NMDAR desensitization changes are a common feature of schizophrenia models and that desensitization itself is an important, yet relatively unexplored, feature of glutamate receptors *in vivo*. This is supported by research linking dysregulation of glycine, another amino acid that reduces NMDAR desensitization, to schizophrenia pathology (Neeman et al. 2005). However, it is still unknown what role NMDAR desensitization plays in the brain.

Most optimistically, let's assume that HCY *does* appear at synapses at the concentrations that reduce desensitization in our study. Even more optimistically, let's assume that the dopamine inputs that arrive in the SC are stimulated during working memory, allowing HCY to arise at NMDAR feedback synapses described in Figure 1.7b. One major constraint on the model put forth by Lisman et al. (1998) and Seung et al. (2000) is that NMDARs desensitize rapidly (Figure 2.1) when exposed to constant glutamate. If NMDARs desensitized during persistent activity, there could be no stacking of feedback EPSCs (Figure 1.7b, Figure 1.10) and NMDARs would stop supporting persistent activity after about 200ms. We know that this is not true, as animals and humans can perform working memory tasks over long delays (Park and Holtzman 1992), and NMDAR mediated persistent activity is thought to support these memories (Arnsten et al. 2012). What prevents NMDARs from desensitizing during persistent activity? Our study confirmed that glycine levels are low enough in intact neural circuits for HCY to modulate desensitization. We also think that we underestimate the amount of desensitization that might occur *in vivo* because cutting slices damages neurons, which contain glycine intracellularly to make proteins; in fact, glycine is the 4<sup>th</sup> most commonly used amino acid in proteins, meaning that intracellular glycine concentrations could impact extracellular concentrations if cells hemorrhage. Models predict glycine to be at ~150nM at synapses (Atwell et al. 1993), a concentration in which NMDAR desensitize almost fully in 200 ms (Mayer et al. 1989). HCY, therefore, may be required for desensitization prevention in the brain, meaning that at sub-pathological concentrations, HCY may be beneficial for brain function. This could be

why the brain uses both COMT *and* DAT as dopamine clearance mechanisms (Figure 1.12): COMT may be necessary for HCY production, which is supported by the fact that COMT is more highly expressed in regions that show persistent activity (eg. PFC, SC). HCY at proper concentrations could be the very mechanism that prevents high frequency excitatory feedback from immediate desensitization (Figure 4.1)

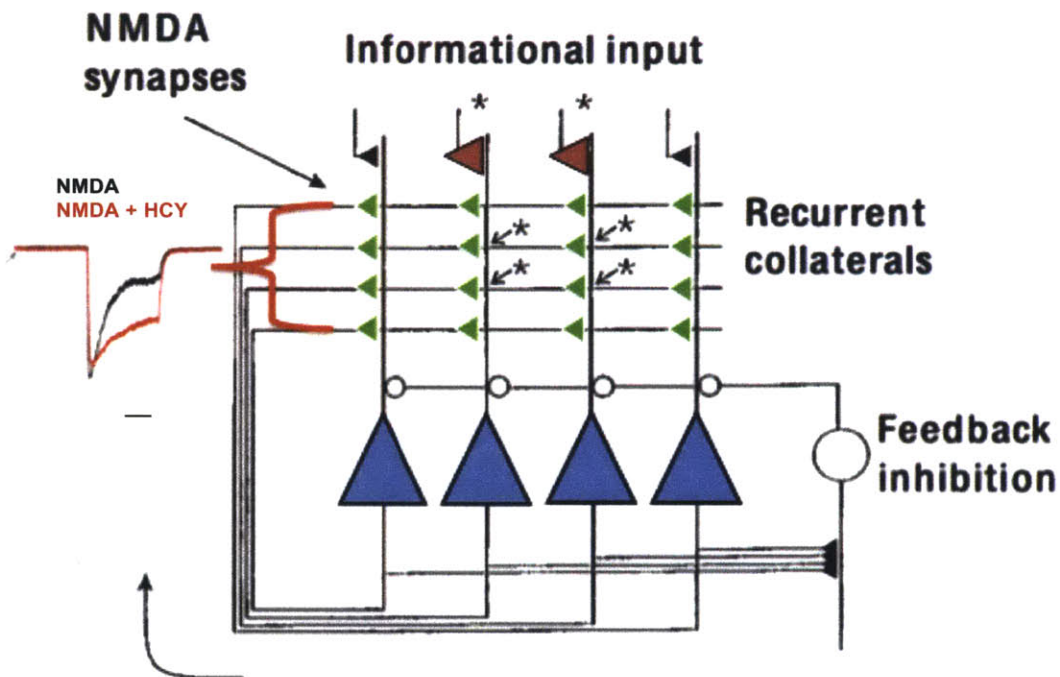


**FIGURE 4.1 - NMDAR feedback model “on HCY”:** If starred neurons are activated by informational input, and store this input via recurrent excitatory activity mediated by NMDARs, some mechanism must exist to prevent NMDARs from desensitizing. The presence of HCY could be the mechanism by which persistently active neurons remain robust to NMDAR desensitization. Scalebar on trace = 500ms.

During pathological states of heightened HCY, two possibilities come into play. First, it is possible that high concentrations of HCY could reduce the amplitude of GluN2B receptors as in our HEK cell study. Reducing the amplitude of GluN2B NMDAR responses would certainly hurt performance of the NMDAR feedback model. GluN2B receptors are present in feedback synapses in the PFC and GluN2B antagonists

reduce persistent activity (Arnsten et al. 2012, Wang et al. 2013). A second possibility is that some NMDAR desensitization is required for *persistent activity to end*. NMDAR desensitization may actually be a built-in mechanism to prevent runaway feedback excitation.

What would be the consequence of runaway persistent activity? My prediction would be that previously correct answers on working memory tasks would remain “on”; that is, the neurons that were activated by previous sensory input would still be saying “remember this target” even after the task is completed. Amazingly, this is the exact pattern by which schizophrenia patients fail working memory tasks. The patients do not simply fail to remember items; they provide previously correct answers (Park and Holtzman 1992), and provide these incorrect answers with high confidence that they are, in fact, correct (Mayer and Park 2012).

**4.1.2 - Issues and future directions concerning the dopamine SC project:** In our dopamine study, we directly sequenced Drd1a and Drd2 mRNA in 3 lanes of 3-4 rat colliculi. These RNA sequencing results showed high expression of only these two receptor subtypes, which is in accordance with some previous literature describing the presence of SC D1 and D2 receptors in the rodent brain (Huang et al. 1992, Mansour et al. 1992, Bouthenet et al. 1991; but see Weiner et al. 1991) and the absence of SC neurons in any Drd3 reporter lines (GENSAT KJ302, KJ291, KI196) or the Drd4 reporter line (GENSAT W18). Although Drd5 was relatively low in the SC (1:7 D5:D2), we did attempt to characterize its location using the only published commercial antibody (Drd5 Santa Cruz). However, this antibody stained Drd5 KO animals strongly so we abandoned Drd5.

One major finding of the dopamine study was that the zona incerta cell group A13 is likely the primary dopamine source to the SC; not the major midbrain dopamine centers (A8, A9, A10). This result was kind of a strange one. First, it had already been documented, in multiple papers (but from the same lab), that a dopamine projection arises from the substantia nigra pars reticulata (Campbell et al. 1991, Takada et al. 1988). This projection was supposed to co-release GABA and dopamine because the neurons expressed GAD (Campbell et al. 1991). Our results in

the VGAT Venus mouse (Figure 3.9b) are in direct contrast to the existence of dopaminergic GABAergic neurons in the SNr. New research *has* pointed to co-release of GABA and dopamine from the SNc and VTA (Tritsch et al. 2012). However, the neurons do not actually make GABA and they use VMAT (vesicular monoamine transporter) to package GABA into vesicles (Sabbatini SFN poster). We identified no neurons in the SNr that use the traditional GABA packaging molecule VGAT and also express the dopamine transporter, which is expressed by 97-99% of TH+ neurons in this region (Tritsch et al. 2012). This fact, coupled to the absence of TH and retrobead co-localization in our retrograde tracing studies, makes Takada and Campbell's projection relatively unlikely.

So what does A13 do? It was relatively easy, when we thought SNr was the dopamine source, to come up with a behavioral role for the dopamine inputs to the SC. The SNr tonically fires upon the SC, keeping it inhibited until orienting movements are generated. This tonic inhibition releases just before movements, and if it is removed in monkeys, saccades are generated freely (Hikosaka and Wurtz 1985, Basso and Wurtz 2002). If dopamine were released from SNr terminals implementing tonic inhibition, it would be relatively easy to fit dopamine's AMPA and resting potential depressing properties into this framework.

A13, however, is a different story. A pubmed search for "A13 superior colliculus" yielded one result, and it was irrelevant. The zona incerta, inside which A13 is embedded at its most medial pole, is an understudied brain structure as well. Interestingly, Romanoswki et al. (1985) identified a projection from the zona incerta to the SC via retrograde labeling. It is clear from this paper that retro-labeled neurons are in the vicinity of A13, but a conclusion cannot be drawn on exact co-localization without a TH stain. Another more recent study found a projection from A13 to the dorsolateral periaqueductal gray; this paper actually mentions, without showing it, an A13 -> SC projection (Messanvi et al. 2013). We therefore seem to be tapping into a real projection with an as yet unknown role in behavior.

Currently, the role of A13 in behavior is completely unknown as far as I can tell. A query for "A13 behavior" yielded only the Messanvi et al. anatomy reference as a relevant hit. Therefore, until somebody studies how A13 is activated, if it truly

releases dopamine, if it is related to working memory at all, or if it is related to traditional Schultz like reward paradigms, it will be very difficult to come up with a functional role for dopamine in the SC.

One missing piece of this thesis is the pattern of axons arising from A13 to the SC; do the axons hit both D1 and D2 enriched zones of the SC? Is there a role for the locus coeruleus in SC dopamine signaling? These questions are being addressed using floxed-GFP AAV injections into TH-Cre mice. I have injected ~30 mice in the last month and will be processing them for histology in the next few weeks to examine the termination patterns of TH+ terminals from the LC and A13.

With regards to the electrophysiology results presented in Chapter 3, I have become very unsatisfied in general with drug wash-on to slices. Schultz (2007) has consistently shown that dopamine neurons are tonically active in the brain; destroying these tonically active connections to the SC upon slicing removes the true dopamine inputs. During wash-on, how do we know we are activating receptors that are targeted by dopamine axons in the brain? To circumvent this problem, we originally intended to use channelrhodopsin injections into the DAT-Cre mouse. Obviously, however, Figure 3.8 showed us that DAT+ terminals are at most an ultra-minor dopamine source (we found axons from time to time, but often times inspected entire SC slices without noticing even one TH+ DAT+ axon). We switched to the TH-Cre mouse, but find that there are hundreds of TH negative Cre+ neurons in the adult, unlike DAT-Cre. In fact, there are many neurons in the SC itself that express TH-Cre. TH expression might occur here during development but the TH-Cre is not a true reporter in the adult.

Moreover, we have already found numerous TH negative cell bodies in A13 that report Cre+ in the TH-Cre; therefore, any electrophysiological effects induced by ChR stimulation of TH-Cre terminals would be suggestive at best.

This does not preclude us from using the TH-Cre for anatomy. False positives are not a problem if you have a control for TH+ identity, which we do with our antibody. We hope to have axons projecting from A13 to the SC labeled soon and will then have an idea about how A13 might influence the D1 and D2 populations in the SC.

Another major point of confusion in Chapter 3 is how to interpret the enrichment of D1 and D2 positive neurons in specific regions of the SC. For example, what does it mean that D2 does not overlap with VGAT in the medial SO? What does it mean that just under those VGAT- cells is a population of small VGAT+ D2+ neurons? How do these results relate to the fact that cutting the SC from a monkey renders it a zombie agent? (Denny Brown 1962). Gidon Felsen at UC Denver is doing very nice work in the rat SC, studying its role in working memory and decision making during a robust odor task. However, using extracellular recordings, as he and Zach Mainen do in the SC, fails to identify the neuron types being recorded. Yes, it is clear that SC neurons are consistently keeping track of variables influencing decisions (Felsen et al. 2008, Krauzlis et al. 2004). But what types of neurons are these and how do descriptions of SC neural circuitry mesh with *in vivo* electrophysiology? At some point, it is important to use *in vivo* imaging, especially on a surface structure like the SC. Watching, in real time, which SC cells are responding during a well-characterized behavioral paradigm will be critical in eventually using findings reported in this thesis to understand dopamine's role. This kind of research may be better served in the zebrafish, where the optic tectum is under intense study and whole brain imaging is becoming more and more feasible.

One low hanging fruit that could be described using our current techniques is whether D1+ and D2+ SC neurons have specific axon projections to regions outside of the SC. Despite being similarly located within the SC, specific subtypes of SC neurons project to distinct structures in the brain. For example, wide-field vertical neurons in the SO project preferentially to the lateral posterior nucleus while non-WFV cells at approximately the same depth project more preferentially to the LGN (Mooney et al. 1988). Do D1 and D2 neurons have distinct projection sites outside the SC? It would not be surprising considering their enrichment in different SC layers. Understanding where D1 and D2 subpopulations project to would shed light on how depression of these cells by dopamine would affect downstream targets of the SC. We have preliminarily begun injecting D1-Cre and D2-Cre mice with AAV-flex-EGFP. One of our preliminary samples is shown here:





**Figure 4.2 – D1-Cre injected with AAV-Flex-EGFP.** We are currently injecting D1 and D2 Cre animals with AAV-Flex-EGFP virus. This will allow us to examine whether D1 and D2 expressing neurons have specific projections to different brain regions.

Interestingly, in addition to traditional target areas of the SC (lateral posterior nucleus, LGN, pons, pretectal nuclei), we have actually seen sparse axon termination in the zona incerta from both D1 and D2 mice. These data, however, are very preliminary and we will have to stain future injections with TH antibody to examine whether this termination is onto A13. We are also performing the same experiments using CLARITY because both D1 and D2 neurons project into the tortuous optic tract. Using CLARITY will avoid having to align multiple slices to reconstruct projection patterns.

Considering our observed possible termination in the ZI from the SC, it is tempting to wonder whether a feedback loop might exist between the SC and A13. Feedback neuromodulation is a very common feature of the SC, as has been most thoroughly shown by Alex Goddard and Eric Knudsen (see Knudsen 2011). One giant hand-waving reach before closing: imagine a scenario where the SC sees an

interesting input in the SGS and orients attention to it via SGI activation. The fact that attention has been grabbed by a stimulus means that it is likely worth analyzing. That is, any new input that arrives before the original stimulus has been analyzed shouldn't be permitted to wrest away attentional resources. If the SC projected to A13, and A13 immediately fed back dopamine that depresses excitability of the SC (decreased AMPA, decreased resting potential), dopamine feedback would prevent the SC from immediately orienting to another stimulus. This could be especially important during working memory tasks. After a spatial stimulus has been presented for memory, cells in the intermediate SC remember the input using persistent activity. During this activity, feedback A13 dopamine may depress the SC from responding to spurious stimuli before an answer has been provided. This would be a highly efficient way of preventing distraction as the circuit tries to hold on to input that is no longer present in the environment.

Although tempting, the previous paragraph is wildly speculative. It is currently unknown whether A13 even participates in working memory, let alone projects feedback dopamine back to the SC during working memory tasks. The first step from here is to implant electrodes into A13 while animals perform working memory tasks. Do A13 neurons show stimulus locked activity to reward predicting items like SN and VTA neurons do? (Schultz 2007). Does A13 receive a strong SC projection that activates dopamine neurons at short latency like it does to SN and VTA neurons? (Comoli et al. 2003). I for one will be answering these questions in frogs, attempting to model working memory deficits in this animal using natural prey capture behaviors. Hopefully this thesis provides a framework for combining molecular and anatomical results with eventual *in vivo* imaging of the tectum during behavior. Optimistically, I hope that I can eventually find out why D1 and D2 cells pattern like they do: why are D1 cells so likely to co-localize with VGAT in the SGS and what does this mean for the function of the circuit? What are D2 islands for? Lots of good questions lie ahead and I hope I am around to see them answered.

## REFERENCE LIST:

1. **Abdolmaleky HM, Cheng K-H, Faraone SV, Wilcox M, Glatt SJ, Gao F, Smith CL, Shafa R, Aeali B, Carnevale J, Pan H, Papageorgis P, Ponte JF, Sivaraman V, Tsuang MT, Thiagalingam S.** Hypomethylation of MB-COMT promoter is a major risk factor for schizophrenia and bipolar disorder. *Hum. Mol. Genet.* 15: 3132–3145, 2006.
2. **Aksay E, Olasagasti I, Mensh BD, Baker R, Goldman MS, Tank DW.** Functional dissection of circuitry in a neural integrator. *Nat Neurosci* 10: 494–504, 2007.
3. **Algaidi SA, Christie LA, Jenkinson AM, Whalley L, Riedel G, Platt B.** Long-term homocysteine exposure induces alterations in spatial learning, hippocampal signalling and synaptic plasticity. *Experimental Neurology* 197: 8–21, 2006.
4. **Applebaum J, Shimon H, Sela BA, Belmaker RH, Levine J.** Homocysteine levels in newly admitted schizophrenic patients. *J Psychiatr Res* 38: 413–416, 2004.
5. **Arce EA, Bennett Clarke CA, Rhoades RW.** Ultrastructural organization of the noradrenergic innervation of the superficial gray layer of the hamster's superior colliculus. *Synapse* 18: 46–54, 1994.
6. **Arencibia-Albite F, Paladini C, Williams JT, Jiménez-Rivera CA.** Noradrenergic modulation of the hyperpolarization-activated cation current (I<sub>h</sub>) in dopamine neurons of the ventral tegmental area. *Neuroscience* 149: 303–314, 2007.
7. **Arnsten AF, Cai JX, Steere JC, Goldman-Rakic PS.** Dopamine D2 receptor mechanisms contribute to age-related cognitive decline: the effects of quinpirole on memory and motor performance in monkeys. *J Neurosci* 15: 3429–3439, 1995.
8. **Arnsten AFT, Wang MJ, Paspalas CD.** Neuromodulation of thought: flexibilities and vulnerabilities in prefrontal cortical network synapses. *Neuron* 76: 223–239, 2012.
9. **Attwell D, Barbour B, Szatkowski M.** Nonvesicular release of

- neurotransmitter. *Neuron* 11: 401–407, 1993.
10. **Aultman JM, Moghaddam B.** Distinct contributions of glutamate and dopamine receptors to temporal aspects of rodent working memory using a clinically relevant task. *Psychopharmacology (Berl)* 153: 353–364, 2001.
  11. **Banke TG, Traynelis SF.** Activation of NR1/NR2B NMDA receptors. *Nat Neurosci* 6: 144–152, 2003.
  12. **Baron A, Montagne A, Cassé F, Launay S, Maubert E, Ali C, Vivien D.** NR2D-containing NMDA receptors mediate tissue plasminogen activator-promoted neuronal excitotoxicity. *Cell Death and Differentiation* 17: 860–871, 2009.
  13. **Basso MA, Wurtz RH.** Modulation of neuronal activity in superior colliculus by changes in target probability. *J Neurosci* 18: 7519–7534, 1998.
  14. **Basso MA, Wurtz RH.** Neuronal activity in substantia nigra pars reticulata during target selection. *J Neurosci* 22: 1883–1894, 2002.
  15. **Benveniste M, Clements J, Vyklicky L, Mayer ML.** A kinetic analysis of the modulation of N-methyl-D-aspartic acid receptors by glycine in mouse cultured hippocampal neurones. *The Journal of Physiology* 428: 333–357, 1990.
  16. **Benz B, Grima G, Do KQ.** Glutamate-induced homocysteic acid release from astrocytes: possible implication in glia-neuron signaling. *Neuroscience* 124: 377–386, 2004.
  17. **Bergeron R, Meyer TM, Coyle JT, Greene RW.** Modulation of N-methyl-D-aspartate receptor function by glycine transport. *Proc Natl Acad Sci USA* 95: 15730–15734, 1998.
  18. **Bi GQ, Poo MM.** Synaptic modifications in cultured hippocampal neurons: dependence on spike timing, synaptic strength, and postsynaptic cell type. *J Neurosci* 18: 10464–10472, 1998.
  19. **Bigl V, Biesold D, Weisz K.** THE INFLUENCE OF FUNCTIONAL ALTERATION ON MONOAMINE OXIDASE AND CATECHOL-O-METHYL TRANSFERASE IN THE VISUAL PATHWAY OF RATS1. *J Neurochem* 22: 505–509, 1974.

20. **Bigl V, Biesold D, Weisz K.** The influence of functional alteration on monoamine oxidase and catechol-O-methyl transferase in the visual pathway of rats. *J Neurochem* 22: 505–509, 1974.
21. **Blom HJ, Wevers RA, Verrips A, TePoele-Pothoff MT, Trijbels JM.** Cerebrospinal fluid homocysteine and the cobalamin status of the brain. *J. Inherit. Metab. Dis.* 16: 517–519, 1993.
22. **Bobb AJ, Addington AM, Sidransky E, Gornick MC, Lerch JP, Greenstein DK, Clasen LS, Sharp WS, Inoff-Germain G, Wavrant-De Vrièze F, Arcos-Burgos M, Straub RE, Hardy JA, Castellanos FX, Rapoport JL.** Support for association between ADHD and two candidate genes: NET1 and DRD1. *Am. J. Med. Genet.* 134B: 67–72, 2005.
23. **Bolton AD, Phillips MA, Constantine-Paton M.** Homocysteine reduces NMDAR desensitization and differentially modulates peak amplitude of NMDAR currents, depending on GluN2 subunit composition. *Journal of Neurophysiology* 110: 1567–1582, 2013.
24. **Broch OJ, Fonnum F.** THE REGIONAL AND SUBCELLULAR DISTRIBUTION OF CATECHOL-O-METHYL TRANSFERASE IN THE RAT BRAIN. *J Neurochem* 19: 2049–2055, 1972.
25. **Campbell KJ, Takada M, Hattori T.** Co-localization of tyrosine hydroxylase and glutamate decarboxylase in a subpopulation of single nigroretinal projection neurons. *Brain Research* 558: 239–244, 1991.
26. **Cannon TD, Huttunen MO, Lonnqvist J, Tuulio-Henriksson A, Pirkola T, Glahn D, Finkelstein J, Hietanen M, Kaprio J, Koskenvuo M.** The inheritance of neuropsychological dysfunction in twins discordant for schizophrenia. *Am. J. Hum. Genet.* 67: 369–382, 2000.
27. **Carmel R, Jacobsen DW.** Homocysteine in health and disease.
28. **Chen L, Muhlhauser M, Yang CR.** Glycine transporter-1 blockade potentiates NMDA-mediated responses in rat prefrontal cortical neurons in vitro and in vivo. *Journal of Neurophysiology* 89: 691–703, 2003.
29. **Chen L, Yang XL.** Hyperpolarization-activated cation current is involved in modulation of the excitability of rat retinal ganglion

- cells by dopamine. *NSC* 150: 299–308, 2007.
30. **Christie LA, Riedel G, Platt B.** Bi-directional alterations of LTP after acute homocysteine exposure. *Behavioural Brain Research* 205: 559–563, 2009.
  31. **Ciliax BJ, Heilman C, Demchyshyn LL, Pristupa ZB, Ince E, Hersch SM, Niznik HB, Levey AI.** The dopamine transporter: immunochemical characterization and localization in brain. *J Neurosci* 15: 1714–1723, 1995.
  32. **Cilz NI, Kurada L, Hu B, Lei S.** Dopaminergic Modulation of GABAergic Transmission in the Entorhinal Cortex: Concerted Roles of  $\alpha 1$  Adrenoreceptors, Inward Rectifier K<sup>+</sup>, and T-Type Ca<sup>2+</sup> Channels. *Cerebral Cortex* (July 10, 2013). doi: 10.1093/cercor/bht177.
  33. **Clements JD, Lester RA, Tong G, Jahr CE, Westbrook GL.** The time course of glutamate in the synaptic cleft. *Science* 258: 1498–1501, 1992.
  34. **Coizet V, Comoli E, Westby GWM, Redgrave P.** Phasic activation of substantia nigra and the ventral tegmental area by chemical stimulation of the superior colliculus: an electrophysiological investigation in the rat. *Eur J Neurosci* 17: 28–40, 2003.
  35. **Coizet V, Overton PG, Redgrave P.** Collateralization of the tectonigral projection with other major output pathways of superior colliculus in the rat. *J Comp Neurol* 500: 1034–1049, 2006.
  36. **Colonnese MT, Constantine-Paton M.** Developmental period for N-methyl-D-aspartate (NMDA) receptor-dependent synapse elimination correlated with visuotopic map refinement. *J Comp Neurol* 494: 738–751, 2006.
  37. **Comoli E, Coizet V, (null), (null), (null), (null), Overton PG, Redgrave P.** A direct projection from superior colliculus to substantia nigra for detecting salient visual events. *Nat Neurosci* 6: 974–980, 2003.
  38. **Compte A.** Computational and in vitro studies of persistent activity: edging towards cellular and synaptic mechanisms of working memory. *Neuroscience* 139: 135–151, 2006.

39. **Constantine-Paton M, Cline HT, Debski E.** Patterned activity, synaptic convergence, and the NMDA receptor in developing visual pathways. *Annu. Rev. Neurosci.* 13: 129–154, 1990.
40. **Dean P, Redgrave P, Sahibzada N, Tsuji K.** Head and body movements produced by electrical stimulation of superior colliculus in rats: Effects of interruption of crossed tectoreticulospinal pathway. *Neuroscience* 19: 367–380, 1986.
41. **Debski EA, Cline HT, Constantine-Paton M.** Activity-dependent tuning and the NMDA receptor. *J. Neurobiol.* 21: 18–32, 1990.
42. **Denny-Brown D.** The Midbrain and Motor Integration. *Proceedings of the Royal Society of Medicine* 55: 527–12, 1962.
43. **Devoto P, Flore G, Saba P, Fà M, Gessa GL.** Co-release of noradrenaline and dopamine in the cerebral cortex elicited by single train and repeated train stimulation of the locus coeruleus. *BMC Neurosci* 6: 31, 2005.
44. **Devoto P, Flore G, Saba P, Fà M, Gessa GL.** Stimulation of the locus coeruleus elicits noradrenaline and dopamine release in the medial prefrontal and parietal cortex. *J Neurochem* 92: 368–374, 2005.
45. **Durstewitz D, Seamans JK.** The Dual-State Theory of Prefrontal Cortex Dopamine Function with Relevance to Catechol-O-Methyltransferase Genotypes and Schizophrenia. *Biological Psychiatry* 64: 739–749, 2008.
46. **Egorov AV, Hamam BN, Fransén E, Hasselmo ME, Alonso AA.** Graded persistent activity in entorhinal cortex neurons. *Nature* 420: 173–178, 2002.
47. **Ehlers MD, Zhang S, Bernhardt JP, Huganir RL.** Inactivation of NMDA receptors by direct interaction of calmodulin with the NR1 subunit. *Cell* 84: 745–755, 1996.
48. **Ewert JP.** *Tectal Mechanism that Underlie Prey-catching and Avoidance Behaviors in Toads.* New York: Plenum Press, 1984.
49. **Felsen G, Mainen ZF.** Neural substrates of sensory-guided locomotor decisions in the rat superior colliculus. *Neuron* 60: 137–148, 2008.

50. **Felsen G, Mainen ZF.** Midbrain contributions to sensorimotor decision making. *Journal of Neurophysiology* 108: 135–147, 2012.
51. **Feng G, Mellor RH, Bernstein M, Keller-Peck C, Nguyen QT, Wallace M, Nerbonne JM, Lichtman JW, Sanes JR.** Imaging neuronal subsets in transgenic mice expressing multiple spectral variants of GFP. *Neuron* 28: 41–51, 2000.
52. **Flint AC, Maisch US, Weishaupt JH, Kriegstein AR, Monyer H.** NR2A subunit expression shortens NMDA receptor synaptic currents in developing neocortex. *J Neurosci* 17: 2469–2476, 1997.
53. **Fu Y, Yuan Y, Halliday G, Rusznák Z, Watson C, Paxinos G.** A cytoarchitectonic and chemoarchitectonic analysis of the dopamine cell groups in the substantia nigra, ventral tegmental area, and retrorubral field in the mouse. *Brain Struct Funct* 217: 591–612, 2011.
54. **Gao WJ, Krimer LS, Goldman-Rakic PS.** Presynaptic regulation of recurrent excitation by D1 receptors in prefrontal circuits. *Proc Natl Acad Sci USA* 98: 295–300, 2001.
55. **Garris PA, Ciolkowski EL, Pastore P, Wightman RM.** Efflux of dopamine from the synaptic cleft in the nucleus accumbens of the rat brain. *J Neurosci* 14: 6084–6093, 1994.
56. **Gjerris A, Werdelin L, Rafaelsen OJ, Alling C, Christensen NJ.** CSF dopamine increased in depression: CSF dopamine, noradrenaline and their metabolites in depressed patients and in controls. *Journal of affective disorders* 13: 279–286, 1987.
57. **Glahn DC, Therman S, Manninen M, Huttunen M, Kaprio J, Lönnqvist J, Cannon TD.** Spatial working memory as an endophenotype for schizophrenia. *Biological Psychiatry* 53: 624–626, 2003.
58. **Goddard CA, Sridharan D, Huguenard JR, Knudsen EI.** Gamma Oscillations Are Generated Locally in an Attention-Related Midbrain Network. *Neuron* 73: 567–580, 2012.
59. **Gogos JA, Morgan M, Luine V, Santha M, Ogawa S, Pfaff D, Karayiorgou M.** Catechol-O-methyltransferase-deficient mice exhibit sexually dimorphic changes in catecholamine levels and behavior. *Proc Natl Acad Sci USA* 95: 9991–9996, 1998.



60. **Goldman-Rakic PS, Muly EC, Williams GV.** D(1) receptors in prefrontal cells and circuits. *Brain Res Brain Res Rev* 31: 295–301, 2000.
61. **Goldman-Rakic PS.** Regional and cellular fractionation of working memory. *Proc Natl Acad Sci USA* 93: 13473–13480, 1996.
62. **Gottesman II.** The Endophenotype Concept in Psychiatry: Etymology and Strategic Intentions. *American Journal of Psychiatry* 160: 636–645, 2003.
63. **Hagler DJ Jr., Sereno MI.** Spatial maps in frontal and prefrontal cortex. *NeuroImage* 29: 567–577, 2006.
64. **Halassa MM, Fellin T, Haydon PG.** The tripartite synapse: roles for gliotransmission in health and disease. *Trends in Molecular Medicine* 13: 54–63, 2007.
65. **Hall WC, Moschovakis AK.** *The Superior Colliculus*. CRC Press, 2003.
66. **Hikosaka O, Wurtz RH.** Modification of saccadic eye movements by GABA-related substances. I. Effect of muscimol and bicuculline in monkey superior colliculus. *Journal of Neurophysiology* 53: 266–291, 1985.
67. **Hogg N.** The effect of cyst (e) ine on the auto-oxidation of homocysteine. *Free Radical Biology and Medicine* 27: 28–33, 1999.
68. **Homayoun H, Moghaddam B.** NMDA receptor hypofunction produces opposite effects on prefrontal cortex interneurons and pyramidal neurons. *J Neurosci* 27: 11496–11500, 2007.
69. **Horwitz GD, Newsome WT.** Separate signals for target selection and movement specification in the superior colliculus. *Science* 284: 1158–1161, 1999.
70. **Howes OD, Kapur S.** The Dopamine Hypothesis of Schizophrenia: Version III--The Final Common Pathway. *Schizophrenia Bulletin* 35: 549–562, 2009.
71. **Huang G, Dragan M, Freeman D, Wilson JX.** Activation of catechol-O-methyltransferase in astrocytes stimulates homocysteine synthesis and export to neurons. *Glia* 51: 47–55,

- 2005.
72. **Ikeda T, Hikosaka O.** Reward-dependent gain and bias of visual responses in primate superior colliculus. *Neuron* 39: 693–700, 2003.
  73. **Ikeda T, Hikosaka O.** Positive and negative modulation of motor response in primate superior colliculus by reward expectation. *Journal of Neurophysiology* 98: 3163–3170, 2007.
  74. **Illing RB.** The mosaic architecture of the superior colliculus. *Prog Brain Res* 112: 17–34, 1996.
  75. **Ingle D.** Focal attention in the frog: behavioral and physiological correlates. *Science* 188: 1033–1035, 1975.
  76. **Ingle DJ.** Visually elicited evasive behavior in frogs. *Bioscience*.
  77. **Isa T, Hall WC.** Exploring the superior colliculus in vitro. *Journal of Neurophysiology* 102: 2581–2593, 2009.
  78. **Jin C, Thetford Smothers C, Woodward JJ.** Enhanced Ethanol Inhibition of Recombinant N-methyl-D-aspartate Receptors by Magnesium: Role of NR3A Subunits. *Alcoholism Clin Exp Res* 32: 1059–1066, 2008.
  79. **Kapur S, Remington G.** Dopamine D 2 receptors and their role in atypical antipsychotic action: still necessary and may even be sufficient. *BPS* 50: 873–883, 2001.
  80. **Katyal S, Zughni S, Greene C, Ress D.** Topography of covert visual attention in human superior colliculus. *Journal of Neurophysiology* 104: 3074–3083, 2010.
  81. **Kean S.** Phineas Gage, Neuroscience's Most Famous Patient  
. *Slate Magazine* May 6 2014 2014.
  82. **Kinney JW, Davis CN, Tabarean I, Conti B, Bartfai T, Behrens MM.** A specific role for NR2A-containing NMDA receptors in the maintenance of parvalbumin and GAD67 immunoreactivity in cultured interneurons. *Journal of Neuroscience* 26: 1604–1615, 2006.
  83. **Knudsen EI.** Control from below: the role of a midbrain network in

- spatial attention. *Eur J Neurosci* 33: 1961–1972, 2011.
84. **Komaroff AL.** Harvard Medical School Family Health Guide - Google Books.
  85. **Krauzlis RJ, Liston D, Carello CD.** Target selection and the superior colliculus: goals, choices and hypotheses. *Vision Res* 44: 1445–1451, 2004.
  86. **Krupp JJ, Vissel B, Heinemann SF, Westbrook GL.** Calcium-dependent inactivation of recombinant N-methyl-D-aspartate receptors is NR2 subunit specific. *Molecular Pharmacology* 50: 1680–1688, 1996.
  87. **Krystal JH, Abi-Saab W, Perry E, D'Souza DC, Liu N, Gueorguieva R, McDougall L, Hunsberger T, Belger A, Levine L, Breier A.** Preliminary evidence of attenuation of the disruptive effects of the NMDA glutamate receptor antagonist, ketamine, on working memory by pretreatment with the group II metabotropic glutamate receptor agonist, LY354740, in healthy human subjects. *Psychopharmacology (Berl)* 179: 303–309, 2004.
  88. **Kussius CL, Popescu GK.** Kinetic basis of partial agonism at NMDA receptors. *Nat Neurosci* 12: 1114–1120, 2009.
  89. **Lacey MG, Mercuri NB, North RA.** Dopamine acts on D2 receptors to increase potassium conductance in neurones of the rat substantia nigra zona compacta. *The Journal of Physiology* 392: 397–416, 1987.
  90. **Langer TP, Lund RD.** The upper layers of the superior colliculus of the rat: a Golgi study. *J Comp Neurol* 158: 418–435, 1974.
  91. **Legendre P, Rosenmund C, Westbrook GL.** Inactivation of NMDA channels in cultured hippocampal neurons by intracellular calcium. *J Neurosci* 13: 674–684, 1993.
  92. **Lerma J, Zukin RS, Bennett MV.** Glycine decreases desensitization of N-methyl-D-aspartate (NMDA) receptors expressed in *Xenopus* oocytes and is required for NMDA responses. *Proc Natl Acad Sci USA* 87: 2354–2358, 1990.
  93. **Lester RA, Jahr CE.** NMDA channel behavior depends on agonist affinity. *J Neurosci* 12: 635–643, 1992.

94. **Levine J, Stahl Z, Sela BA, Gavendo S, Ruderman V, Belmaker RH.** Elevated homocysteine levels in young male patients with schizophrenia. *The American journal of psychiatry* 159: 1790–1792, 2002.
95. **Lidow MS, Goldman-Rakic PS, Gallager DW, Rakic P.** Distribution of dopaminergic receptors in the primate cerebral cortex: quantitative autoradiographic analysis using [3H]raclopride, [3H]spiperone and [3H]SCH23390. *NSC* 40: 657–671, 1991.
96. **Lipton SA, Kim WK, Choi YB, Kumar S, D'Emilia DM, Rayudu PV, Arnelle DR, Stamler JS.** Neurotoxicity associated with dual actions of homocysteine at the N-methyl-D-aspartate receptor. *Proc Natl Acad Sci USA* 94: 5923–5928, 1997.
97. **Lisman JE, Fellous JM, Wang XJ.** A role for NMDA-receptor channels in working memory. *Nat Neurosci* 1: 273–275, 1998.
98. **Lovejoy LP, Krauzlis RJ.** Inactivation of primate superior colliculus impairs covert selection of signals for perceptual judgments. *Nat Neurosci* 13: 261–266, 2010.
99. **Luca P, Laurin N, Misener VL, Wigg KG, Anderson B, Cate-Carter T, Tannock R, Humphries T, Lovett MW, Barr CL.** Association of the dopamine receptor D1 gene, DRD1, with inattention symptoms in families selected for reading problems. *Mol Psychiatry* 12: 776–785, 2007.
100. **Luciana M, Depue RA, Arbisi P, Leon A.** Facilitation of working memory in humans by a D2 dopamine receptor agonist. *Journal of cognitive neuroscience* 4: 58–68, 1992.
101. **Lukasiewicz PD, Lawrence JE, Valentino TL.** Desensitizing glutamate receptors shape excitatory synaptic inputs to tiger salamander retinal ganglion cells. *J Neurosci* 15: 6189–6199, 1995.
102. **MacDonald AW, Chafee MV.** Translational and developmental perspective on N-methyl-D-aspartate synaptic deficits in schizophrenia. *Dev Psychopathol* 18: 853–876, 2006.
103. **Magleby KL.** Modal gating of NMDA receptors. *Trends in Neurosciences* 27: 231–233, 2004.

104. **Martina M, Gorfinkel Y, Halman S, Lowe JA, Periyalwar P, Schmidt CJ, Bergeron R.** Glycine transporter type 1 blockade changes NMDA receptor-mediated responses and LTP in hippocampal CA1 pyramidal cells by altering extracellular glycine levels. *The Journal of Physiology* 557: 489–500, 2004.
105. **Martina M, Krasteniakov NV, Bergeron R.** D-Serine differently modulates NMDA receptor function in rat CA1 hippocampal pyramidal cells and interneurons. *The Journal of Physiology* 548: 411–423, 2003.
106. **Mayer JS, Park S.** Working memory encoding and false memory in schizophrenia and bipolar disorder in a spatial delayed response task. *J Abnorm Psychol* 121: 784–794, 2012.
107. **Mayer ML, Armstrong N.** Structure and function of glutamate receptor ion channels. *Annu Rev Physiol* 66: 161–181, 2004.
108. **Mayer ML, BENVENISTE M, PATNEAU DK, VYKLIICKY L.** Pharmacologic Properties of NMDA Receptors. *Annals of the New York Academy of Sciences* 648: 194–204, 1992.
109. **Mayer ML, Vykllicky L, Clements J.** Regulation of NMDA receptor desensitization in mouse hippocampal neurons by glycine. *Nature* 338: 425–427, 1989.
110. **Mehta MA, Manes FF, Magnolfi G, Sahakian BJ, Robbins TW.** Impaired set-shifting and dissociable effects on tests of spatial working memory following the dopamine D2 receptor antagonist sulpiride in human volunteers. *Psychopharmacology (Berl)* 176: 331–342, 2004.
111. **Mehta MA, Sahakian BJ, McKenna PJ, Robbins TW.** Systemic sulpiride in young adult volunteers simulates the profile of cognitive deficits in Parkinson's disease. *Psychopharmacology (Berl)* 146: 162–174, 1999.
112. **Mehta MA, Swainson R, Ogilvie AD, Sahakian B, Robbins TW.** Improved short-term spatial memory but impaired reversal learning following the dopamine D2 agonist bromocriptine in human volunteers. *Psychopharmacology (Berl)* 159: 10–20, 2001.
113. **Mehta MA.** Sulpiride and mnemonic function: effects of a dopamine D2 receptor antagonist on working memory, emotional

- memory and long-term memory in healthy volunteers. *Journal of Psychopharmacology* 19: 29–38, 2005.
114. **Mejias-Aponte CA, Drouin C, Aston-Jones G.** Adrenergic and Noradrenergic Innervation of the Midbrain Ventral Tegmental Area and Retrorubral Field: Prominent Inputs from Medullary Homeostatic Centers. *Journal of Neuroscience* 29: 3613–3626, 2009.
115. **Meltzer LT, Christoffersen CL, Serpa KA.** Modulation of dopamine neuronal activity by glutamate receptor subtypes. *Neurosci Biobehav Rev* 21: 511–518, 1997.
116. **Merker B.** Consciousness without a cerebral cortex: A challenge for neuroscience and medicine. *Behavioral and Brain Sciences* 30, 2007.
117. **Metzger M, Britto LRG, Toledo CAB.** Monoaminergic markers in the optic tectum of the domestic chick. *Neuroscience* 141: 1747–1760, 2006.
118. **Misener VL, Luca P, Azeke O, Crosbie J, Waldman I, Tannock R, Roberts W, Malone M, Schachar R, Ickowicz A, Kennedy JL, Barr CL.** Linkage of the dopamine receptor D1 gene to attention-deficit/hyperactivity disorder. *Mol Psychiatry* 9: 500–509, 2003.
119. **Monyer H, Burnashev N, Laurie DJ, Sakmann B, Seeburg PH.** Developmental and regional expression in the rat brain and functional properties of four NMDA receptors. *Neuron* 12: 529–540, 1994.
120. **Mooney RD, Nikolettseas MM, Ruiz SA, Rhoades RW.** Receptive-field properties and morphological characteristics of the superior collicular neurons that project to the lateral posterior and dorsal lateral geniculate nuclei in the hamster. *Journal of Neurophysiology* 59: 1333–1351, 1988.
121. **Munoz DP, Wurtz RH.** Saccade-related activity in monkey superior colliculus. I. Characteristics of burst and buildup cells. *Journal of Neurophysiology* 73: 2313–2333, 1995.
122. **Muntjewerff JW, Kahn RS, Blom HJ, Heijer Den M.** Homocysteine, methylenetetrahydrofolate reductase and risk of schizophrenia: a meta-analysis. *Mol Psychiatry* 11: 143–149, 2006.

123. **Müller JR, Philiastides MG, Newsome WT.** Microstimulation of the superior colliculus focuses attention without moving the eyes. *Proc Natl Acad Sci USA* 102: 524–529, 2005.
124. **Myles-Worsley M, Park S.** Spatial working memory deficits in schizophrenia patients and their first degree relatives from Palau, Micronesia. *Am. J. Med. Genet.* 114: 609–615, 2002.
125. **Neeman G, Blanaru M, Bloch B, Kremer I, Ermilov M, Javitt DC, Heresco-Levy U.** Relation of plasma glycine, serine, and homocysteine levels to schizophrenia symptoms and medication type. *The American journal of psychiatry* 162: 1738–1740, 2005.
126. **Newcomer JW, Krystal JH.** NMDA receptor regulation of memory and behavior in humans. *Hippocampus* 11: 529–542, 2001.
127. **Nicodemus KK, Kolachana BS, Vakkalanka R, Straub RE, Giegling I, Egan MF, Rujescu D, Weinberger DR.** Evidence for statistical epistasis between catechol-O-methyltransferase (COMT) and polymorphisms in RGS4, G72 (DAOA), GRM3, and DISC1: influence on risk of schizophrenia. *Hum. Genet.* 120: 889–906, 2007.
128. **Northmore DP, Levine ES, Schneider GE.** Behavior evoked by electrical stimulation of the hamster superior colliculus. *Experimental brain research Experimentelle Hirnforschung Expérimentation cérébrale* 73: 595–605, 1988.
129. **Onn S-P, Wang X-B, Lin M, Grace AA.** Dopamine D1 and D4 receptor subtypes differentially modulate recurrent excitatory synapses in prefrontal cortical pyramidal neurons. *Neuropsychopharmacology* 31: 318–338, 2006.
130. **Papouin T, Ladépêche L, Ruel J, Sacchi S, Labasque M, Hanini M, Groc L, Pollegioni L, Mothet J-P, Oliet SHR.** Synaptic and Extrasynaptic NMDA Receptors Are Gated by Different Endogenous Coagonists. *Cell* 150: 633–646, 2012.
131. **Park S, Holzman PS, Goldman-Rakic PS.** Spatial Working Memory Deficits in the Relatives of Schizophrenic Patients. *Arch Gen Psychiatry* 52: 821, 1995.
132. **Park S, Holzman PS.** Schizophrenics show spatial working memory deficits. *Arch Gen Psychiatry* 49: 975–982, 1992.

133. **Pettit DL, Helms MC, Lee P, Augustine GJ, Hall WC.** Local excitatory circuits in the intermediate gray layer of the superior colliculus. *Journal of Neurophysiology* 81: 1424–1427, 1999.
134. **Phillips MA, Colonnese MT, Goldberg J, Lewis LD, Brown EN, Constantine-Paton M.** A synaptic strategy for consolidation of convergent visuotopic maps. *Neuron* 71: 710–724, 2011.
135. **Pickel VM, Colago EE, Mania I, Molosh AI, Rainnie DG.** Dopamine D1 receptors co-distribute with N-methyl-D-aspartic acid type-1 subunits and modulate synaptically-evoked N-methyl-D-aspartic acid currents in rat basolateral amygdala. *NSC* 142: 671–690, 2006.
136. **Pirkola T, Tuulio-Henriksson A, Glahn D, Kieseppä T, Haukka J, Kaprio J, Lönngqvist J, Cannon TD.** Spatial working memory function in twins with schizophrenia and bipolar disorder. *Biological Psychiatry* 58: 930–936, 2005.
137. **Podda MV, Riccardi E, D'Ascenzo M, Azzena GB, Grassi C.** Dopamine D1-like receptor activation depolarizes medium spiny neurons of the mouse nucleus accumbens by inhibiting inwardly rectifying K<sup>+</sup> currents through a cAMP-dependent protein kinase A-independent mechanism. *Neuroscience* 167: 678–690, 2010.
138. **Poddar R, Paul S.** Homocysteine-NMDA receptor-mediated activation of extracellular signal-regulated kinase leads to neuronal cell death. *J Neurochem* 110: 1095–1106, 2009.
139. **Popescu G, Auerbach A.** Modal gating of NMDA receptors and the shape of their synaptic response. *Nat Neurosci* 6: 476–483, 2003.
140. **Priestley T, Laughton P, Myers J, Le Bourdellés B, Kerby J, Whiting PJ.** Pharmacological properties of recombinant human N-methyl-D-aspartate receptors comprising NR1a/NR2A and NR1a/NR2B subunit assemblies expressed in permanently transfected mouse fibroblast cells. *Molecular Pharmacology* 48: 841–848, 1995.
141. **Ratcliff R.** A Comparison of Macaque Behavior and Superior Colliculus Neuronal Activity to Predictions From Models of Two-Choice Decisions. *Journal of Neurophysiology* 90: 1392–1407, 2003.
142. **Regland B, Abrahamsson L, Blennow K, Grenfeldt B, Gottfries C-G.** CSF-methionine is elevated in psychotic patients. *J Neural*



- Transm* 111: 631–640, 2004.
143. **Regland B.** Schizophrenia and single-carbon metabolism. *Progress in Neuro-Psychopharmacology and Biological Psychiatry* 29: 1124–1132, 2005.
  144. **Robertson SD, Plummer NW, de Marchena J, Jensen P.** Developmental origins of central norepinephrine neuron diversity. *Nature Publishing Group* 16: 1016–1023, 2013.
  145. **Robinson DA.** Eye movements evoked by collicular stimulation in the alert monkey. *Vision Res* 12: 1795–1808, 1972.
  146. **Roffman JL, Gollub RL, Calhoun VD, Wassink TH, Weiss AP, Ho BC, White T, Clark VP, Fries J, Andreasen NC, Goff DC, Manoach DS.** MTHFR 677C --> T genotype disrupts prefrontal function in schizophrenia through an interaction with COMT 158Val --> Met. *Proc Natl Acad Sci USA* 105: 17573–17578, 2008.
  147. **Roffman JL, Weiss AP, Deckersbach T, Freudenreich O, Henderson DC, Wong DH, Halsted CH, Goff DC.** Interactive effects of COMT Val108/158Met and MTHFR C677T on executive function in schizophrenia. *Am. J. Med. Genet.* 147B: 990–995, 2008.
  148. **Romanowski CA, Mitchell IJ, Crossman AR.** The organisation of the efferent projections of the zona incerta. *Journal of anatomy* 143: 75, 1985.
  149. **Romo R, Brody CD, Hernández A, Lemus L.** Neuronal correlates of parametric working memory in the prefrontal cortex. *Nature* 399: 470–473, 1999.
  150. **Rosenberg D, Artoul S, Segal AC, Kolodney G, Radzishevsky I, Dikopoltsev E, Foltyn VN, Inoue R, Mori H, Billard J-M, Wolosker H.** Neuronal D-serine and glycine release via the Asc-1 transporter regulates NMDA receptor-dependent synaptic activity. *Journal of Neuroscience* 33: 3533–3544, 2013.
  151. **Roux MJ, Supplisson S.** Neuronal and glial glycine transporters have different stoichiometries. *Neuron* 25: 373–383, 2000.
  152. **Saito Y, Isa T.** Electrophysiological and morphological properties of neurons in the rat superior colliculus. I. Neurons in the intermediate layer. *Journal of Neurophysiology* 82: 754–767, 1999.

153. **Saito Y, Isa T.** Local excitatory network and NMDA receptor activation generate a synchronous and bursting command from the superior colliculus. *Journal of Neuroscience* 23: 5854–5864, 2003.
154. **Sather W, Dieudonné S, MacDonald JF, Ascher P.** Activation and desensitization of N-methyl-D-aspartate receptors in nucleated outside-out patches from mouse neurones. *The Journal of Physiology* 450: 643–672, 1992.
155. **Sather W, Johnson JW, Henderson G, Ascher P.** Glycine-insensitive desensitization of NMDA responses in cultured mouse embryonic neurons. *Neuron* 4: 725–731, 1990.
156. **Sawaguchi T, Goldman-Rakic PS.** D1 dopamine receptors in prefrontal cortex: involvement in working memory. *Science* 251: 947–950, 1991.
157. **Sawaguchi T, Goldman-Rakic PS.** The role of D1-dopamine receptor in working memory: local injections of dopamine antagonists into the prefrontal cortex of rhesus monkeys performing an oculomotor delayed-response task. *Journal of Neurophysiology* 71: 515–528, 1994.
158. **Sawaguchi T, Iba M.** Prefrontal cortical representation of visuospatial working memory in monkeys examined by local inactivation with muscimol. *Journal of Neurophysiology* 86: 2041–2053, 2001.
159. **Sawaguchi T, Matsumura M, Kubota K.** Effects of dopamine antagonists on neuronal activity related to a delayed response task in monkey prefrontal cortex. *Journal of Neurophysiology* 63: 1401–1412, 1990.
160. **Sawaguchi T.** The effects of dopamine and its antagonists on directional delay-period activity of prefrontal neurons in monkeys during an oculomotor delayed-response task. *Neurosci Res* 41: 115–128, 2001.
161. **Schell MJ, Brady RO, Molliver ME, Snyder SH.** D-serine as a neuromodulator: regional and developmental localizations in rat brain glia resemble NMDA receptors. *J Neurosci* 17: 1604–1615, 1997.

162. **Schiller PH, Stryker M.** Single-unit recording and stimulation in superior colliculus of the alert rhesus monkey. *J Neurophysiol* 35: 915–924, 1972.
163. **Schnieder TP, Dwork AJ.** Searching for Neuropathology: Gliosis in Schizophrenia. *BPS* 69: 134–139, 2011.
164. **Schultz W.** Multiple Dopamine Functions at Different Time Courses. *Annu. Rev. Neurosci.* 30: 259–288, 2007.
165. **Seamans J.** Losing inhibition with ketamine. *Nat. Chem. Biol.* 4: 91–93, 2008.
166. **Seamans JK, Durstewitz D, Christie BR, Stevens CF, Sejnowski TJ.** Dopamine D1/D5 receptor modulation of excitatory synaptic inputs to layer V prefrontal cortex neurons. *Proceedings of the National Academy of Sciences* 98: 301–306, 2001.
167. **Seamans JK, Gorelova N, Durstewitz D, Yang CR.** Bidirectional dopamine modulation of GABAergic inhibition in prefrontal cortical pyramidal neurons. *Journal of Neuroscience* 21: 3628–3638, 2001.
168. **Seong HJ, Carter AG.** D1 Receptor Modulation of Action Potential Firing in a Subpopulation of Layer 5 Pyramidal Neurons in the Prefrontal Cortex. *Journal of Neuroscience* 32: 10516–10521, 2012.
169. **Sesack SR, Hawrylak VA, Matus C, Guido MA, Levey AI.** Dopamine axon varicosities in the prelimbic division of the rat prefrontal cortex exhibit sparse immunoreactivity for the dopamine transporter. *J Neurosci* 18: 2697–2708, 1998.
170. **Seung HS, Lee DD, Reis BY, Tank DW.** Stability of the memory of eye position in a recurrent network of conductance-based model neurons. *Neuron* 26: 259–271, 2000.
171. **Sooksawate T, Isa K, Isa T.** Cholinergic responses in crossed tecto-reticular neurons of rat superior colliculus. *Journal of Neurophysiology* 100: 2702–2711, 2008.
172. **Sooksawate T, Yanagawa Y, Isa T.** Cholinergic responses in GABAergic and non-GABAergic neurons in the intermediate gray layer of mouse superior colliculus. *Eur J Neurosci* 36: 2440–2451, 2012.

173. **Sornarajah L, Vasuta OC, Zhang L, Sutton C, Li B, El-Husseini A, Raymond LA.** NMDA receptor desensitization regulated by direct binding to PDZ1-2 domains of PSD-95. *Journal of Neurophysiology* 99: 3052–3062, 2008.
174. **Sparks DL, Hartwich-Young R.** The deep layers of the superior colliculus. *Rev Oculomot Res* 3: 213–255, 1989.
175. **Strehler BL.** Where is the self? A neuroanatomical theory of consciousness. *Synapse* 7: 44–91, 1991.
176. **Surtees R, Leung DYM, Bowron A, Leonard J.** Cerebrospinal Fluid and Plasma Total Homocysteine and Related Metabolites in Children with Cystathionine  $\beta$ -Synthase Deficiency: The Effect of Treatment. *Pediatr Res* 42: 577–582, 1997.
177. **Takada M, Li ZK, Hattori T.** Dopaminergic nigrotectal projection in the rat. *Brain Research* 457: 165–168, 1988.
178. **Tauscher J, Hussain T, Agid O, Verhoeff NPLG, Wilson AA, Houle S, Remington G, Zipursky RB, Kapur S.** Equivalent occupancy of dopamine D1 and D2 receptors with clozapine: differentiation from other atypical antipsychotics. *The American journal of psychiatry* 161: 1620–1625, 2004.
179. **Tecuapetla F, Patel JC, Xenias H, English D, Tadros I, Shah F, Berlin J, Deisseroth K, Rice ME, Tepper JM, Koos T.** Glutamatergic Signaling by Mesolimbic Dopamine Neurons in the Nucleus Accumbens. *Journal of Neuroscience* 30: 7105–7110, 2010.
180. **Tong G, Shepherd D, Jahr CE.** Synaptic desensitization of NMDA receptors by calcineurin. *Science* 267: 1510–1512, 1995.
181. **Townsend M, Yoshii A, Mishina M, Constantine-Paton M.** Developmental loss of miniature N-methyl-D-aspartate receptor currents in NR2A knockout mice. *Proc Natl Acad Sci USA* 100: 1340–1345, 2003.
182. **Trantham-Davidson H, Kroner S, Seamans JK.** Dopamine Modulation of Prefrontal Cortex Interneurons Occurs Independently of DARPP-32. *Cerebral Cortex* 18: 951–958, 2007.
183. **Tritsch NX, Ding JB, Sabatini BL.** Dopaminergic neurons inhibit striatal output through non-canonical release of GABA. *Nature* 490:

262–266, 2012.

184. **Tunbridge E, Harrison P, Weinberger D.** Catechol-o-Methyltransferase, Cognition, and Psychosis: Val158Met and Beyond. *Biological Psychiatry* 60: 141–151, 2006.
185. **Tunbridge EM, Harrison PJ, Warden DR, Johnston C, Refsum H, Smith AD.** Polymorphisms in the catechol-O-methyltransferase (COMT) gene influence plasma total homocysteine levels. *Am. J. Med. Genet. B Neuropsychiatr. Genet.* 147B: 996–999, 2008.
186. **Tunbridge EM.** Catechol-O-Methyltransferase Inhibition Improves Set-Shifting Performance and Elevates Stimulated Dopamine Release in the Rat Prefrontal Cortex. *Journal of Neuroscience* 24: 5331–5335, 2004.
187. **van Zundert B, Yoshii A, Constantine-Paton M.** Receptor compartmentalization and trafficking at glutamate synapses: a developmental proposal. *Trends in Neurosciences* 27: 428–437, 2004.
188. **Versteeg DH, Van der Gugten J, De Jong W, Palkovits M.** Regional concentrations of noradrenaline and dopamine in rat brain. *Brain Research* 113: 563–574, 1976.
189. **Vicini S, Wang JF, Li JH, Zhu WJ, Wang YH, Luo JH, Wolfe BB, Grayson DR.** Functional and pharmacological differences between recombinant N-methyl-D-aspartate receptors. *Journal of Neurophysiology* 79: 555–566, 1998.
190. **Villarroel A, Regalado MP, Lerma J.** Glycine-independent NMDA receptor desensitization: localization of structural determinants. *Neuron* 20: 329–339, 1998.
191. **Vyklicky L, Benveniste M, Mayer ML.** Modulation of N-methyl-D-aspartic acid receptor desensitization by glycine in mouse cultured hippocampal neurones. *The Journal of Physiology* 428: 313–331, 1990.
192. **Wang M, Vijayraghavan S, Goldman-Rakic PS.** Selective D2 receptor actions on the functional circuitry of working memory. *Science* 303: 853–856, 2004.
193. **Wang M, Yang Y, Wang C-J, Gamo NJ, Jin LE, Mazer JA, Morrison**

- JH, Wang X-J, Arnsten AFT.** NMDA Receptors Subserve Persistent Neuronal Firing during Working Memory in Dorsolateral Prefrontal Cortex. *Neuron* 77: 736–749, 2013.
194. **Wang XJ.** Synaptic reverberation underlying mnemonic persistent activity. *Trends in Neurosciences* 24: 455–463, 2001.
195. **Wang Y, Kakizaki T, Sakagami H, Saito K, Ebihara S, Kato M, Hirabayashi M, Saito Y, Furuya N, Yanagawa Y.** Fluorescent labeling of both GABAergic and glycinergic neurons in vesicular GABA transporter (VGAT)-Venus transgenic mouse. *Neuroscience* 164: 1031–1043, 2009.
196. **Weller ME, Rose S, Jenner P, Marsden CD.** In vitro characterisation of dopamine receptors in the superior colliculus of the rat. *Neuropharmacology* 26: 347–354, 1987.
197. **Werner P, Hussy N, Buell G, Jones KA, North RA.** D2, D3, and D4 dopamine receptors couple to G protein-regulated potassium channels in *Xenopus* oocytes. *Molecular Pharmacology* 49: 656–661, 1996.
198. **Whorton MR, MacKinnon R.** X-ray structure of the mammalian GIRK2- $\beta\gamma$  G-protein complex. *Nature* 498: 190–197, 2013.
199. **Wilcox KS, Fitzsimonds RM, Johnson B, Dichter MA.** Glycine regulation of synaptic NMDA receptors in hippocampal neurons. *Journal of Neurophysiology* 76: 3415–3424, 1996.
200. **Williams GV, Goldman-Rakic PS.** Modulation of memory fields by dopamine D1 receptors in prefrontal cortex. *Nature* 376: 572–575, 1995.
201. **Williams PJ, MacVicar BA, Pittman QJ.** A dopaminergic inhibitory postsynaptic potential mediated by an increased potassium conductance. *NSC* 31: 673–681, 1989.
202. **Wolosker H.** D-Serine Regulation of NMDA Receptor Activity. *Science Signaling* 2006: pe41–pe41, 2006.
203. **Yamamoto T, Rossi S, Stiefel M, Doppenberg E, Zauner A, Bullock R, Marmarou A.** CSF and ECF glutamate concentrations in head injured patients. *Acta Neurochir. Suppl.* 75: 17–19, 1999.

204. **Zahrt J, Taylor JR, Mathew RG, Arnsten AF.** Supranormal stimulation of D1 dopamine receptors in the rodent prefrontal cortex impairs spatial working memory performance. *J Neurosci* 17: 8528–8535, 1997.
205. **Zhang W, Howe JR, Popescu GK.** Distinct gating modes determine the biphasic relaxation of NMDA receptor currents. *Nat Neurosci* 11: 1373–1375, 2008.
206. **Zhong J, Russell SL, Pritchett DB, Molinoff PB, Williams K.** Expression of mRNAs encoding subunits of the N-methyl-D-aspartate receptor in cultured cortical neurons. *Molecular Pharmacology* 45: 846–853, 1994.
207. **Zilberter Y, Uteshev V, Sokolova S, Khodorov B.** Desensitization of N-methyl-D-aspartate receptors in neurons dissociated from adult rat hippocampus. *Molecular Pharmacology* 40: 337–341, 1991.
208. **Zucker RS, Regehr WG.** Short Term Synaptic Plasticity. *Annu Rev Physiol* 64: 355–405, 2002.